Aus der Medizinischen Klinik und Poliklinik I Großhadern
Klinik der Ludwig-Maximilians-Universität München
Direktor: Prof. Dr. med. Steffen Massberg

Enhanced recombinant adeno-associated virus (rAAV) in vivo transduction efficacy via surface modified PAMAM nanoparticles precoating

Dissertation
zum Erwerb des Doktorgrades der Humanbiologie
an der Medizinischen Fakultät der
Ludwig-Maximilians-Universität zu München

Vorgelegt von
Seungmin Lee
Aus
Daegu, Republic of Korea
Jahr
2015

Mit Genehmigung der Medizinischen Fakultät

der Universität München

Berichterstatter:	Prof. Dr. med. Christian Kupatt
Mitberichterstatter:	Prof. Dr. rer. nat. Sabine Marten-Steffens
	Prof. Dr. Andreas Dendorfer
	Prof. Dr. Christian Hagl
Mitbetreuung durch den Promovierten Mitarbeiter:	
Dekan:	Prof. Dr. med. dent. Reinhard Hickel
Tag der mündliche Prüfung:	17.12.2015

Real knowledge is to know the extent of one's ignorance

- Confucius

Eidesstattliche Versicherung

Lee, Seungmin

Name, Vorname

Ich erkläre hiermit an Eides statt,
dass ich die vorliegende Dissertation mit dem Thema

Enhanced recombinant adeno-associated virus (rAAV) in vivo transduction efficacy via surface modified PAMAM nanoparticles precoating

selbständig verfasst, mich außer der angegebenen keiner weiteren Hilfsmittel bedient und alle Erkenntnisse, die aus dem Schrifttum ganz oder annähernd übernommen sind, als solche kenntlich gemacht und nach ihrer Herkunft unter Bezeichnung der Fundstelle einzeln nachgewiesen habe.

Ich erkläre des Weiteren, dass die hier vorgelegte Dissertation nicht in gleicher oder in ähnlicher Form bei einer anderen Stelle zur Erlangung eines akademischen Grades eingereicht wurde.

13.07.2015

Ort, Datum

Unterschrift Doktorandin/Doktorand

TABLE OF CONTENTS

1. INTRODUCTION

1.1 . Gene therapy

Gene therapy is the use of genetic information to treat human diseases by the selective delivery of DNA into a patient's cells defective or missing DNA sequences. Gene therapy was first conceptualized by Theodore Friedmann and Richard Roblin [1]. Martin Cline conducted the first gene therapy trial involving recombinant DNA in 1980. The first successful FDA approved gene therapy study was targeting ADA-SCID in the United States in 1990. Since then, the number of studies for gene therapy rapidly increased to > 2.000 completed or ongoing trials today. AAV-based gene therapy was first applied in 1997, and a decade later [2] reported improvement of human eyesight by using an AAV-mediated gene transfer.

1.1.1. Viral vectors

Viral and non-viral vectors are used for targeted gene delivery. Viral vectors are the most efficient for gene therapy, but their approach is limited by their immunogenicity, the available packaging size of DNA and their oncogenic potential. The most popular viral vectors for gene delivery are adenovirus [59], adeno-associated virus [14], retrovirus and lentivirus [60]. In principle, they display varying features: For example, the adenovirus has a naked coat, an icosahedral capsid, lacks virion polymerase, but provides a transient transgene expression and a packaging capacity of 7.5 kb. The adeno-associated virus has a naked coat, an icosahedral capsid, no virion polymerase, but provides long lasting transgene expression, and a packaging capacity of 4.5 kb. In contrast, retroviruses/lentiviruses have an enveloped coat, an icosahedral capsid, possess a virion polymerase, insert into the host genome, and provide a packaging capacity of 8 kb (Table 1).

	Adenovirus	AAV	Retro-/Lenti-virus
Family	Adenoviridae	Parvoviridae	Retroviridae
Coat	Naked	Naked	Enveloped
Capsid	Icosahedral	Icosahedral	Icosahedral
Genome	dsDNA	ssDNA	ssRNA(+)
Virion polymerase	Negative	Negative	Positive
Virion diameter	70 - 90 nm	18 - 26 nm	80 - 130 nm
Genome size	39 - 38 kb	5 kb	3 - 9 kb
Infection/tropism	Dividing and non-dividing cells	Dividing and non-dividing cells	Dividing cells
Host genome interaction	Non-integrating	Non-integrating	Integrating
Transgene expression	Transient	Potential long lasting	Long lasting
Packaging capacity	7.5 kb	4.5 kb	8 kb

Table 1 | Characterization of viral vectors. dsDNA, double-stranded DNA; ssDNA, single-stranded DNA. (Modified from Gene Therapy Net; http://www.genetherapynet.com/viral-vectors.html).

1.1.2. Non-viral vectors

Non-viral vectors possess several advantages compared to viral vectors, such as large capacity, a low production costs, a low immunogenicity as well as a low toxicity. The main limitation of non-viral vectors is their low continuous transfer efficiency compared to viral vectors in gene delivery. Nonetheless, recent studies of non-viral vectors show substantial progress [4].

Currently used non-viral vectors are inorganic, polymer, lipid-based or hybrid [8]. Specially, inorganic particles including gold nanoparticles, calcium phosphate, magnetic nanoparticles, and carbon nanotubes (CNTs) are commonly used for gene delivery materials. These particles possess advantages, such as easy preparation, quick transfection, wide availability, and high transfection efficiency. But they are toxic, non-biocompatible and imply low transferring efficiency.

Polymer-based particles include cationic polymer, polysaccharide particle, polyethylenimin (PEI) polymers, dendrimers, poly lactic-co-glycolic acid (PLGA)-based nanoparticles, and poly-ion complex micelles (PICs). In addition to other advantages, they display high protection against enzymatic degradation, easy

preparation, low toxicity and a high cationic potential. But they also feature low biodegradability and low transferring efficiency.

Cationic lipids, cationic emulsions, and cationic liposomes are lipid-based particles commonly utilized for gene delivery to target cells. These particles have safe preparation, low immunogenicity, but a toxic in high dose, and difficult to prepare as well as transfer efficient.

Hybrid particles contain two groups, such as liposome-polycation-DNA (LPD) particles and multilayered nanoparticles. These particles consist of polyplexes and liposomes, called as lipopolyplexes. Most of the polyplexes contain complexes of polymers with DNA, e.g. cationic polymers (such as NH_2 surfaced-dendrimers) and their production is regulated by ionic interactions. One advantage compared to other non-viral vectors is their high transfection efficiency, similar to viral vectors. The properties, advantages, and disadvantages of these non-viral vectors are presented in Tables 2 [8].

Vectors	Toxicity	Advantages	Disadvantages
Inorganic	Frequently toxic	Short time of transfection, easy preparation, wide availability, rich functionality, high transfection efficiency, potential capability for targeted delivery and controlled release	Most of them are instable, toxic and non-biocompatible
Polymer	Low toxicity	Small size, narrow distribution, more stability, high protection against enzymatic degradation, low toxicity and high cationic potential	Low biodegradability, low efficacy
Lipid	Toxic	Safe preparation, low immunogenicity	Toxicity at high dose, difficult preparation, low transformation efficiency
Hybrid	Low toxicity	Improved the loading dose of DNA cellular uptake, controlling the release of the DNA and target delivery compared to other non-viral vectors	Toxicity at very high dose

Table 2 | Different type of non-viral vectors in gene delivery. Toxicity; Cellular toxicity. (Modified from Dizaj et al., Nanoscale Research Letters 2014 [8]).

1.2 . Adeno-associated virus

Given the range of vector systems described above, adeno-associated viruses are a promising vector system for human gene therapy, since they are not known for human pathogenity, provide a long lasting effect at low immunologic side effects. The first serotype was discovered in 1965, isolated from a contaminant of simian adenovirus preparations [5]. AAVs are small viruses with a non-enveloped icosahedral capsid of a size between 18 ~ 26 nm (Figure 1) [6]. Although about 40-60% (depending on regional differences) of adults are sero-positive for AAV serotype 2 (AAV2), the infection has not been associated with any symptoms or disease. Because AAV serotypes are members of the Parvoviridae family and belong to the genus Dependovirus, they require a helper virus, such as adenovirus, to support productive infection and replication. The capsid structure controls in different tissues specificity and transduction efficiency [12]. The tropisms of each AAV serotypes are indicated as in Table 3.

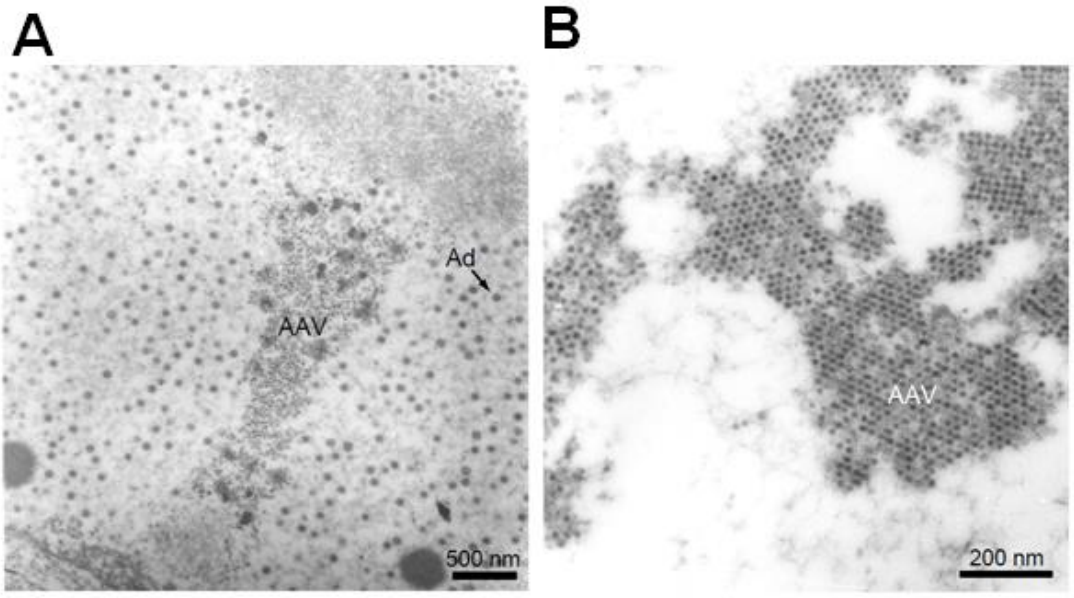

Figure 1 | Transmission electron microscopy image of AAV2 and Ad5. **A**, AAV2 and Ad5 particles in the nucleus of a HeLa cell at 48 hours after co-infection. Magnification: × 15,000. **B**, AAV2 virions in a HeLa cell at 48 hours after co-infection with Ad5. Magnification: × 40,000. (Adapted from Gonçalves MA, Virology Journal 2005 [6]).

Serotype	Origin	Receptor	Co-receptor
AAV1	Muscle, CNS	2.3N/2,6N-sialic acid	Unknown
AAV2	Muscle, liver, Kidney	HSPG	FGFR-1, integrin, HGFR, LamR
AAV3	Inner ear	HSPG	FGFR-2, HGFR, LamR
AAV4	CNS, Eye	2.3O-sialic acid	Unknown
AAV5	Lung, CNS, Photoreceptor cells	2.3N-sialic acid	PDGFR
AAV6	Skeletal muscle	2.3N/2,6N-sialic acid	EGFR
AAV7	Skeletal muscle	N-sialic acid	PDGFR
AAV8	Heart, Liver, Pancreas, Skeletal muscle	Unknown	LamR
AAV9	Heart, Liver, Skeletal muscle, Lung	N-galactose	LamR

Table 3 | Tropisms, receptors and co-receptors of AAV serotype vectors. HSPG; heparan sulfate proteoglycan, FGFR; Fibroblast growth factor receptor, HGFR; hepatic growth factor receptor, PDGFR; platelet derived growth factor receptor, LamR; 37/67 KD laminin receptor, EGFR; epidermal growth factor receptor, CNS; Central nervous system. (Modified from Zhijian Wu et al., Molecular Therapy 2006 [10] and Hyun-Joo Nam et al., J Virol 2007 [12]).

1.2.1. Structure of AAV

The virion shell of AAV has as a small (about 18~26 nm), naked coat, a T=1 icosahedral capsid, negative virion polymerase, and a single stranded DNA genome (capacity ~4.7 kb). The AAV genome is packaged into T=1 icosahedral capsids consisting of 60 subunits of capsid proteins (CPs). The inverted terminal repeats (ITRs; ~145 kb) flank the two viral open reading frames (ORFs) *rep* (replication) and *cap* (capsid) encoding non-structural and structural proteins [6]. The ITRs are required for genome replication and packaging. The *rep* non-structural ORF, encodes four replication proteins responsible for site-specific integration, nicking, and helicase activity. The *cap* structural ORF contain three viral proteins (VPs): VP1, VP2 and VP3, which assemble the capsid by 2-, 3-, and 5-fold symmetry-related interactions in proportions of about 1:1:10 (Figure 2) [7].

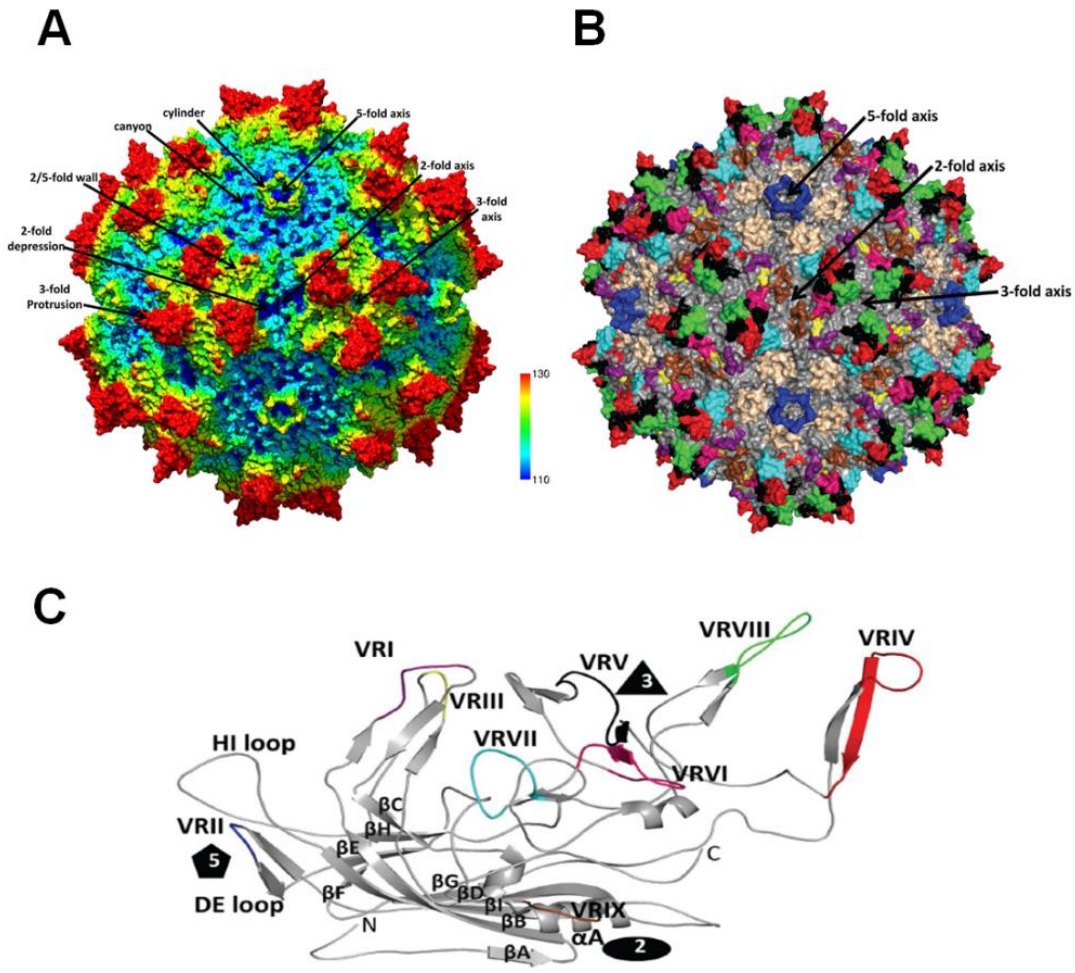

Figure 2 | Three-dimensional structure of AAV capsid and variable regions. A, Radially color-cued (from capsid center to surface: blue-green-yellow-red; ~110–130 Å) of the AAV1 capsid generated from 60 VP monomers (RCSB PDB # 3NG9). The approximate icosahedral two-, three-, and five-fold symmetry axes are as well as the AAV capsid surface features are indicated by the arrows and labeled and indicated by the filled oval, triangle, and pentagon, respectively in (**A & B**). **B**, The capsid surface of AAV2 with VR-I to VR-IX colored (I: purple, II: blue, III: yellow, IV: red, V: black, VI: hot pink, VII: cyan, VIII: green, and IX: brown) and labeled as in (**B & C**). **C**, A ribbon diagram representation of the ordered over lapping VP3 monomer region of AAV1. The conserved β-barrel core motif (βBIDG-βCHEF, gray), conserved αA helix, DE loop (between βD and βE), HI loop (between βH and βI), VR-I to VR-IX are colored as in (**B**). The N and C labels are the N- and C-terminal ends of the ordered VP region, respectively. The (**A**) image was generated using the Chimera program. (**B & C**) were generated with the PyMOL program. (Adapted from Tseng et al., Front Immunol 2014 [7]).

Three-dimensional structures have been determined for several serotypes of AAV (about AAV1-AAV9) by X-ray crystallography or cryo-reconstruction. These AAV serotypes are representatives of the over 100 AAV genomic isolates and 13 human and non-human serotypes. The AAVs have a sequence similarity that ranges from ~55 to 99% [7, 9, 12, 21, 22]. These capsid proteins of 60 subunits have been positioned by three rules (Figure 2A, B):

1. They assemble the capsid in 2-, 3-, and 5-fold symmetry-related interactions in proportions of about 1:1:10 [9].
2. 3-fold axes and 5-fold axes are at vertices joining 3-fold protrusions and 5-fold cylinders, respectively, and 2-fold depressions bisect neighboring 3-folds [7].
3. The 2-, 3-, 5-fold axes from a triangle (2-fold axes, as dimple, surrounding a cylindrical channel at the 5-fold axes, as canyon, and protrusions surrounding the 3-fold axes) and It may be repeated sixty-fold with icosahedral symmetry operators to generate the entire capsid [9, 12].

The ribbon diagram of VP region consists of a eight stranded anti-parallel (bB-bI) β-barrel core motives, conserving alpha helix (αA), DE loop, HI loop, VR-I to VR-IX (Figure 2C). These VRs contribute to local topological differences between the AAV capsid surfaces. They assemble such that VR-I, III, VII, and IX contribute to the 2/5-fold wall; VR-VI and VR-VII form their base; VR-IV, V, and VIII form the top of the 3-fold protrusion and VR-II forms the top of the 5-fold channel. Furthermore, they are dictate that including receptor attachment, antigenic reactivity, transduction efficiency, and functional differences [12, 13, 21, 22].

1.2.2. The tissue tropism of AAV serotypes

The transduction of AAV starts by binding to a receptor and/or co-receptor complex. The course of AAV transduction requires five steps (Figure 3): (1) cellular attachment, (2) initial interaction with receptors or co-receptors on the cell surface molecules, cf. (Table 3), (3) internalization of virion by the host cell, virus intracellular trafficking through the endosomal compartment, escape of the virus from the endosome, and virion uncoating, (4) entry into the nucleus and release of the single stranded vector genomes with subsequent viral genome conversion from single stranded to a double stranded DNA, and (5) chromosomal integration before gene expression. Of note, hybridization of complementary input genomes can occur from a double stranded template, or (6) deletion integration and gene expression.

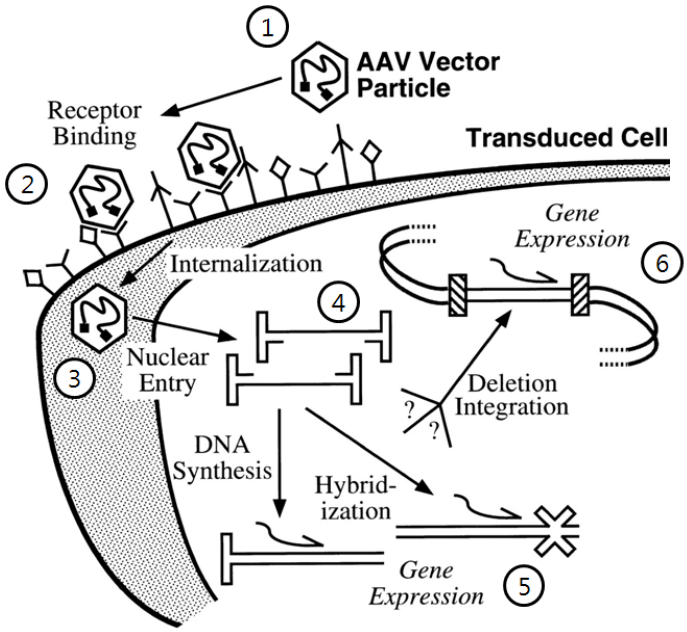

Figure 3 | Cell entry and trafficking of AAV. AAV enters the cell through receptor-mediated endocytosis. The transduction by AAV vectors showing six steps. The AAV vector particles are binding to cellular attachment (**1**) and an initial interaction with a variety of receptors or co-receptors on the cell surface molecules (**2**), as in (Table 3). Internalization of virion (**3**), nuclear entry and release of the single stranded vector genomes (**4**). Chromosomal integration before gene expression, and/or hybridization of complementary input genomes can occur from a double stranded template (**5**), or deletion integration and gene expression (**6**). (Modified from Russel DW et al., Blood 1999 [11]).

The AAV pseudotyping experiments demonstrate that the varying cell tropism and transduction efficiencies are dictated by specific capsid viral protein (VP) amino acids [7, 9, 12, 21, 22]. Each serotype of AAV capsids mediates binding to a cellular receptor before cell entry (Table 3). For example, AAV serotype 2 makes its initiates first contact with the target cell by attaching to the receptor heparan sulfate proteoglycan (HSPG), which might be enhanced by co-receptors (as αVβ5 integrin, fibroblast growth factor receptor-1; FGFR-1, and hepatocyte growth factor receptor; HGFR) [10, 11, 21]. Each AAV serotype has specific binding receptors. However, the target specificity may be altered by AAV surface modification [15, 21], e.g., engineering of AAV2 capsid virion protein. Thus, deletion of heparan binding site (R484 and R585) diminishes hepatic expression and augments cardiac expression (Figure 4).

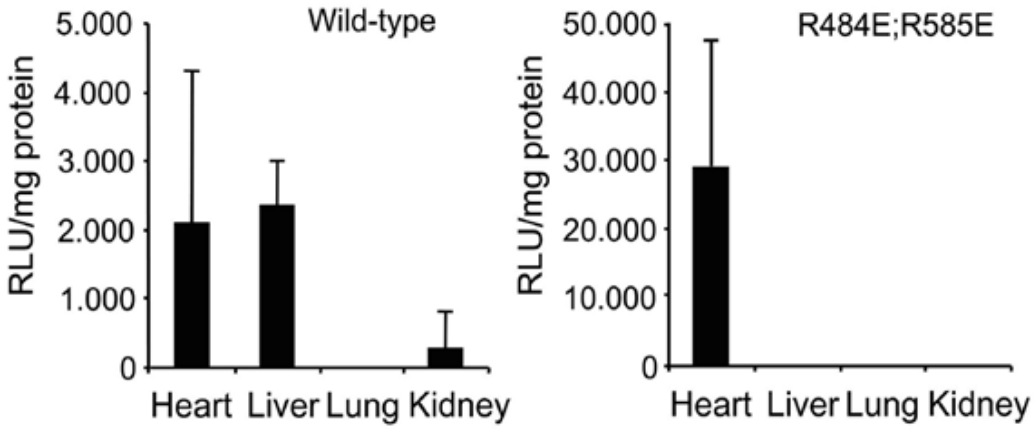

Figure 4 | In vivo distribution of wild-type rAAV and rAAV mutant (R484E/R585E) in mouse tissues. Luciferase activities in different organs after intravenous injection of 1011 wild-type capsids or rAAV mutated in R484E and R585E, 3 weeks post infecion. Luciferase activities are depicted in relative light units (RLU) per milligram of protein. Error bars indicate standard deviations. (Adapted from A. Kern et al., J Virol 2003 [21]).

1.3. Nanoparticles

Surface modification of AAV vectors comprises several possibilities, including peptide expression at privileged sites of the vector capsid [49] or shuffling of the capsid gene sequences of various strains [85]. A novel and promising approach consists of coating of vector capsids with dendrimeric nanoparticles.

Dendrimers are repetitively branched macro molecules (three-dimensional polymers) with spherical, branched structures. Commonly used dendrimers are polyamines, polyamides, or polyesters. These molecules possess the central core, branches (which give rise to dendrimer generations) and surface peripheries (Figure 5).

A

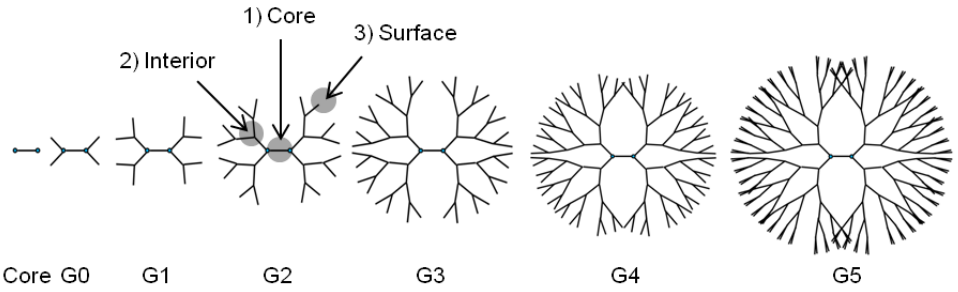

B

Generation	MW	Molecular formula	Hydro dynamic diameter(nm)	No. of NH_2 surface groups
0	609	$C_{24}H_{52}N_{10}O_4S_2$	1.5	4
1	1,522	$C_{64}H_{132}N_{26}O_{12}S_2$	2.2	8
2	3,348	$C_{144}H_{292}N_{58}O_{28}S_2$	2.9	16
3	7,001	$C_{304}H_{612}N_{122}O_{60}S_2$	3.6	32
4	14,307	$C_{824}H_{1252}N_{250}O_{124}S_2$	4.5	64
5	28,918	$C_{1264}H_{2582}N_{508}O_{252}S_2$	5.4	128

Figure 5 | Schematic representation of polyamidoamine (PAMAM) dendrimers. A, In contrast to traditional polymers, dendrimers are unique core-shell structures possessing three basic architectural components: (**1**) a core, (**2**) an interior of shells (an increase in generation number (G0 to G5) consisting of repeating branchpoints, and (**3**) surface functional groups. **B**, The characterization of generation of PAMAM. MW; Molecular Weight (Modified from Donald A et al., Materialstoday 2005 [34]).

The first report of repetitive growth with branching was provided by Buhleier in 1978 [31]. The polyamineamide (PAMAM) dendrimers are the most common group of dendrimers suitable for applications of nano-medicine. These macromolecules constitute a class of hyperbranched polymers developed by Tomalia in 1979 [32]. PAMAM nanomolecules are readily used in non-viral gene delivery system for enhancing transduction efficiency (Figure 6) [33, 34].

PAMAMs are highly variable in their molecule structure. An increase in generation number (G0 to G10) is provided by interiors. Five core types (cystamine, diaminobutane, diaminohexane, diamonododecane, and ethylenediamine core), and nine functional surface groups (amine, amidoethylethanolamine, amidoethanol, sodium carboxylate, succinamic acid, hexylamide, carbomethoxypyrrolidinone, tris-hydroxymethyl-amidomethane, and poly-ethyleneglycol) add to their variability (Figure 5A).

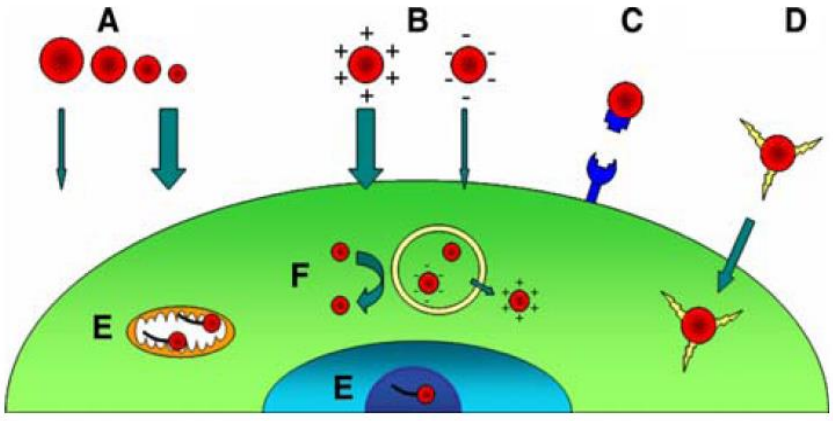

Figure 6 | Factors affecting nanoparticle cellular uptake. A, Given similar surface characteristics, smaller nanoparticles are more efficiently internalized than larger nanoparticles. **B**, Cationic surface nanoparticles are preferentially taken up by cells. **C**, Cell specific targeting by a surface modified-nanoparticles (target cell membrane specific ligand conjugated ligands). **D**, Rapid uptake by conjugating protein transduction domains to the surface of the nanoparticle. **E**, Application of oligodeoxynucleotide (ODN) was found to aid in specific internal cellular localization. **F**, Positive surface charged nanoparticles can escape from endosomes. (Adapted from K. Ted Thurn et al., Nanoscale Res Lett 2007 [30]).

Furthermore, these PAMAMs display various external charge patterns: there are positively charged amino-termini (cationic), neutral hydroxyl-termini (neutral), or negatively charged carboxyl-termini (anionic) provided by the surface molecules [37]. The PAMAMs of generation 2 (PAMAM G2: 3,348 MW) and PAMAMs of generation 5 (PAMAM G5: 28,918 MW) as used in this study are positively charged and have 16 or 128 of NH_2 surface groups, respectively (Figure 5B).

The high density of surface functional groups on PAMAM dendrimers, which may be differently charged, enables the polymers to electrostatically interact with other charged surfaces like the plasmalemm of a cell (Figure 7). Commonly, most particles are transported and taken up by four major routes:

1) Paracellular aqueous pathway, e.g. water-soluble agents, 2) passive diffusion, 3) carrier mediated, and 4) endocytosis via adsorption, receptor mediation or fluid phase. Most likely, PAMAM dendrimers are transported by routes 1) and 4) [35-38].

The microvascular endothelium contains highly polar glycosaminoglycans (GAGs) on the surface [39]. The GAGs are classified by four groups, as heparin/heparan sulfate (HSGAGs), chondroitin/dermatan sulfate (CSGAGs), keratan sulfate and hyaluronic acid [40]. The heparin contain the highest negative charge density within GAGs. Therefore, the observed extravasation of cationic PAMAM dendrimers molecules may also be a function of the electrostatic interactions between the polymers and the negatively charged endothelium as in Figure 7 [38].

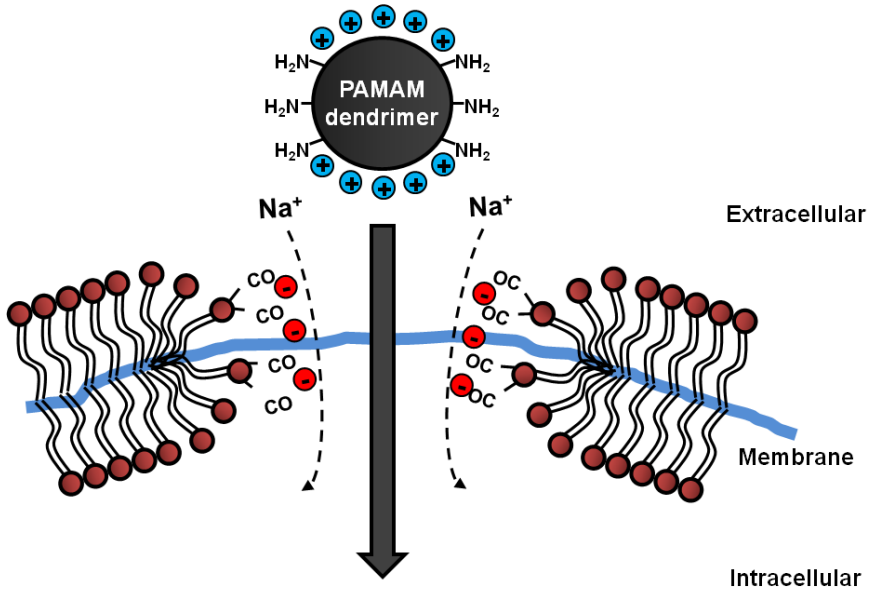

Figure 7 | Schematic representation of cellular uptake of PAMAM dendrimer. The electrostatic interactions between the PAMAM dendrimer (cationic dendrimers; positive charged -NH_2 surface) and the negatively charged endothelium. (Modified from Adamson RH et al., J Physiol. 1992 [36, 38]).

1.4. Phage display

In addition to utilization of nanoparticles to alter the negatively charged surface of the virus capsid, selective targeting can be achieved by peptides binding with high affinity to a specific cell-type. We attempted to select endothelial-targeted peptides via phage display and biopanning in endothelial cells.

The phage display method is an efficient tool for affinity selection of target-specific peptides [45]. This technology was discovered by George P. Smith in 1985 [41], when he demonstrated that foreign DNA fragments inserted into filamentous phages (= bacteriophages = a virus that infects and replicates only within a bacterium) are displayed as fusion proteins with a random sequence.

By selecting and sequencing the motives, protein-peptide, protein-protein, and protein-DNA interactions can be distinguished. The most common bacteriophages used in phage display are filamentous bacteriophage (M13 [25] and fd) and lytic phage (T4 and T7 [26]), shown as in Figure 8.

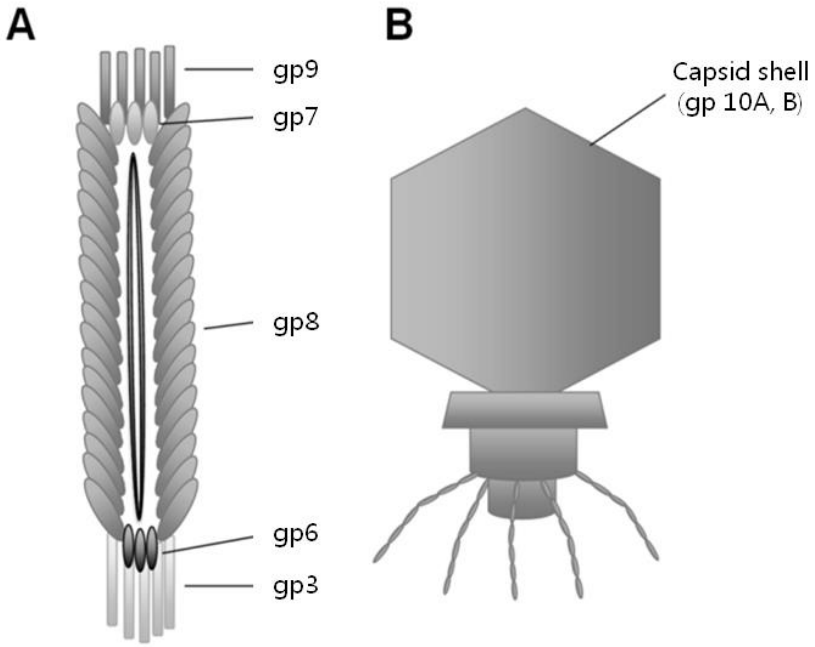

Figure 8 | Structure of bacteriopahge. A filamentous M13 phage (**A**) and a lytic T7 phage (**B**). (Adapted from Keisuke Fukunaga et al., Journal of Nucleic Acids 2012 [45]).

The phage display technology allows for identification of specific interactions between randomized phage library peptides on the phage and target proteins, peptides, or other molecules [24]. The M13 CX7C phage display library system (C; cystein, X7; 7-mer random aa) is based on a vector of M13 phage encoding N-terminal library random peptide fused to a gp3 coat protein. The gp3 plays a critical role for phage infection, since randomized 7-mer aa peptides are fused in all five copies of the gp3. Infectivity of the M13 phage can be significantly affected by a random sequence of the displaying peptides. Amplification efficiency of the each selected-M13 phage clone is determined by a combination of the infection and secretion rates. A M13 phage library displaying CX7C random peptides was screened to enrich phage that selectively bind to target, as cells or other molecules shown as in Figure 9.

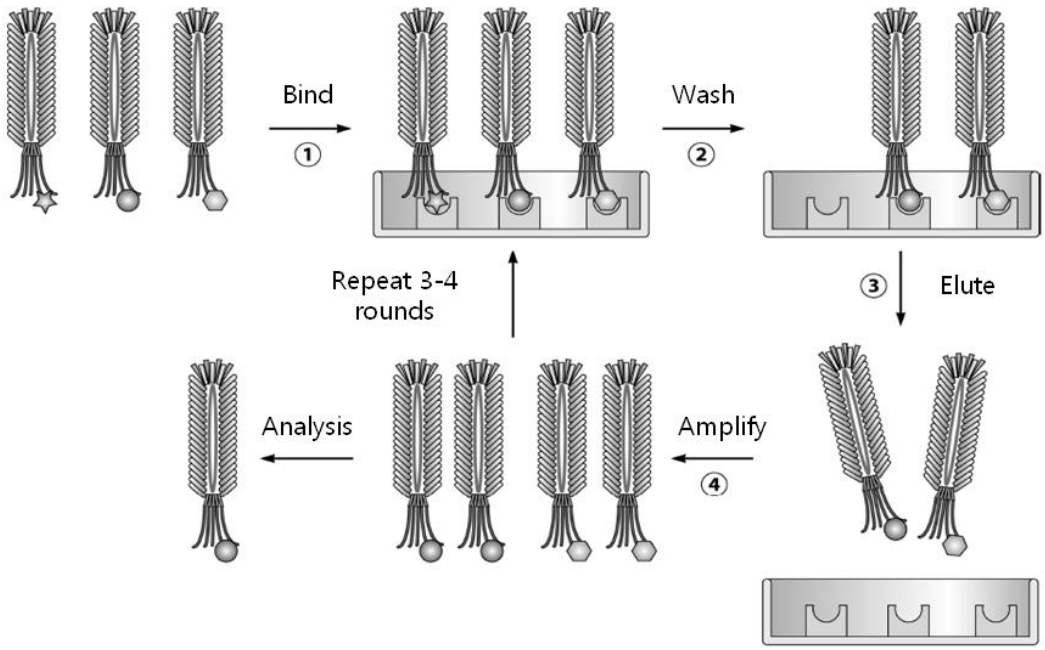

Figure 9 | Procedural of biopanning by phage-display library. The sequence of events that are followed in phage display screening to identify polypeptides that bind with high affinity to desired target protein or DNA sequence. A typical procedure of the biopanning. **1**) binding, **2**) washing, **3**) eluting of the selected phage, **4**) amplification of the phage library subset, which bound to the bait, **5**) repeating 3-4 times (rounds; 1 to 4), and analysis of bound phages. (Adapted from Keisuke Fukunaga et al., Journal of Nucleic Acids 2012 [45]).

1.5. Aim of study

In this study, we aim at retargeting an AAV2/9 virus strain towards endothelial transduction. Since all AAV strains have a low transduction efficacy in endothelium (Figure 10-a), we utilized surface modifications of the virus capsid to achieve endothelial retargeting. We used a three-step strategy to achieve this aim.

1. First, we tested the combination of AAV2/9 and two cationic PAMAM dendrimer (G2 and G5) for endothelial transduction in vivo (figure 10-b).
2. Secondly, we identified endothelial targeting peptide motifs of 7 amino-acid length, by M13 phage-display technology.
3. Thirdly, we linked the endothelial targeting peptide to PAMAMs for targeting endothelial cells in vivo (figure 10-c).

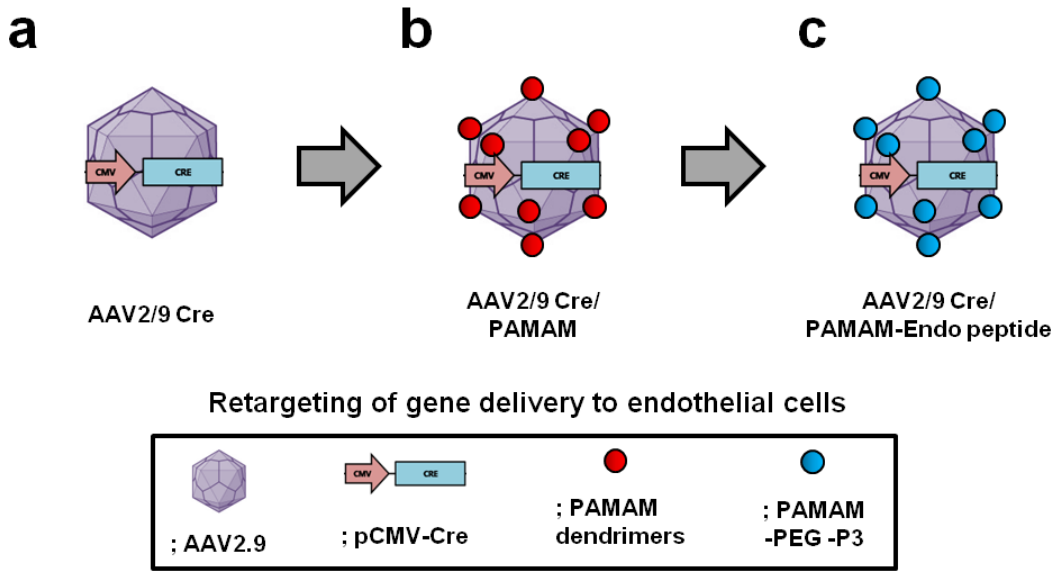

Figure 10 | Design of gene delivery system by surface modified AAVs by different type of PAMAM dendrimers. a, AAV2/9CMV-Cre virus have a tropism in heart. **b**, Cationic PAMAM dendrimer (G2 or G5) coated AAV2/9CMV-Cre virus. **c**, AAV2/9CMV-Cre/PAMAM G2-PEG linker-Endo peptide; Endothelial cell target motives (P1 or P3) are displayed on PAMAM surface (PEG linker pre-conjugated G2 PAMAM) and thereafter coated to AAV2/9CMV-Cre virus.

2. MATERIALS AND METHODS

2.1. Materials

2.1.1. Chemicals, solutions and enzymes

Product	Company
Acetonitril	Roth GmbH, Lübeck, Germany
Agarose	Life tech. GmbH, Darmstadt , Germany
Ampicillin	Sigma-Aldrich GmbH, Munich, Germany
APS	Merck, Darmstadt, Germany
Bacto-agar	BD GmbH, Heidelberg, Germany
Bacto-tryptone	BD GmbH, Heidelberg, Germany
Bovine Serum Albumine (BSA)	Sigma-Aldrich GmbH, Munich, Germany
Calcium Chloride	Sigma-Aldrich GmbH, Munich, Germany
Claycomb medium	Sigma-Aldrich GmbH, Munich, Germany
Dimethyl sulfoxide (DMSO)	Sigma-Aldrich GmbH, Munich, Germany
DMEM	Invitrogen GmbH, Darmstadt, Germany
DNA Ladder 50 bp	NEB GmbH, Frankfurt, Germany
DNA Ladder 1k bp	NEB GmbH, Frankfurt, Germany
DTT	Sigma-Aldrich GmbH, Munich, Germany
EDTA	Invitrogen GmbH, Darmstadt, Germany
Endothelial medium 200	Invitrogen GmbH, Darmstadt, Germany
Ethanol	Roth GmbH, Lübeck, Germany
Ethidium Bromide	Roth GmbH, Lübeck, Germany
FCS	Invitrogen GmbH, Darmstadt, Germany
Glycerol	Roth GmbH, Lübeck, Germany

Glycine	Roth GmbH, Lübeck, Germany
HEPES	Sigma-Aldrich GmbH, Munich, Germany
IPTG	Sigma-Aldrich GmbH, Munich, Germany
Isopropanol	Roth GmbH, Lübeck, Germany
KAPA HiFi DNA polymerase	PEQLAB Biotech., Erlangen, Germany
Macro-prep high S	BioRad GmbH, Munich, Germany
Magnesium Chloride	Sigma-Aldrich GmbH, Munich, Germany
NHS-PEG-OPSS	Rapp Polymere GmbH, Tübingen, Germany
NP-40	Sigma-Aldrich GmbH, Munich, Germany
Nuclease Free Water (NFW)	Promega GmbH, Mannheim, Germany
O.C.T. compound	Sakura Finetek Germany GmbH, Germany
Opti-MEM	Invitrogen GmbH, Darmstadt, Germany
PAMAM dendrimers (G2 or G5)	Dendritic Nanotech. Inc, Michigan, USA
PEG 8000	Sigma-Aldrich GmbH, Munich, Germany
Penicillin/Streptomycin	Invitrogen GmbH, Darmstadt, Germany
Peptide (no.1 or no.3)	Biosyntan GmbH, Berlin, Germany
RPMI-1640 medium	Sigma-Aldrich GmbH, Munich, Germany
Sephadex G-25 superfine	Sigma-Aldrich GmbH, Munich, Germany
Skim-milk	Roth GmbH, Lübeck, Germany
Sodium chloride	Roth GmbH, Lübeck, Germany
Sodium Dodecyl Sulfate (SDS)	Sigma-Aldrich GmbH, Munich, Germany
Sodium Phosphate	Sigma-Aldrich GmbH, Munich, Germany
Spectra/Por membranes	Spectrum Lab. Inc, Breda, Netherlands
Sucrose	Sigma-Aldrich GmbH, Munich, Germany
T4 DNA Ligase	Invitrogen GmbH, Darmstadt, Germany
TEMED	Sigma-Aldrich GmbH, Munich, Germany

Tetracycline	Sigma-Aldrich GmbH, Munich, Germany
TFA	Roth GmbH, Lübeck, Germany
TNBS	Sigma-Aldrich GmbH, Munich, Germany
Tris	Sigma-Aldrich GmbH, Munich, Germany
Triton X 100	Roth GmbH, Lübeck, Germany
TRIzol	Ambion GmbH, Darmstadt, Germany
Trypsin-EDTA	Invitrogen GmbH, Darmstadt, Germany
Tween 20	Roth GmbH, Lübeck, Germany
Vectashield H-1200	Vector Lab. Inc., Burlingame, CA, USA
X-gal	Roth GmbH, Lübeck, Germany
Yeast extract	BD GmbH, Heidelberg, Germany

The water was used as purified by Milli-Q, Millipore Centrifugal filter units Amicon Ultra 0.5ml, 3K and 50K from Millipore GmbH (Darmstadt, Germany). All other chemicals were bought from Sigma-Aldrich (Munich, Germany), Invitrogen GmbH (Darmstadt, Germany) or Roth GmbH (Karlsruhe, Germany).

2.1.2. Standard kits

Product	Company
DNeasy Kit	Roche Diagnostics GmbH, Penzberg, Germany
EndoFree Plasmid Kits	Macherey-Nagel GmbH, Düren, Germany
Gel Extraction Kit	Macherey-Nagel GmbH, Düren, Germany
KAPA Mouse genotyping kit	PEQLAB Biotech., Erlangen, Germany
PCR Purification Kit	Macherey-Nagel GmbH, Düren, Germany
Ph.D. CX7Cphage display library	NEB GmbH, Frankfurt, Germany
Reverse transcription system kit	Promega GmbH, Mannheim, Germany
SYBR Green kit	BioRad GmbH, Munich, Germany
TMB Substrate Kit	Thermo GmbH., Bonn, Germany

2.1.3. Plasmids

1. pAAV-CMV-eGFP: EGFP cDNA controlled by the human cytomegalovirus (CMV) promoter with Ampicillin resistance.
2. pAAV-CMV-Cre: Cre cDNA controlled by the human cytomegalovirus (CMV) promoter with Ampicillin resistance.
3. pAdΔF6: PolyFlo®Purified Plasmid pAdΔF6 (P.O. Number 03032012 Lot# C30JA) from Puresyn Inc. (Malvern, PA) [16, 17].
4. pVP2: AAV based helper plasmid containing the AAV2 Rep and Cap open reading frame (ORF) with Ampicillin resistance [20].
5. pVP2/6: AAV based helper plasmid containing the AAV2/6 Rep and Cap open reading frame (ORF) with Ampicillin resistance.
6. pVP2/9: AAV based helper plasmid containing the AAV2/9 Rep and Cap open reading frame (ORF) with Ampicillin resistance [16, 17].
7. pVP2/9Endo: AAV based helper plasmid containing the AAV2/9Endo, Endothelial cell target peptide (SLRSPPS) displayed on virion, Rep and Cap open reading frame (ORF) with Ampicillin resistance [24].
8. pAAV-CMV-S1FG: S1FG cDNA controlled by the human cytomegalovirus (CMV) promoter with Ampicillin resistance [55].

2.1.4. Primers

M13 phage PCR primer (forward; 5’- TTA TTC GCA ATT CCT TTA GTG G -3’, reverse; 5’- CCC TCA TAG TTA GCG TAA CG -3’All primers have been purchased from MVG (Ebersberg, Germany).

2.1.5. Antibodies

Name	Immunogen	Manufacturer
CD31 PerCP	human	eBioscience
Troponin I Alexa647	human	BD Biosciences
CD45 eFluor450	mouse	eBioscience
CD144 eFluor660	mouse	eBioscience
IgG2a K PerCP	rat	eBioscience
M13-pIII	M13 coat protein III	NEB GmbH
M13-pVIII	M13 coat protein VIII	Abcam plc

2.1.6. Bacteria strain

ER2738: The host cell of M13phage.

DH5α: The host cell of viral vectors for transformation.

2.1.7. Cell lines

bEnd3: Mouse brain endothelial cell line [16].

HEK293: Human embryonic kidney cells [17].

HL-1: Mouse cardiomyocyte.

HMEC: Human microvascular cells.

HUVEC: Human umbilical vein endothelial cells.

2.2. Methods

2.2.1. Viral vectors

All vectors were designed to express transgenes or reportergenes (Cre reporter genes) under the control of two promoters. The pAAV-CMV-eGFP and pAAV-CMV-Cre vectors carry a cytomegalovirus (CMV) enhancer promoter. The constructed plasmids (pAAV-CMV-eGFP and pAAV-CMV-Cre), contain 5'- Inverted terminal repeats (ITR), a CMV promoter, a transgene (eGFP or Cre), a posttranscriptional regulatory element (WPRE), a bovine growth hormone polyadenylation signal (bGHpA), 3'- ITR, a region for resistance to the antibiotic Ampicillin (Amp) Figure 11-A. The viral vector plasmids were provided by James Wilson, University of Pennsylvania, Philadelphia, USA and Oliver J. Müller, University of Heidelberg, Germany.

2.2.2. Recombinant AAV production

All production of recombinant AAV was performed using a triple plasmid transfection method in principle as described [20]. Briefly, the triple plasmids were an adenovirus (Ad) helper plasmid (pAdΔF6), a chimeric trans plasmid containing the AAV2 rep gene fused to the capsid gene of the AAV serotype of interest (crosspackaging of pseudotyped vectors), and a ITRs-positive rAAV vector plasmid. AAVs were produced with triple the pAdΔF6 as Ad helper plasmid. rAAV2-CMV-eGFP virus was produced by cotransfection of U293 cells with pAAV-CMV-eGFP and pDG (R484E/R585E) containing mutations of two amino acids involved in heparin binding of AAV2 (R484E/R585E) [21]. rAAV2/6-CMV-eGFP virus used pAAV-CMV-eGFP and pDP6. The rAAV2/9-CMV-eGFP and rAAV2/9-CMV-Cre virus used each a pAAV-CMV-eGFP or pAAV-CMV-Cre with pDP9. Furthermore, the cross packaging of rAAV2/9Endo-Cre virus pseudotyped vector was accomplished with pAAV-CMV-Cre and Endo endothelial cell targeting peptide (SLRSPPS) inserted on the surface of A589 of AAV9 capsid (p5E18-VD-2/9- SLRSPPS) [24]. After 2-3 days, cells were harvested and viruses were

purified using standard cesium sedimentation as previously described [22]. The titer of rAAVs viral particle was determined using real-time PCR against the untranslated region of the DNA encoded transcript in each AAV vectors. The bGHpA primer sequences were forward 5′-TCT AGT TGC CAG CCA TCT GTT GT-3′, and reverse 5′-TGG GAG TGG CAC CTT CA-3′, Cre primer sequences were forward 5'- AGA GGA AAG TCT CCA ACC TG -3', reverse 5′- ACA CAG ACA GGA GCA TCT TC -3', and eGFP primer sequences were forward 5'- GCC ACA ACG TCT ATA TCA TGG -3', reverse 5′- GGT GTT CTG CTG GTA GTG GT -3'. Real-time PCR was performed using SYBR Green for 40 cycles (30 seconds at 95°C, 30 seconds at 58°C, 30 seconds at 72°C) by an iQ-Cycler (Bio-Rad, Germany). Cross packaging constructs of pseudotyped vectors were provided by Oliver J. Müller, University of Heidelberg, Heidelberg, Germany [25].

2.2.3. Coating of AAVs with PAMAM dendrimer

The complexes of rAAVs and nanoparticles (PAMAM G2, PAMAM G5), at times carrying endothelial targeting peptides P1 and P3 (PAMAM G2 P1, and PAMAM G2-P3) were formed by diluting indicated amounts of AAVs in Opti-MEM (Invitrogen, Germany). Viral particles were added to the PAMAM diluted solution, immediately mixed by gentle aspiration with the pipet tip and allowed to incubate for at RT/30 min before further use, as in Figure 11-B.

2.2.4. Panning

In this study we use a phage peptide library Ph.D. CX7C M13KE kit. 2.0E+11 plaque forming units (pfu) of the phage library was incubated with 1 ml of 1% BSA/DMEM in 1.0E+07 cells/tube of the HMEC or HUVEC cells and incubated for 120 min at 4°C with gently rolling. After washing 5 times with TBST (TBS/0.1% Tween 20) and spinning down at RT/1200 rpm/5 min, bound phages were eluted with a 1 ml of 0.2M Glycine-HCl (pH 2.2)/1 mg/ml BSA by centrifugation at 4°C/13000 rpm/5 min. The

supernatant of elute was neutralized with a 200 µl of Tris-HCl (pH 8.0).

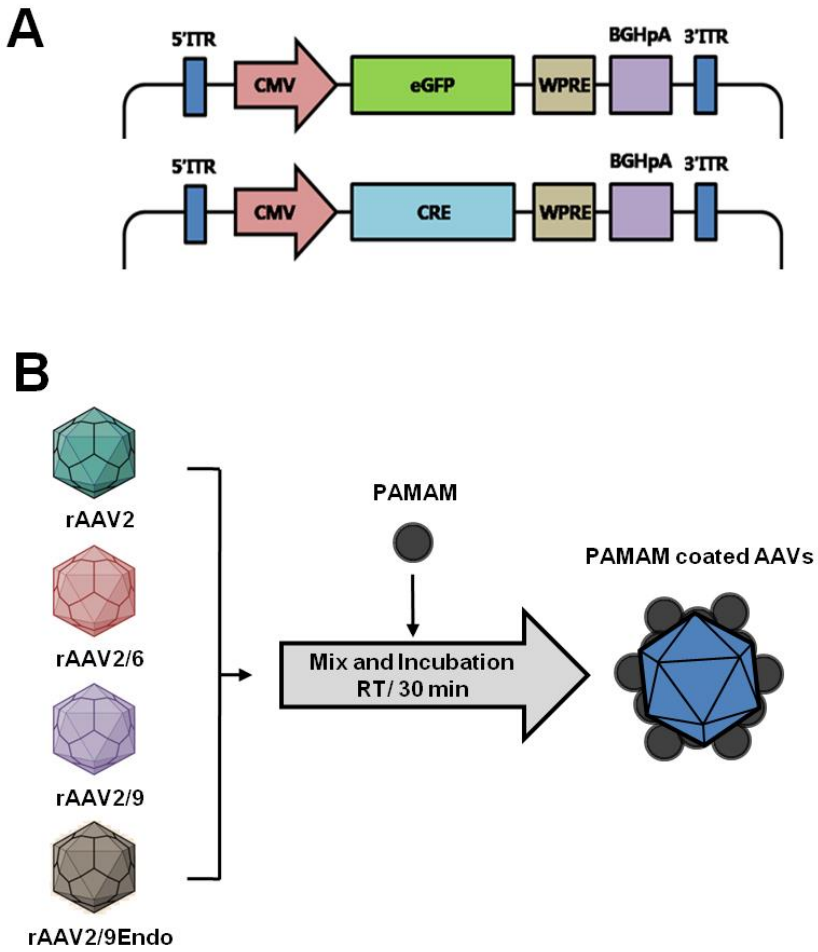

Figure 11 | Construction of gene delivery viral vector and modifications by PAMAM with or without peptide linkage. A, pAAV-CMV-eGFP vector (upper part) and pAAV-CMV-Cre vector (lower part). **B**, PAMAM dendrimers (G2, G2P1, G2P3, or G5) coated to AAV (rAAV2, rAAV2/6, rAAV2/9 or rAAV2/9Endo) at RT/30 min.

2.2.5. Amplification of selected phage clones

1 ml of selected phage eluate was incubated with 20 ml of an E. coli ER2738 bacteria suspension (A600 nm 0.5) by vigorous shaking at 37°C/4.5 hr in 250 ml volume. The amplified phage was purified according to the method in principle as described [27, 28]. Briefly, recovered phages were centrifuged at 4°C/13000 rpm/20 min. Then, the upper 80% of supernatant were transferred to a fresh tube with 1/6 volume of 20% PEG/2.5M NaCl and incubated overnight at 4°C. Thereafter, the phage was pelleted by spinning

down at 4°C/13000 rpm/15 min and the supernatant was discarded. The phage pellet was completely resuspend with 1 ml of TBS by gently rocking overnight at 4°C. Residual pellets were spun down at 4°C/13000 rpm/20 min and the supernatant was purified by syringe filter with 0.45 µm (Life Sciences, Germany). Each round of eluted solutions was used for determination of phage titration by plaque assay [26]. The amplified phage was used as input for the next round and the phage titration used as output data.

2.2.6. Direct phage PCR and sequencing

10 µl of phage elutes (2 and 3 rounds) were incubated overnight with 300 µl of an E. coli ER2738 bacteria suspension (A600 nm OD 0.5) and 3 ml of prewarmed TOP-agar medium (10 g Bacto-Tryptone, 5 g yeast extract, 5 g NaCl, and 7 g Bacto-agar per liter) onto a LB/IPTG/X-gal plates (1l LB medium, 15 g/l agar, 0.05 g of IPTG, and 0.04 g of X-gal per liter). Each of 488 single blue (positive) plaques were random selected and amplified with 2 ml of an E. coli ER2738 bacteria suspension (A600 nm OD 0.5) by vigorous shaking at 37°C/4.5 hr. Each of purified plaques (488 single positive plagues) were reselected by direct PCR. The direct PCR enrichment was performed using DNA polymerase for 35 cycles by an iQ-Cycler. Then, 169 phage (positive of direct PCR products) were selected by gel electrophoresis. 58 phage DNA sequences were identified by sequencing analysis, and finally 10 phage DNA sequences were selected. The M13 phage primer sequences were forward 5'- TTA TTC GCA ATT CCT TTA GTG G -3', reverse 5'- CCC TCA TAG TTA GCG TAA CG -3'. The direct PCR enrichment was performed using KAPA HiFi DNA polymerase (peqlab, Germany) for 35 cycles with the following cycling parameters: 3 minutes at 98°C; 35 cycles of 15 seconds at 98°C, 30 seconds at 53°C, 30 seconds at 72°C; 30 seconds at 72°C by an iQ-Cycler (Bio-Rad, Germany). Thereafter PCR products were separated by DNA gel electrophoresis compact XS/S (Biometra, Germany). The sequences of the PCR products (selected phage DNA) were identified by MWG (Eurofins MWG Operon,

Germany).

2.2.7. Phage ELISA

10,000 cells/well of HUVEC, and HMEC cells were incubated in a micro 96-well plate (Nunc, Germany) overnight at 37°C in 5% CO_2. The cell plates were washed with 1x phosphate buffered saline (PBS) and fixed with 4% PFA at RT/15 min. Thereafter they were washed and blocked at RT for 30 min with 100 µl/well of 2% skim-milk in 1x TBST (as blocking buffer). The blocking buffer was removed and individual 10 amplified phage clones were incubated at RT for 60 min with in endothelial cell (HUVEC or HMEC). 50 µl/well of 1:200 HRP-conjugated M13 PVIII antibody were added in 2% skim-milk in 1x TBST (as primary antibody solution) and incubate overnight at 4°C. Plates were washed 5 times with 100 µl/well of 1x TBST. 100µL/well of TMB Substrate (Thermo Fisher Scientific, Germany) were added and incubated at RT for 15 min. After adding 100µL/well of TMB Stop Solution, the absorbance at 450nm (A450) was analyzed.

2.2.8. Nanoparticle synthesis

The PAMAM G2 dendrimer (Figure 12-A) and PAMAM G5 dendrimer (Figure 12-B) were synthesized by Dendritic Nanotech. Inc, Michigan, USA. The conjugation of a PAMAM G2 dendrimer, a NHS-PEG-OPSS linker and endothelial cell specific transduction peptides (P1 or P3) was performed according to [29]. Briefly, 1 µmol of G2 (MW = 3,284 Da) was incubated with 4 µmol of NHS-PEG-OPSS (2 kDa) dissolved in DMSO at 37°C/3 hr. The reaction mixtures were loaded on a cation-exchange column (Macro-Prep High S; BioRad) and fractioned with a salt gradient from 0.6 to 3 M NaCl in 20 mM HEPES (pH 7.4) solution. Thereafter, the product was filterated by centrifuge filter devices (Amicon Ultra 3K) and the G2 content of the conjugate was determined by TNBS assay. For G2P1 (Figure 12-C) and G2P3 (Figure 12-D) synthesis, 1.98 µmol of peptides in 75 µl of 30% acetonitrile, 70% H2O, 0.1% TFA (trifluoroacetic acid)

solution and 0.79 μmol of G2 with PEG-OPSS linker in 3.6 ml of HBS solution were mixed and incubated at room temperature. The mixtures were loaded on a cation-exchange column with varying salt gradients from 0.6 to 3 M NaCl in 20 mM HEPES including 10% acetonitrile (pH 7.4) solution. Thereafter, the product was filtered by a centrifuge filter devices (Amicon Ultra 50K and 3K) and the G2 content of the conjugate was determined by TNBS assay. The amount of P1 or P3 was calculated via the extinction coefficient at 280 nm.

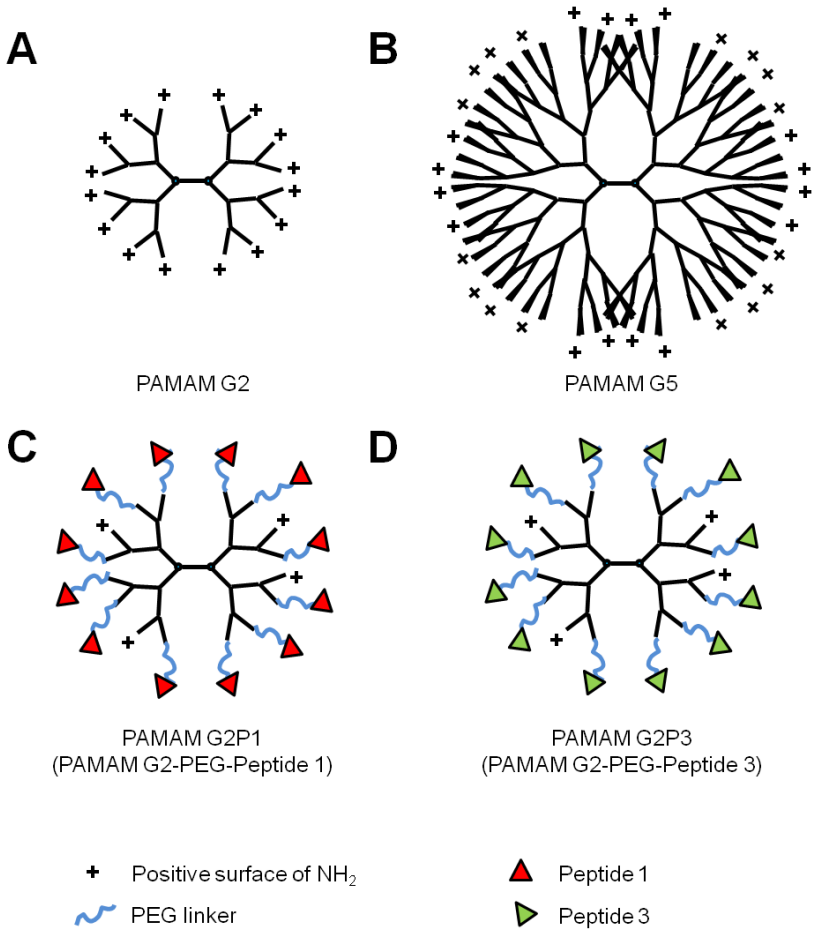

Figure 12 | Cationic PAMAM dendrimers & surface modified PAMAM dendrimers. A, PAMAM G2 is a cationic (16 of NH_2) generation 2 PAMAM dendrimer. **B**, PAMAM G5 is a cationic (128 of NH_2) generation 5 PAMAM dendrimer, **C**, PAMAM G2P1 is surface modified, adding P1 (CSLRSPPS) with PEG linker conjugated on the surface, PAMAM G2 dendrimer. **D**, PAMAM G2P3 is surface modified, adding P3 (CNNSGMRN) with PEG linker conjugated on the surface, PAMAM G2 dendrimer.

2.2.9. Cell culture

For in vitro studies, human microvascular endothelial cells (HMEC), mouse brain endothelial cell line (bEnd3), and human embryonic kidney 293 cells (HEK293) were cultured in Dulbecco's modified Eagle's medium (DMEM). Mouse cardiomyocyte (HL-1) were cultured in Claycomb medium, 0.1 mM Norepinephrine. Human umbilical vein endothelial cells (HUVEC) were cultured in endothelial medium 200. All cell culture medias were supplemented with 10% fetal calf serum (FCS), 1 % penicillin-streptomycin solution (100 units/ml penicillin, 100 µg/mL streptomycin), and 1% L-alanine-L-glutamine (200 mM) at 37°C in 5% CO2.

2.2.10. Animals

dTomato mice care and all experimental procedures were performed in to the Guide for the Care and Use of Laboratory Animals published by the NIH (NIH publication no. 85-23, revised 1996), and were approved by the Bavarian Animal Care and Use Committee (AZ 55.2-1-54-2531-130-8 and 35-12). All animal experiments were conducted at the Walter Brendel Centre of Experimental Medicine.

2.2.11. ROSA mT/mG mice (tdTomato mice)

The Cre/loxP system has been widely used for site-specific mutagenesis in mice [3, 46]. The Cre recombination activity at specific sites, called lox sites, is instrumental for temporal and spatial resolution of the recombination event. The ROSA mT/mG mouse strain (B6.129(Cg)–Gt(ROSA)26Sortm4 (ACTB-tdTomato,-EGFP)Luo/J, (The Jackson Laboratory, www.jax.org) is a double color fluorescent Cre reporter mouse strain that expresses cell membrane-targeted red fluorescence, tandem dimer Tomato (mT) in its native state prior to Cre recombinase exposure. In contrast, cell membrane-targeted green fluorescent protein (mG) is expressed after Cre-mediated activation of mG, and excision of mT as shown in Figure 13 A-C.

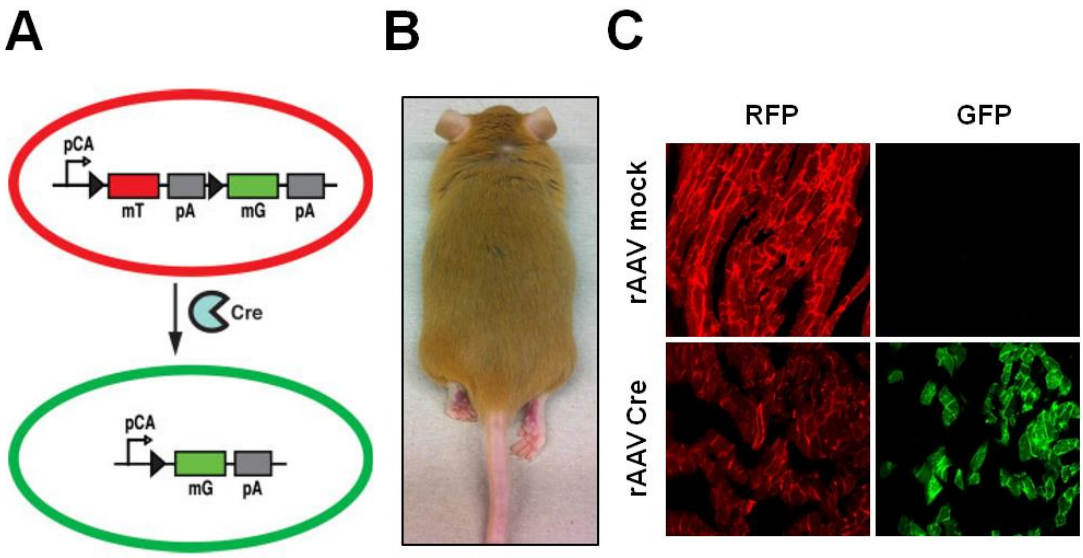

Figure 13 | Tomato reporter gene mice, mT/mG mutation mice; Gt(ROSA)26Sor. A, Tomato mice are characterized by a mT/mG combined in the ROSA locus as displayed in this map. Mice homozygous for this mT/mG mutation are viable and fertile. These mice possess *loxP* sites on either side of a membrane-targeted tdTomato (mT) cassette and express strong red fluorescence in all tissues. Tail or whole body epi-fluorescence is sufficient to identify mT/mG homozygotes. When bred to Cre recombinase expressing mice, the resulting offspring have the mT cassette deleted in the *cre* expressing tissues, allowing expression of the membrane-targeted EGFP (mG) cassette located just downstream. **B**, The phenotype of tomato mice. **C**, An example of tomato mice after Cre gene transduction. The Cre gene mediated mT expression change to mG compared to the mock transfected heart. (Figure A is adaptied from Muzumdar et al., Genesis 2007 [3]).

2.2.12. Genotyping of dTomato mice

Offspring from matings of a heterozygote Gt (ROSA) 26Sor mouse and a heterozygote Gt (ROSA) 26Sor mouse were biopsied at weaning age, and total DNA was prepared from the mice tail clip (approx 2 mm) by manual DNA isolation, incubated with 100 µl of solution A (25 mM NaOH/0.2 mM EDTA) during 60 min 95°C and vortexed briefly with 100 µl of solution B (40 mM Tris-HCl). Thereafter, the mixture was centrifuged at 2000 rpm for 10 min, and 100 µl of supernatant were removed and used as 1 µl per 25 µl PCR reaction. The total DNA was analyzed by PCR for the presence of the respective transgenes. Primers (wild type for 5′- CTC TGC TGC CTC CTG GCT TCT -3′, wild

type rev 5′- CGA GGC GGA TCA CAA GCA ATA -3′, and mutant type rev 5′- TCA ATG GGC GGG GGT CGT T -3′) were used for the Gt (ROSA) 26Sor allele PCR. The direct PCR enrichment was performed using KAPA HiFi DNA polymerase (peqlab, Germany) for 35 cycles with the following cycling parameters: 3 minutes at 98°C; 35 cycles of 15 seconds at 98°C, 30 seconds at 53°C, 30 seconds at 72°C; 30 seconds at 72°C by an iQ-Cycler. Thereafter, PCR products were separated by DNA gel electrophoresis compact XS/S. The resulting PCR products were mutant type (250 bp), wild type (330 bp), and heterozygote type (250 bp and 330 bp) in size.

2.2.13. Transduction efficiency test in vitro

Surface modified PAMAM dendrimers coated rAAV transductions were performed using HEK293, HL1, bEnd3 and HMEC cell lines with 24hr, 48hr, and 72hr incubation time. The PAMAM dendrimer (G2, G2P1, G2P3 or G5) coating doses ranged from 50 to 800 ng per well, rAAV vector (AAV2-eGFP, AAV2/6-eGFP, AAV2/9-eGFP, AAV2/9-Cre, AAV2/9Endo-Cre, as in Figure 14-A & -B) dose were 1.0E+05 virus particles per cell or 1.0E+06 virus particles per cell.

2.2.14. Transduction efficiency test in vivo

The dtTomato reporter mouse carries a RFP (red) fluorescing reportergene, which upon Cre activity switches to GFP (green). Mice of this strain were injected intravenously (i.v.) 2.5E+12 virus particles coated with 45 ng or 90 ng of surface modified dendrimers (G2, G2P1, G2P3 or G5) or AAV2/9Endo coated with the same amount of cationic surface dendrimers (G2 or G5). Successful pCMV-Cre gene transduction of tdTomato mouse organs (heart, liver, lung, kidney, spleen, brain, upper limb, and lower limb) was analyzed 21 days after viral injection. In this study experimental groups consist of AAV2Cre, AAV2/6Cre, AAV2/9Cre, AAV2/9Endo-Cre [24], AAV2/9Cre/G2, AAV2/9Cre/G5, AAV2/9Endo-Cre/G2, AAV2/9Endo-Cre/G5, AAV2/9Cre/G2P1, and AAV2/9Cre/G2P3.

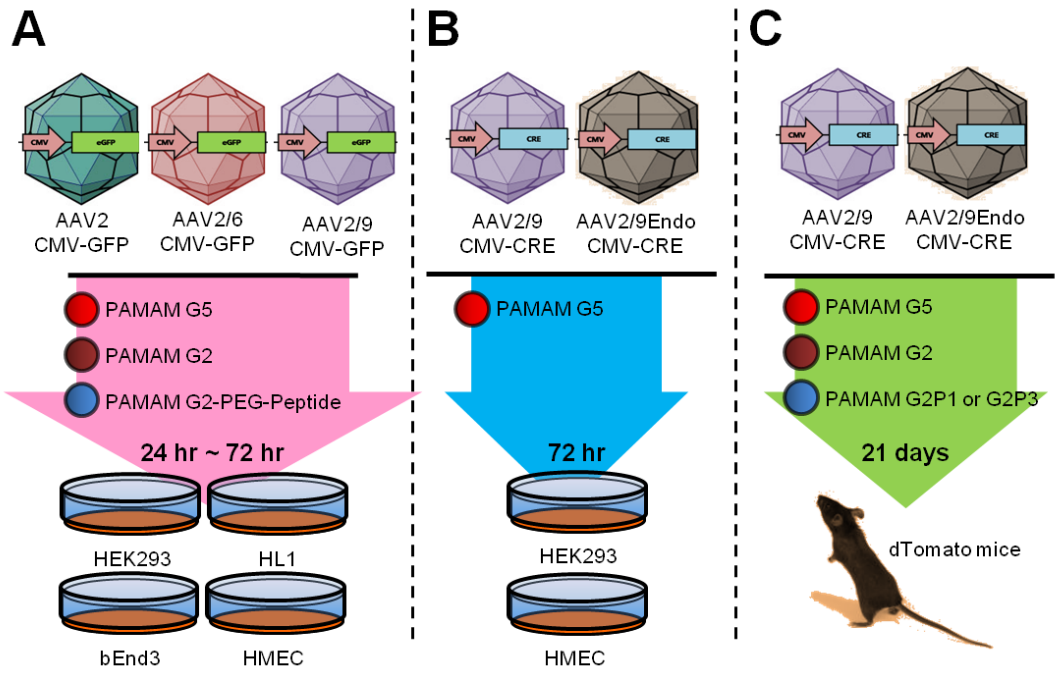

Figure 14 | Gene transduction by surface modified PAMAM coated AAVs in vitro and in vivo. A, In vitro transduction test of PAMAM coated AAV encoding for CMV-eGFP. G2 and G5 coated AAV2, AAV2/6, and AAV2/9 were applied to human embryonic kidney 293 cells (HEK 293), human microvascular endothelial cells (HMEC), and AT-1 mouse atrial cardiomyocyte tumor lineage cells (HL-1) during 24 hr to 72 hr. **B**, In addition, the AAV2/9 Endo displaying endothelial targeting peptide 1 (P1) directly on the capsid was coated with G5 in vitro. **C**, The surface modified PAMAM coated AAV2/9 CMV-Cre or AAV2/9Endo CMV-Cre are applied by tail vein injection into tdTomato mice. After 3 weeks, the mice tissues (heart, liver, lung, kidney, spleen, brain, upper limb and lower limb) are harvested for transduction analysis.

2.2.15. Tissue processing

The tomato mouse organs were removed and fixed for 4 hours by cold 4% PFA in 0.1 M PBS, pH7.4. Then fixed mouse tissues were incubated in 25% sucrose solution at 4°C overnight followed by O.C.T. compound (Tissue-Tek, Sakura) for 20 min and stored at -80°C until sectioned. Frozen whole organs were cut into 5 micron sections using by freezing cryotome (Leica, Germany). For each organ, approximately 30 sections were analyzed (5 to 10 slides per group). The sections were examined using by laser-scanning confocal microscope system LSM 510 (Leica, Germany) as in Figure 15.

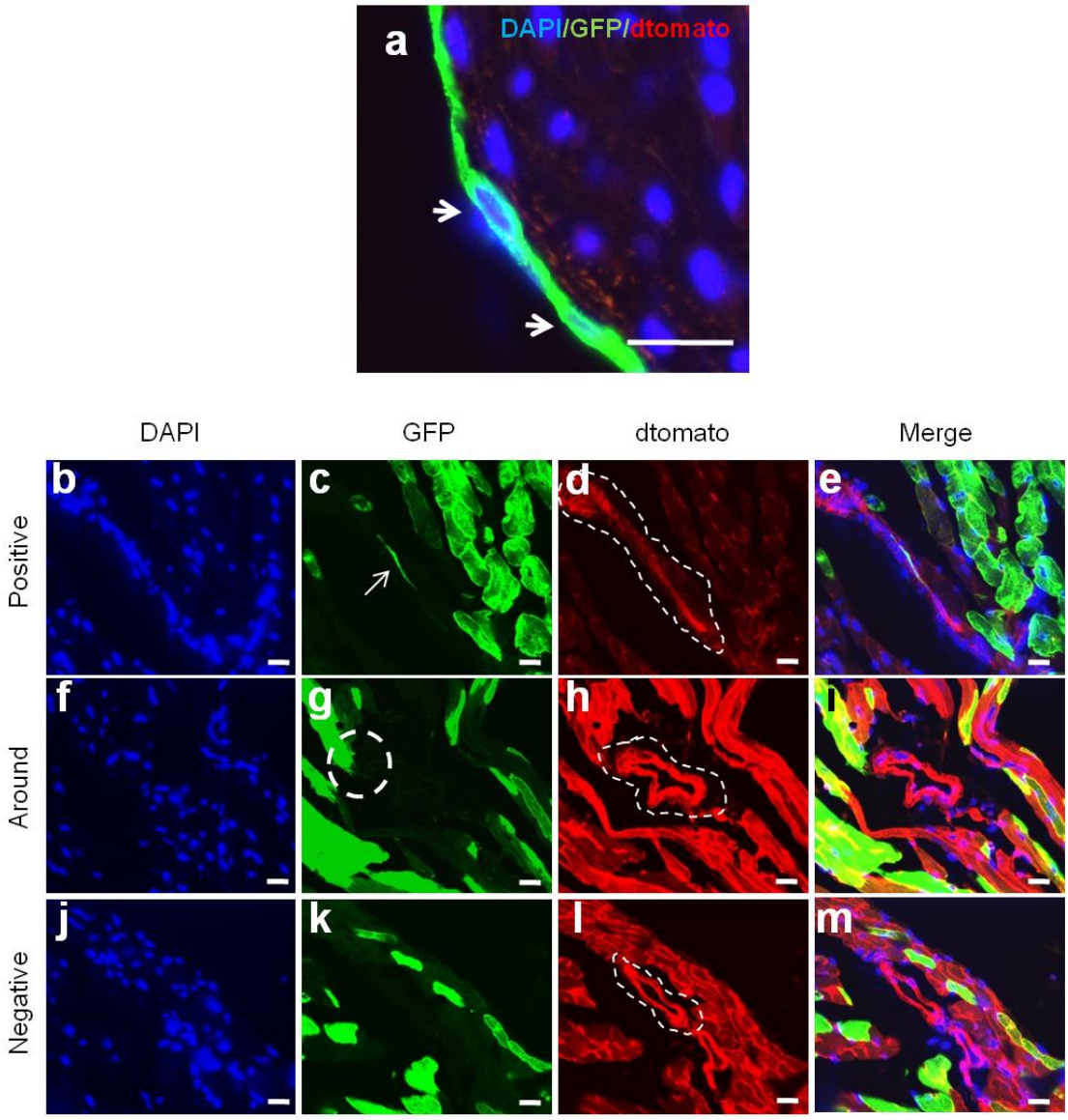

Figure 15 | Identification of Cre expression in vivo. a, The Cre gene expressed (green) in endothelial cell. **b-e**, Cre positive expression in endothelium of muscular artery. **f-i**, positive expression of cardiomyocyte in near muscular artery area. **j-m**, Cre negative expression of muscular artery. DAPI; nuclear counterstain, GFP; Cre positive expression, RFP; dtomato gene expression, merge; GFP with RFP. Scale Bar; 20 μm.

2.2.16. Mouse heart dissociation

Whole hearts of dTomato mice were washed 3 times in 0.9% NaCl and dissociated into single cell suspension by digestion in Collagenase II solution (1mg/ml PBS, Gibco) with DNase (50 µg/ml + 3mM $MgCl_2$ 3mM), and incubated at 37°C. Detached cells were resuspended in PBS/2% FCS and kept on ice with gentle agitation until staining.

2.2.17. Flow cytometry analysis

Whole hearts cell-suspensions were stained in ice-cold PBS containing 1% FCS using the following surface antibody cocktail. Antibodies against cell-surface markers (human CD31, mouse CD45, and mouse CD144) or against internal cell markers (human cardiac Troponin I) were incubated for 30 min. Cells were washed, resuspended in FACS staining buffer, processed using the Gallios Flow Cytometer, and analyzed using FlowJo X software (Beckman Coulter). Endothelial cell (CD31+, CD45-) and cardiomyocytes (Troponin I+) sorting gates were set according to unstained control, isotype control (rat IgG2a K) and single staining control.

2.2.18. Whole-mount preparation of the cremaster muscle

C57Bl/6 mice were anesthesized and placed on a heating pad to maintain body temperature. Intravital microscopy of leukocyte adhesion in the cremaster muscle preparation was performed by surgically preparation [54]. Briefly, after incision of the scrotum of the C57Bl/6 mouse, cremaster muscle was exteriorized and opened through a longitudinal incision. Thereafter, live cremaster images were recorded by intravital microscopy. The intravital microscopy was conducted on a BX 51 WI microscope (Olympus, Munich, Germany) equipped with a charge-coupled device camera (KAPPA CF8 HS) and a saline immersion objective (Olympus MplanFI/RI; 0.8 numerical aperture). The post-capillary venules were recorded at least 1 min and up to 3 min. Leukocyte adhesion, such as defined as non-moving cells or displacement less than one

cell diameter during 60 seconds, was analyzed by number of adherent cells per square millimeter. Blood flow velocity was measured by a dual-slit photodiode live measuring device (Circusoft Instrumentation, Hockessin, DE) and blood counts were determined through Idexx Procyte Dx hematology analyzer (Idexx Europe, Hoofddorp, Netherlands).

2.2.19. Statistics

Data are given as mean ± SD. $p < 0.05$ was considered statistically significant. All data were assessed using the Student's t-test was performed (http://studentsttest.com) or ANOVA followed by Student-Newman-Keuls-test for more 3 groups. The gradations were used in this analysis to illustrate the magnitude of significance (*: $p < 0.05$, **: $p < 0.005$, ***: $p < 0.0005$).

3. RESULTS

3.1. Optimization of Transduction efficiency of AAV/PAMAM complexes in vitro

For the in vitro optimization of AAV vectors using PAMAM dendrimers, complexes of AAV2/9-CMV-eGFP/G5 were first characterized in cell culture (Figure 16). A human embryonic kidney cell line (HEK 293; Figure 16-A) or human microvascular endothelial cells (HMECs; Figure 16-B) were transduced with two doses of AAV2/9-CMV-GFP virus particles (1.0E+05 vp/cell or 1.0E+06 vp/cell) either alone or coated with 3, 8, 12, or 16 pg/cell of PAMAM G5, a 48 h incubation period at 37°C. Cell images were analyzed by fluorescence microscopy (Zeiss) with image J v1.47 (http://rsb.info.nih.gov/ij/index.html). As shown, optional conditions for transduction (> 60%) were the 16 pg/cell of PAMAM G5 coating 1.0E+06 vp/cell AAV2/9-CMV-eGFP (Figure 16-C & -D).

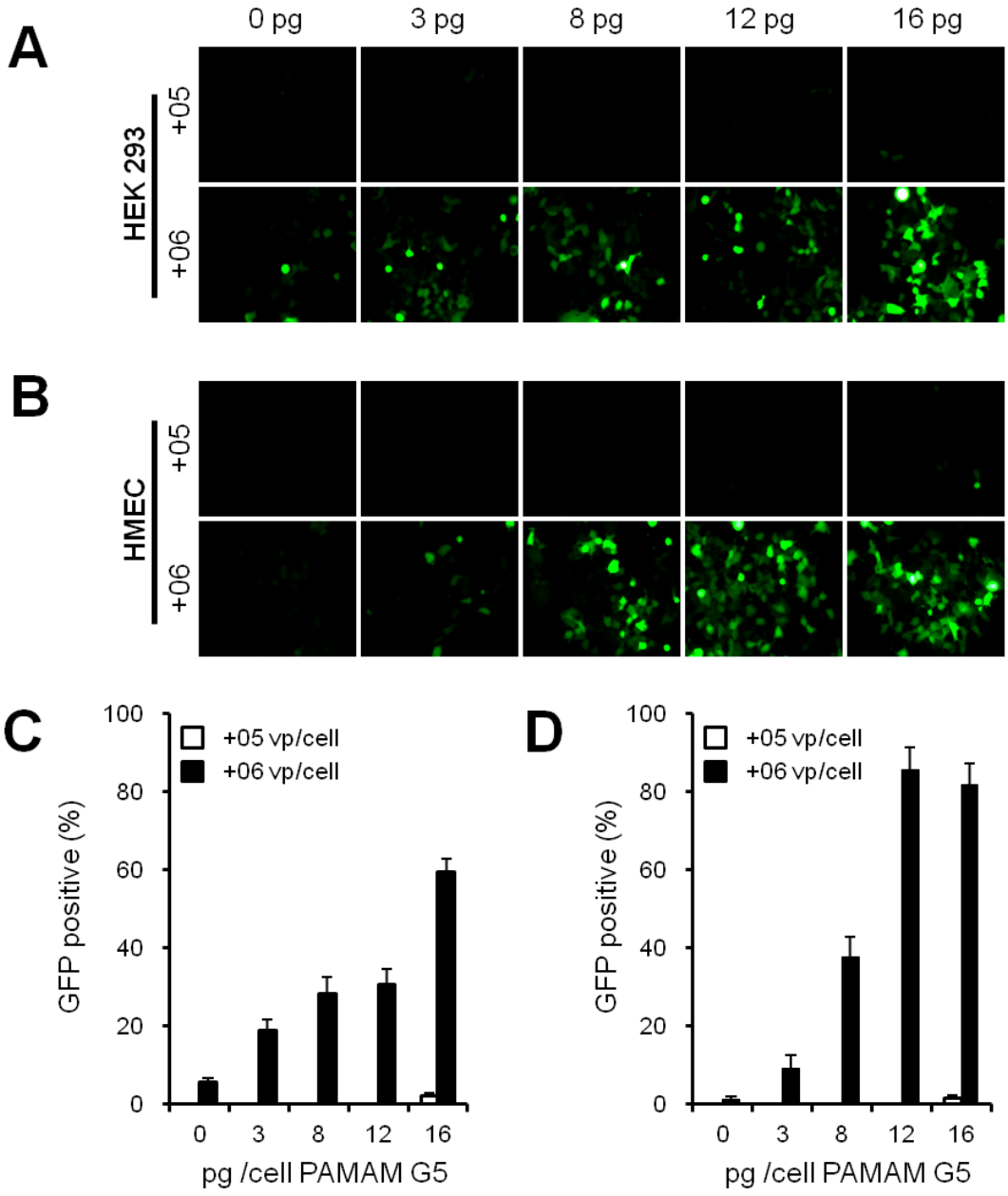

Figure 16 | Transduction efficiency characterization of AAV2/9-CMV-eGFP and AAV2/9-CMV-eGFP/PAMAM complexes in vitro. HEK 293 (**A & C**) or HMEC (**B & D**) were transduced with two doses of AAV2/9-CMV-GFP virus particles, as shown (open bars; 1.0E+05 vp/cell, black bars; 1.0E+06 vp/cell), either alone or coated with 3, 8, 12, or 16 pg/cell of PAMAM G5. Values represent the mean ± SD (n=3).

3.2. *Transduction efficiency by different serotypes of AAVs*

Transduction efficacies of wildtype AAV2-CMV-eGFP or AAV2/6-CMV-eGFP were altered by coating with PAMAM G5 in vitro (Figure 17). HMECs or murine cardiomyocytic cell line HL-1 cells were transduced with AAV2-CMV-GFP (Figure 17-A & -C) or AAV2/6-CMV-GFP (Figure 17-B & -D) virus particles (1.0E+06 vp/cell), either alone or coated with 2, 6, or 10 pg/cell of PAMAM G5. Thereafter, transduction efficacy was analyzed by fluorescence microscopy and quantified.

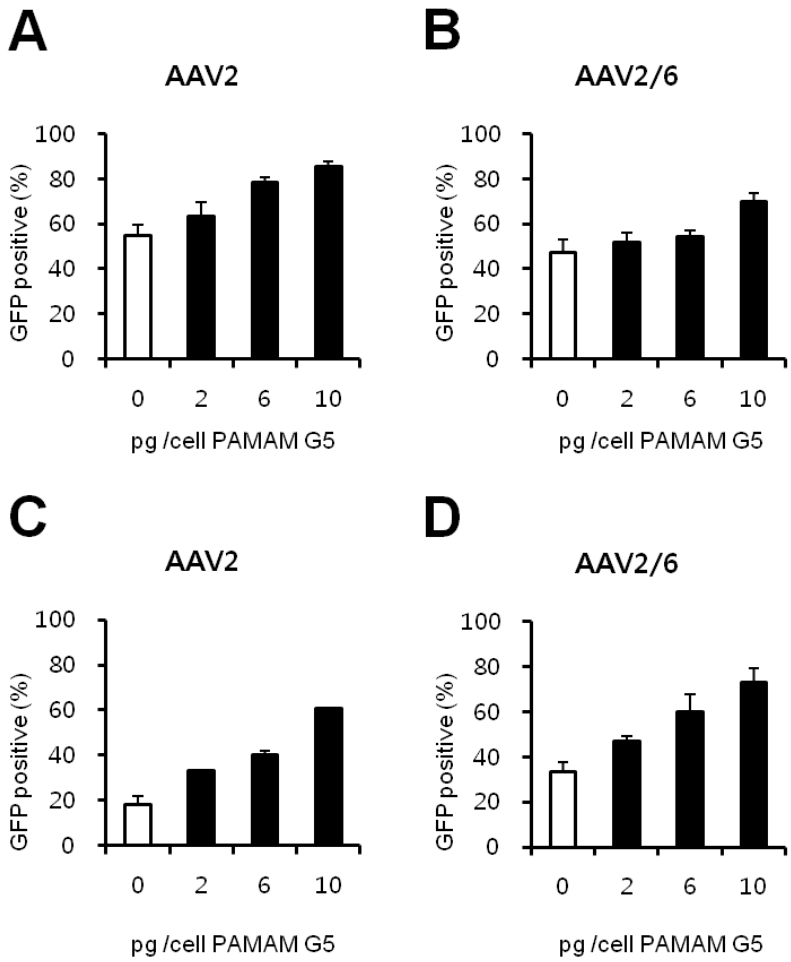

Figure 17 | AAV2 and AAV2/6 virus strains were incubated at 37°C/72 h with PAMAM G5. HMECs (**A & B**) or cardiomyocytic HL-1 cells (**C & D**) were transduced with AAV2-CMV-GFP (**A & C**) or AAV2/6-CMV-GFP (**B & D**) virus particles (1.0E+06 vp/cell), either alone (open bars) or coated with 2, 6, or 10 pg/cell of PAMAM G5 (black bars) after a 72 h incubation period at 37°C. Transduction efficiency of G5/AAV complexes were analyzed by fluorescence microscopy and quantified. Values represent the mean ± SD (n=3).

3.3. Transduction efficacies of G2 and G5 PAMAM dendrimers

Transduction efficacies of G2 PAMAM versus G5 PAMAM coating were characterized in vitro (Figure 18) at 37°C/72 h. Human microvascular endothelial cells (HMECs; Figure 18-A), or mouse brain endothelial cell line (bEnd.3 cells; Figure 18-B), were transduced with AAV2/6-CMV-eGFP virus particles (1.0E+06 vp/cell), either alone or after coating with 2, 4, or 6 pg/cell of PAMAM dendrimers (PAMAM G2 or G5). As a result, 6 pg/cell of PAMAM G5 with AAV2/6-CMV-eGFP complexes (38.30 ± 4.21 % in HMECs, 39.35 ± 6.63 % in bEnd.3 cells) were more efficient than only AAV2/6-CMV-eGFP 11.54 ± 7.19 % in HMEC, 2.34 ± 1.35 % in bEnd.3 cells) in vitro. As shown, the most efficient condition of PAMAM/AAV -combinations was the 6 pg/cell of PAMAM dendrimers (PAMAM G2 or G5).

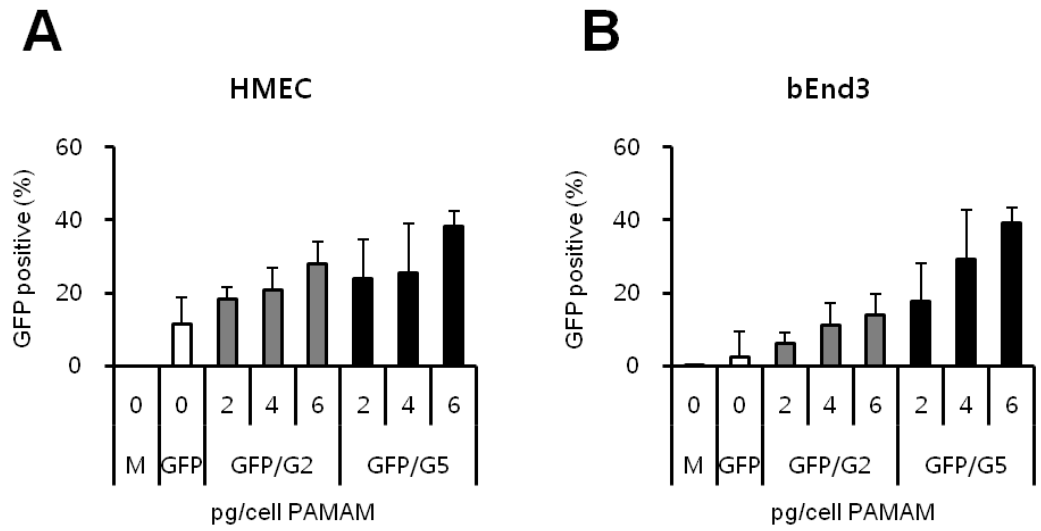

Figure 18 | Comparison of G2 vs G5 PAMAM coated AAV2/6-CMV-GFP in endothelial cells at 37°C/72 h. HMECs (**A**; n=3) or bEndo.3 cells (**B**; n=5) were transduced with AAV2/6-CMV-eGFP virus particles (1.0E+06 vp/cell), either alone (open bars) or coated with 2, 4, or 6 pg/cell of PAMAM dendrimers (G2: gray bars or G5: black bars). Bars present transduced cells/total cells, M; mock, GFP; AAV2/6-CMV-eGFP, GFP/G2; PAMAM G2 coated AAV2/6-CMV-eGFP, GFP/G5; PAMAM G5 coated AAV2/6-CMV-eGFP. Values represent the mean ± SD.

3.4. Biopanning

In order to improve the efficacy of PAMAM-mediated transduction and achieve a retargeting of the AAV vectors towards endothelial cells, we next selected endothelium-affine peptides from a M13 phage library (Figure 19-A1). $2x10^{11}$ plaque forming units (pfu) of the CX7C M13KE phage library were incubated with 1 ml of 1% BSA/DMEM in each $1x10^{7}$ cells/plate of the HMEC or HUVEC cells for 120 min at room temperature (RT) (Figure 19-A2). The results of phage selection are shown in Figure 19.

According to our prediction, the eluted solutions from the third round (HUVEC; $5.3x10^{6} \pm 3.3x10^{6}$ pfu, HMEC; $1.9x10^{6} \pm 1.5x10^{6}$ pfu) were binding with higher affinity to endothelial cells as compared to outputs from first (HUVEC; $5.1x10^{1} \pm 5.0x10^{1}$ pfu, HMEC; $2.6x10^{1} \pm 2.5x10^{1}$ pfu) and second round (HUVEC; $3.5x10^{3} \pm 1.5x10^{3}$ pfu, HMEC; $3.3x10^{3} \pm 2.5x10^{2}$ pfu, cf. Figure 19-B & C).

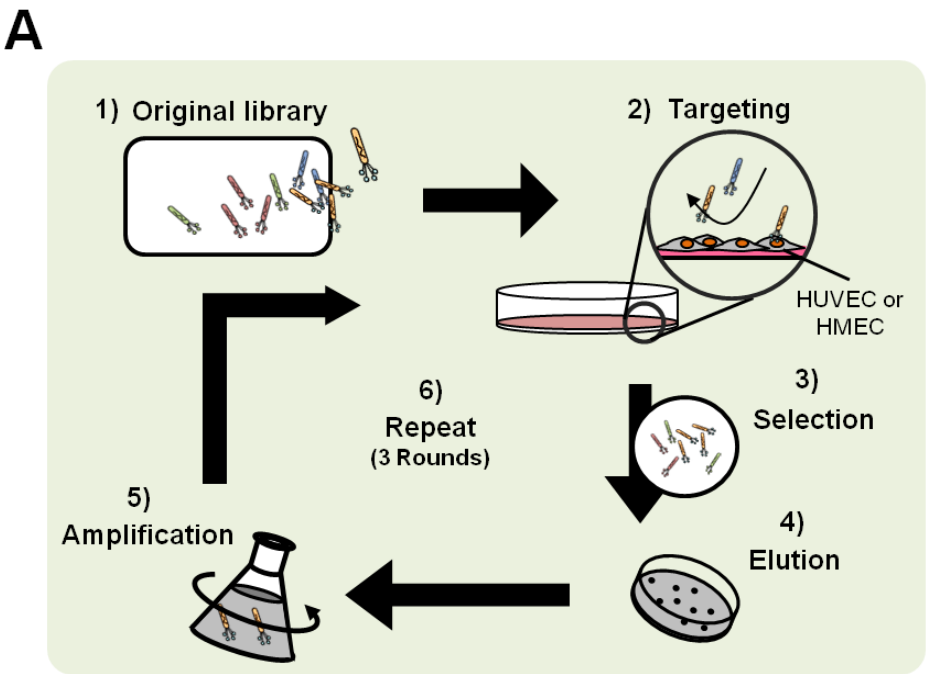

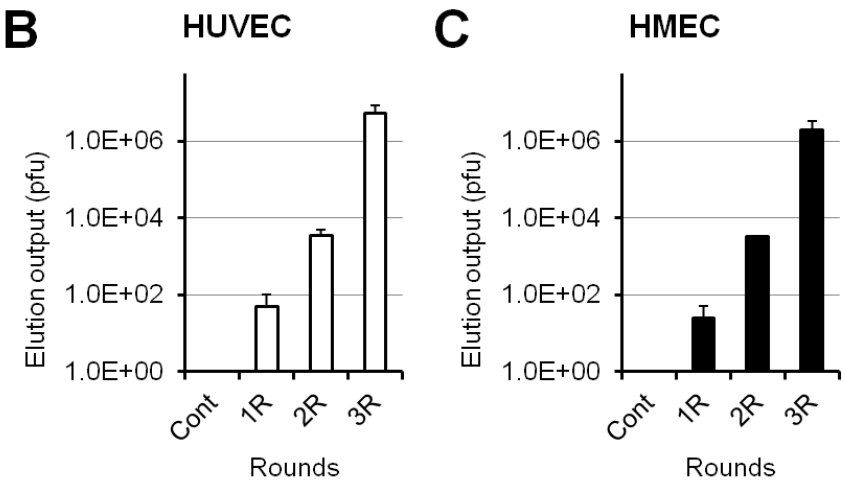

Figure 19 | Panning procedure of motif selection for targeting endothelial cells. A, a CX7C M13KE phage library **1)** was incubated with a HUVEC or a HMEC at 4'C for 120 min **2)**. The endothelial cell bound phages were selected by rigid washing of non-bound phages **3)**. Bound phages were eluted **4)**. The eluted phages were amplified in E. coli ER2738 **5)** and subjected to the next round of selection for up to 3 rounds (3R) **6)**. **B and C**, The phage titers of elutions of each round were measured using plaque assays in HUVEC (**B**) or HMEC (**C**). Cont; original CX7C M13KE phage library, 1R; first round elution, 2R; second rounds elution, 3R; third rounds elution, values represent the mean ± SD (n=3).

3.5. Direct phage PCR and sequencing

Each of 488 single blue (positive) plaques were selected from eluted phages on the LB/IPTG/X-gal plate (the results of 2 rounds and 3 rounds) and amplified in small volume with an E. coli ER2738 bacteria suspension (A600 nm OD 0.5) by vigorous shaking at 37°C/4.5 h. After purification, 1 µl of selected phage was analyzed by PCR with M13 phage PCR primers (forward; 5'- TTA TTC GCA ATT CCT TTA GTG G -3', reverse; 5'- CCC TCA TAG TTA GCG TAA CG -3').

3.6. Phage ELISA

Individual 10 phage clones (4 phage clones screened in HUVEC and 6 phage clones screened in HMEC) were tested for binding to target cells by incubation at RT for 120 min in endothelial cells (HUVEC or HMECs) and removed of non-bound phage clones. The bound phage clones were incubated with HRP-conjugated M13 PVIII antibody at

4’C for O/N and analyzed by TMB Substrate for absorbance at 450 nm. U1 to U4 phage clones were selected after panning from HUVEC, M1 to M6 phage clones were selected after panning from HMEC (Figure 20). U4, M1, M4, and M6 phages bound with high affinity to both endothelial cell, but M2 and M3 phages bound only in HMEC.

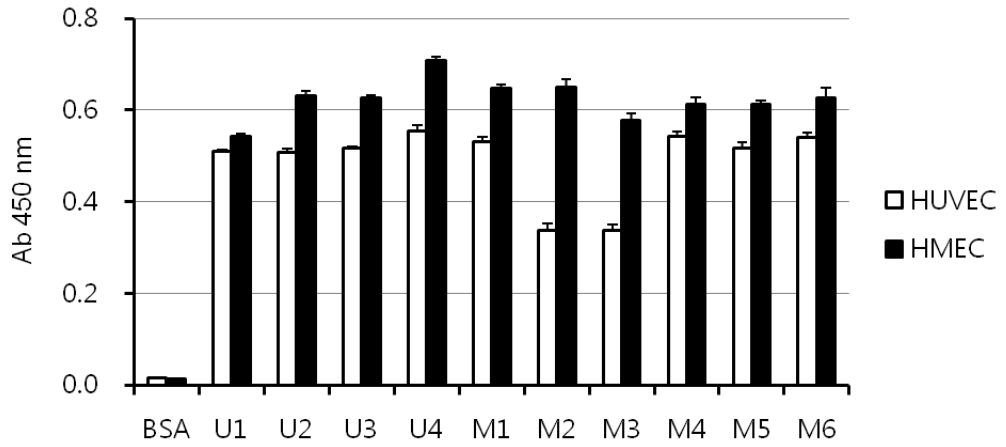

Figure 20 | Selected phages target to endothelial cell by Phage ELISA. Individual 10 phage clones were incubated with in HUVEC (open bars) or HMEC (black bars) and analyzed absorbance at 450 nm. U1 to U4; phage clones were selected from HUVEC, M1 to M6; phage clones were selected from HMEC. Values represent the mean ± SD (n=4).

3.7. Identification of predominant motifs

The graphical sequence logo represents predominant motifs of 10 identified amino acid phage sequences. The conserved sequence pattern was generated using WebLogo3 (Figure 21). As shown, the predominant motif was identified with the first 4 site of amino acid sequence N (Asn; Asparagine), N, S (Ser; Serine), G (Gly; Glycine), and last one amino acid sequence is also N. The unknown sequences, as fifth and sixth amino acid sequence, were decided according to phage ELISA results and alignment analysis of the 10 peptide sequences using Clustal W program (Figure S1). The final selected two novel endothelium target motifs were peptide no.2; CNNVGGWN and peptide no.3; CNNSGMRN (Table 4).

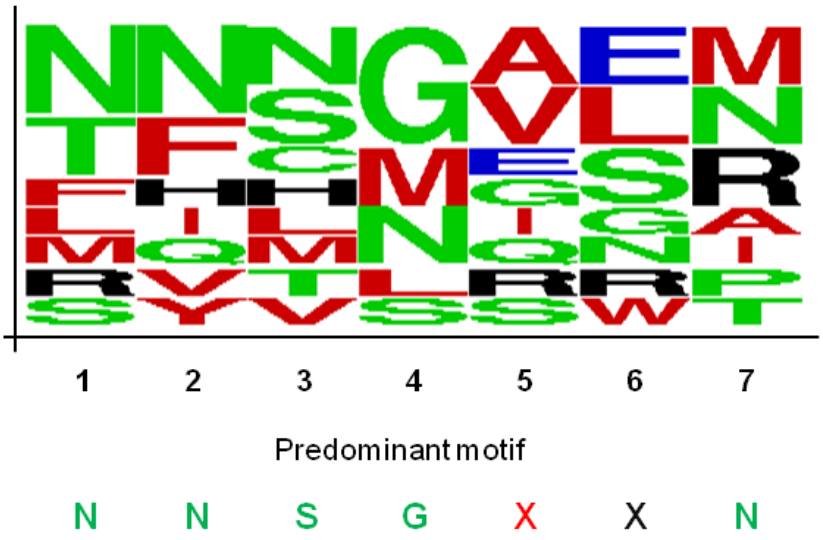

Figure 21 | Graphical sequence logo representation of predominant motif. The conserved sequence pattern was generated using WebLogo3 (http://weblogo.berkeley.edu/). Hydrophilic amino acid (green letters); QNSTCGP, hydrophobic amino acid (red letters); AILMFWYV, positive charged amino acid (black letters); RHK, negative charged amino acid (blue letters); DE, X of red letter); hydrophobic amino acid and X of black letter; positive charged amino acid.

No.	Sequence	Homologous	Identifications	Function	Accession no.
1	CSLRSPPS	CSLCSPPS	Fibroblast growth factor receptor 3	Cell-surface receptor	P22607
2	CNNVGGWN	VGGWN	Actin-binding protein IPP	Organizing the actin cytoskeleton	Q9Y573
3	CNNSGMRN	CNNRGM	Stabilin-2	ER* for heparin internalization	Q8R4U0

Table 4 | Identification of homologous. Peptides were analyzed using the National Center for Biotechnology Information BLAST search against the SWISSPROT database, using the option for short nearly exact matches, to identify human proteins with homologous sequences. ER*; Endocytosis receptor.

3.8. Surface modified nano complexes

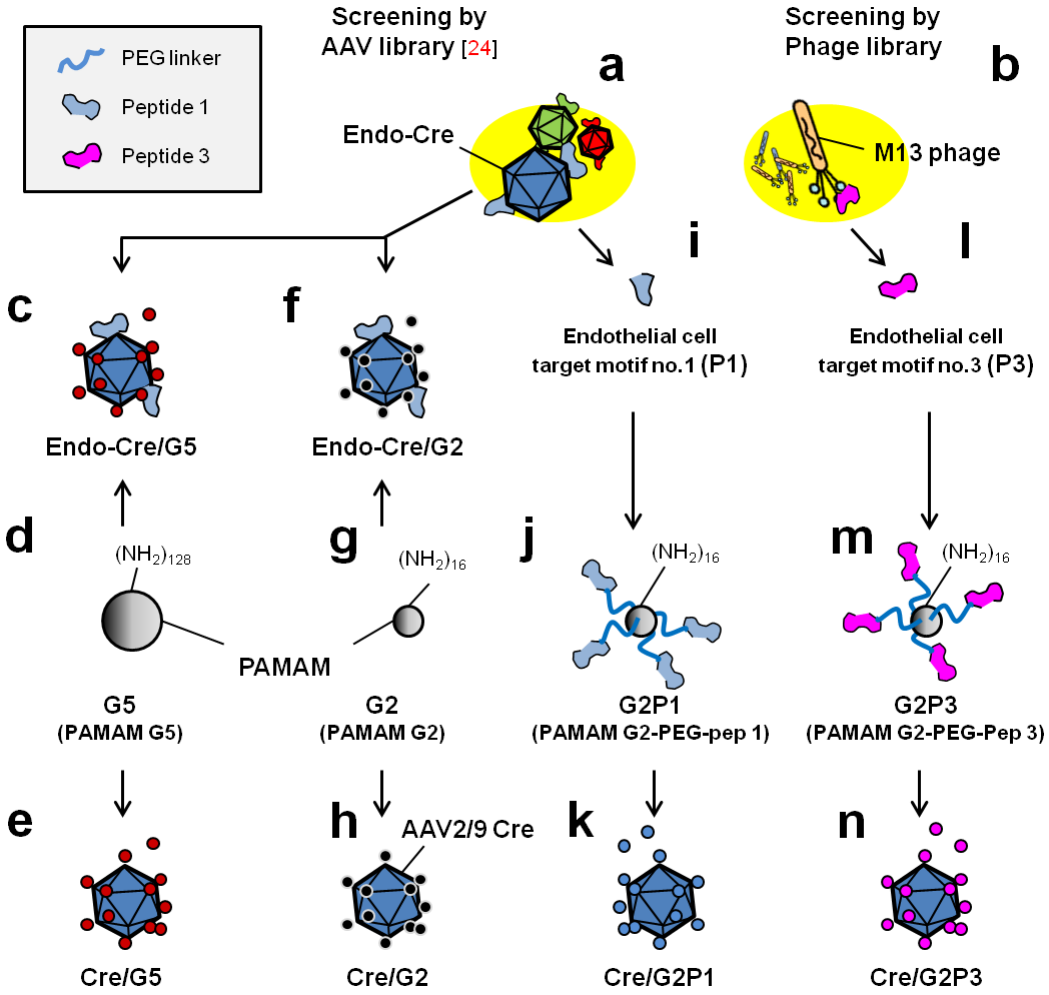

Figure 22 | Design of surface modified PAMAM dendrimers coated AAV2/9. Endo-Cre/G5 **c)** or Cre/G5 **e)** coating an AAV2/9Endo-Cre (Endo-Cre) or AAV2/9Cre (Cre) compexed with G5 PAMAM **d)**, and Endo-Cre/G2 **f)** or Cre/G2 **h)** coating an Endo-Cre or Cre with G2 PAMAM **g)**. Endothelial cell target motifs peptide no.1 (P1) **i)** or peptide no.3 (P3) **l)**, as CX7 peptides, were identified by AAV display library **a)** or M13 phage display library **b).** Thereafter, they were synthesized and displayed on the surface of G2 PAMAMs. Cre/G2P1 **k)** or Cre/G2P3 **n)** contribute an AAV2/9Cre with G2P1 **j)** or G2P3 **m)**.

In this study, we studied two cationic surfaced PAMAM dendrimers, namely G2 (-(NH_2)16; Figure 22-g) or G5 (-(NH_2)128; Figure 22-d), and two surface modified PAMAM dendrimers, such as G2-PEG linker-P1 (G2P1) or G2-PEG linker-P3 (G2P3) for transduction efficiency of cardiomyocyte and endothelial cells in heart. The two PAMAM dendrimers with cationic surface were synthesized by Dendritic Nanotech. Inc, Michigan, USA, whereas surface modifications of PAMAM dendrimers were performed in our lab in cooperation with Manfred Ogris (Pharmazie, LMU). The two endothelium target motifs, pentavalent amino acid peptide no.1 (P1) and peptide no.3 (P3), of surface modified PAMAM dendrimers were identified either by AAV display library (K. Varadi et al., Gene Therapy 2012 [24]) or by the M13 phage display library (Ph.D. CX7C M13KE, New England Biolabs, see Methods section), respectively (Figure 22-b). The identified P1 (CSLRSPPS-amind; MW: 845.99) and P3 (CNNSGMRN-amind; MW: 894.98) were synthesized (Figure 22-I & -l) and conjugated to the G2-PEG linker (NHS-PEG-OPSS), such as G2P1 (Figure 22-j) or G2P3 (Figure 22-m).

The pAAV-CMV-Cre plasmid was used in a model of systemic gene transduction (tail vein injection of AAV2/9-CMV-Cre virus (Cre)) in dTomato mice. The mice are characterized by stop loxP cassettes before mG sites on either side of a membrane-targeted dTomato (mT) cassette and default red fluorescence in all tissues. When exposed to Cre recombinase, the mT cassette is deleted and expression of the membrane-targeted EGFP (mG) cassette is enabled. The surface modified PAMAM dendrimers (G2P1 or G2P3) were coated with pAAV2/9-Cre by incubation at 30 min at the room temperature, such as Cre/G2P1 (Figure 22-k) or Cre/G2P3 (Figure 22-n). We also used endothelial cell targeting peptide no.1 (SLRSPPS) inserted on the surface of A589 of AAV9 capsid, termed Endo-Cre (p5E18-VD-2/9-SLRSPPS-Cre). Endo-Cre/G5 (Figure 22-c) or Endo-Cre/G2 (Figure 22-f) were complexes of AAV2/9Endo-Cre (Endo-Cre) with G5 or G2 PAMAMs. Cre/G5 (Figure 22-e) or Cre/G2 (Figure 22-h) were complexes of AAV2/9-Cre with G5 or G2.

3.9. Transduction efficiency by peptide-modified G2 in vitro

Transduction efficiency of unmodified PAMAM dendrimers versus surface modified G2 PAMAMs were characterized after coating AAV2/6-CMV-eGFP and application in endothelial cells in vitro (Figure 23).

5.0E+05 vp/cell of AAV2/6-CMV-eGFP virus particles (low virus dose) were transduced without or with 2 pg/cell of each different surface the modified G2 PAMAM dendrimers in HMECs at 37°C/72 h (Figure 23-A), and intensity of GFP expression per total RFP area was analyzed (Figure 23-B). The transduction efficiency of AAV2/6-CMV-eGFP/G2 (AAV/G2; 6.20 ± 3.13 %), AAV2/6-CMV-eGFP/G5 (AAV/G5; 7.08 ± 4.29 %), AAV2/6-CMV-eGFP/G2P1 (AAV/G2P1; 10.87 ± 6.31 %), and AAV2/6-CMV-eGFP/G2P3 (AAV/G2P3; 15.04 ± 5.77 %) was increased compared AAV2/6-CMV-eGFP only (AAV; 3.76 ± 1.29 %) in HMECs. As shown below (figure 23), G2-PEG-P3 (G2P3) coated AAV2/6-CMV-eGFP virus was highly transduced in HMECs.

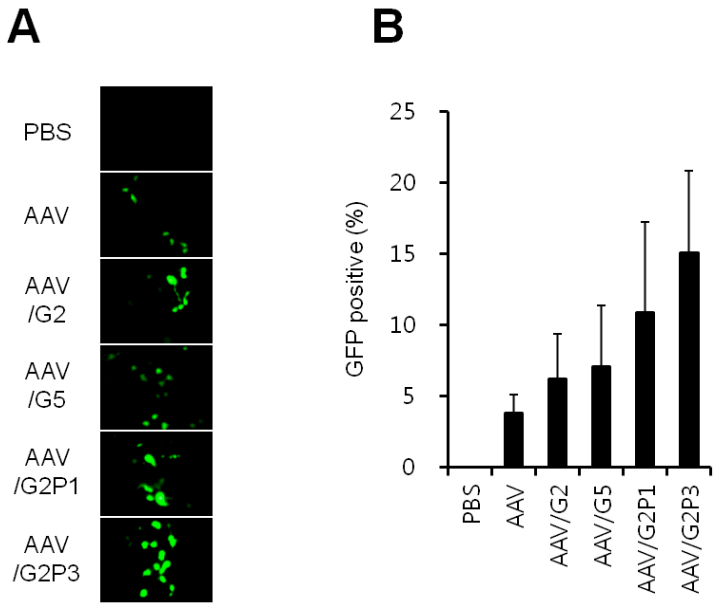

Figure 23 | Transduction efficiency characterization of peptide modified G2 with AAV2/9-CMV-eGFP complexes in endothelial cell. AAV2/6-CMV-eGFP virus particles (5.0E+05 vp/cell) were transduced with alone or 2 pg/cell of each different surface modified PAMAM dendrimers in HMEC at 37°C/72 h. **A,** Transduced cells signal (green) were indicated by AAV2/6-CMV-eGFP. **B,** Bars present transduced cells/total cells. Values represent the mean ± SD (n=3).

3.10. Dose effects of G5 coating to AAV2/9-Cre in dTomato mice (in vivo)

In this study, we focused to arteries (A), (muscular arteries; 250 ± 50 μm, arteriole; 28 ± 15 μm, and capillaries; 3.3 ± 0.5 μm)[86], of heart or hind limb for several artery disease causing (ex, atherosclerosis; a specific type of arteriosclerosis) in vivo model.

AAV2/9Cre was coated by incubation of 2.0E+12 vp of AAV2/9Cre virus with 45 μg/mouse or 90 μg/mouse of G5 in 30 min at RT, as Cre/G5-45 or Cre/G5-90. Those were administered into the tail vein of dTomato mice (7 ~ 9 month) and the mice were sacrificed after injection 3 week (21 days) later (Figure 24).

In the AAV2/9Cre/G5-90 group, the vector transduced both the cardomyocyte of artery (A) area (45.23 ± 7.72 A.U.; Figure 24-A & B) and muscle area (64.98 ± 7.20 A.U.; Figure 24-C & D) more efficiently than the AAV2/9Cre group (A area; 20.58 ± 5.84 A.U., muscle area; 28.78 ± 4.14 A.U.) by intensity (A.U.; arbitrary units) in the dTomato heart. The AAV2/9Cre/G5-45 group was significantly higher transduced (A area; 28.17 ± 3.14 A.U., muscle area; 45.07 ± 19.70 A.U.) compared to the AAV2/9Cre group. Values the mean ± SD (n=1).

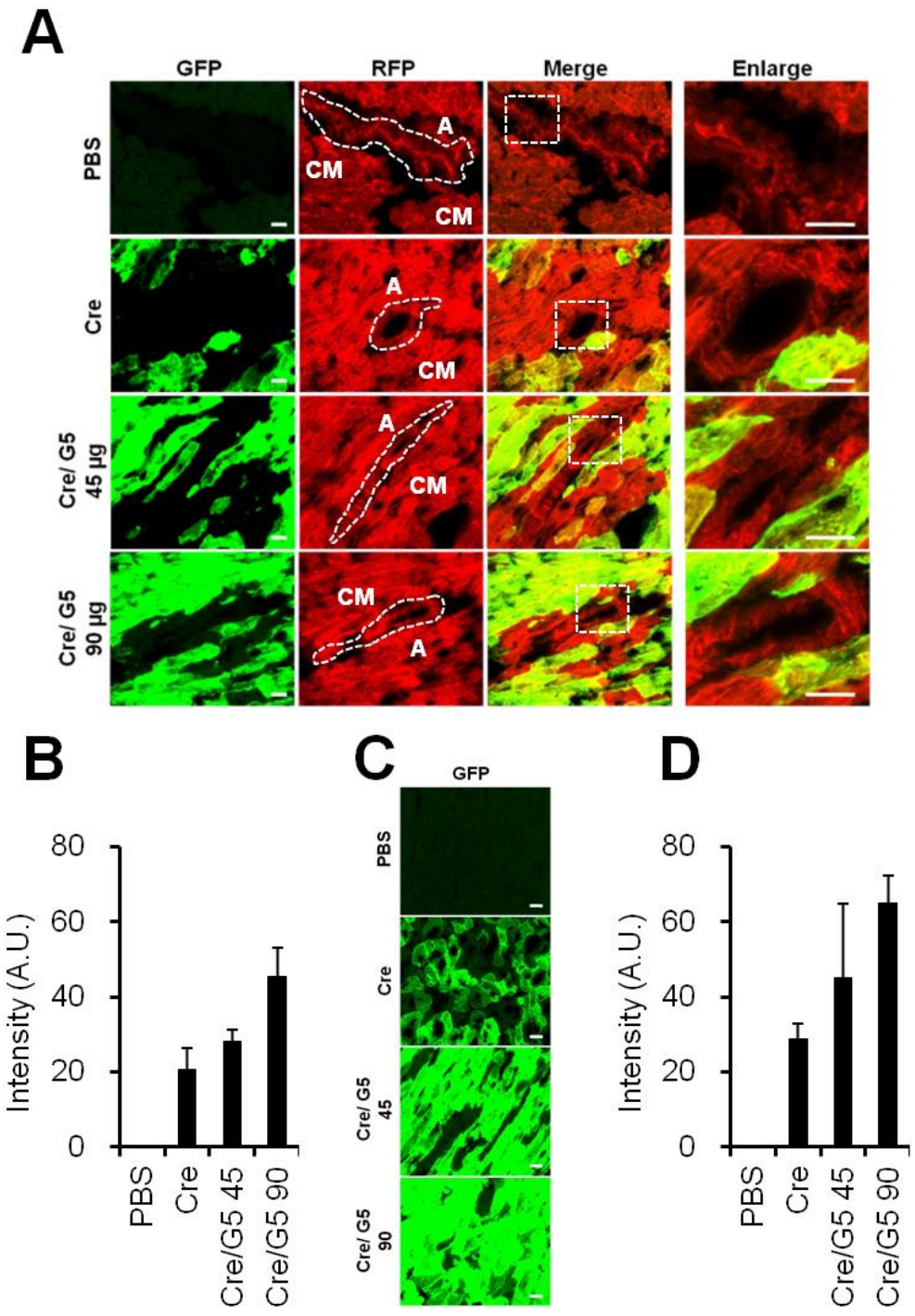

Figure 24 | Transduction efficacy of G5 in dTomato mice heart. A, Transduction efficacy in the artery. GFP; Cre positive expression, RFP; dtomato gene expression, merge; GFP with RFP, enlarge; 3 fold large image of white dashed line square box, A; artery (white dashed line), CM; cardiomyocyte, scale bar; 20 µm. **B**, Intensity (A.U.; arbitrary units) of GFP expression per total RFP area. **C**, Gene delivery efficacy in the cardiomyocyte of dTomato. GFP; Cre positive expression, scale bar; 20 µm. **D**, Intensity (A.U.; arbitrary units) of GFP expression per total RFP area. Values represent the mean ± SD (n=1).

3.11. PAMAM G5 coating of AAV2/9Endo-Cre in vivo

The cross packaging of AAV2/9Endo-Cre virus was accomplished with pAAV-CMV-Cre plasmid and endothelial cell targeting peptide (SLRSPPS) inserted on the surface of A589 of AAV9 capsid (p5E18-VD-2/9-SLRSPPS) [24]. 2.0 x 10^{12} vp of AAV2/9Endo-Cre virus were coated with 25 µg/mouse or 45 µg/mouse of G5 in 30 min at RT, as AAV2/9Endo-Cre/G5-25 or AAV2/9Endo-Cre/G5-45. Those were administered into the tail vein of dTomato mice (7 to 9 month) and the mice were sacrificed after injection 3 week (21 days) later. The images were analyzed by confocal microscopy (LSM 510) with image J v1.47 (Figure 25).

In the AAV2/9Endo-Cre/G5-45 group, we found a higher transduction of arteries (A) (posi; 33.3 %, around; 25.9 %, and nega; 40.7 %) than in the unmodified AAV2/9Cre group (posi; 12.5 %, around; 75.0 %, and nega; 12.5 %) or the capsid-modified AAV2/9Endo-Cre group (posi; 0.0 %, around; 10.0 %, and nega; 90.0 %). Of note, transduction efficacy of AAV2/9Endo-Cre/G5-45 group was reduced in both, the arteries area (2.03 ± 4.81 A.U., p-value < 0.0005) (Figure 25-A & C) and the muscle area (1.69 ± 2.13 A.U., p-value < 0.0005) (Figure 25-D) compared to the AAV2/9Cre group (A area; 59.08 ± 26.15 A.U. muscle area; 154.28 ± 18.13 A.U.).

The results of AAV2/9Endo-Cre/G5-45 group shown that coating G5 PAMAM can help to increase transduction efficacy to targeted cell types according to specific affinities of the coated virus type.

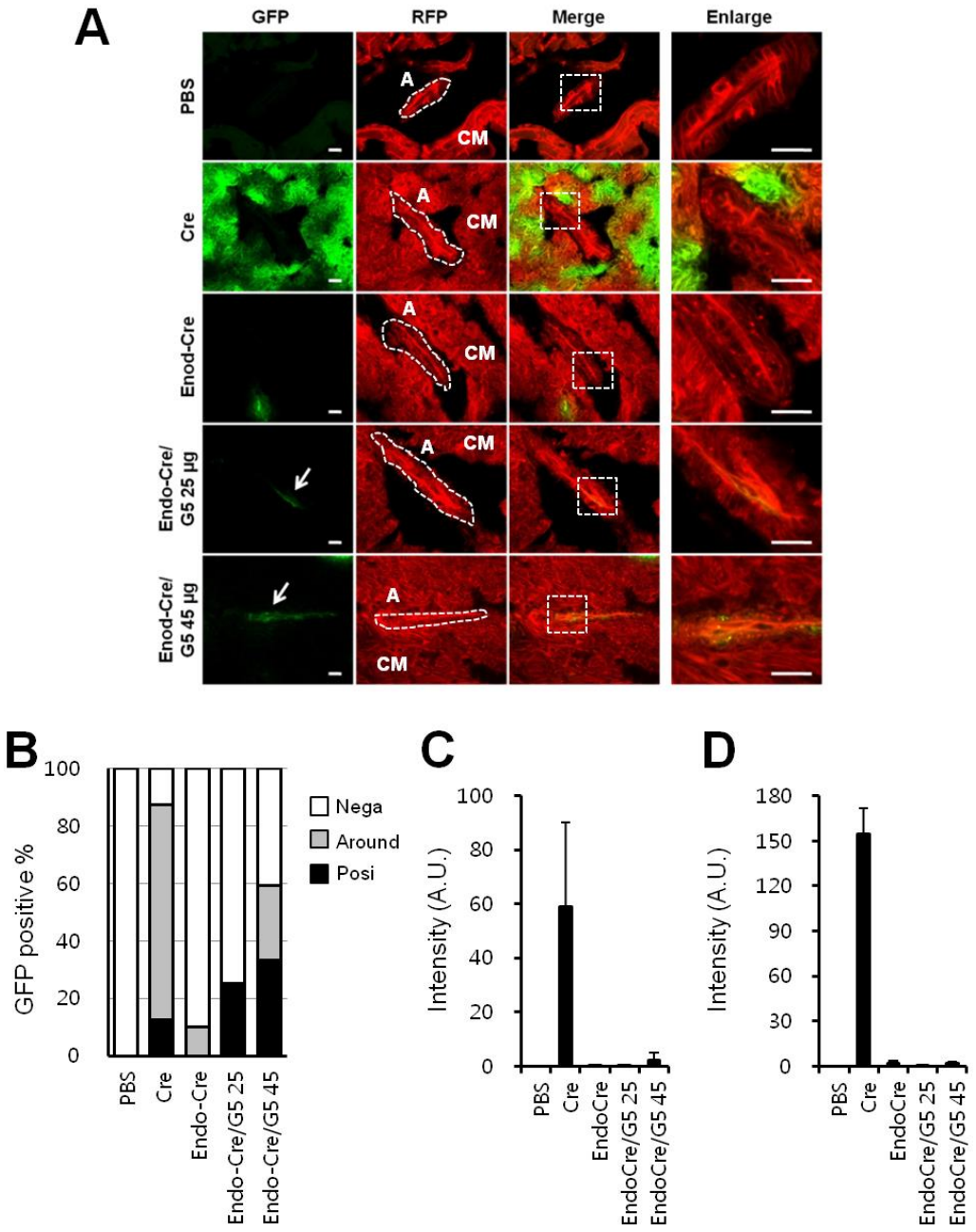

Figure 25 | Transduction efficacy of AAV2/9Endo-Cre/G5 in dTomato mice heart. A, Transduction efficacy in arteries. The white arrows were indicated Cre positive expression (green) of endothelium in arteries. GFP; Cre positive expression, RFP; dtomato gene expression, merge; GFP with RFP, enlarge; 3 fold large image of white dashed line square box, A; arteries (white dashed line), CM; cardiomyocyte, Scale Bar; 20 µm. **B**, demonstration of Cre positive revel (percentage; Cre positive expressed arteries per total arteries), as shown in **A)**. posi (black bars), around (gray bars), and nega (strip bars). **C**, Intensity (A.U.; arbitrary units) of GFP expression per total RFP area, as shown in **A)**. Values represent the mean ± SD. **D**, Intensity (A.U.; arbitrary units) of GFP expression per total RFP area in cardiomyocyte. Values represent the mean ± SD.

3.12. AAV2/9Cre/G2 transduction of dTomato mice in vivo

The AAV2/9Cre virus particles were coated by incubation with 2.0 x 10^{12} vp of AAV2/9Cre virus and 45 µg/mouse of PAMAM dendrimers (G2 or G5) in 30 min at RT, as Cre/G2 or Cre/G5. Those vectors were administered into the tail vein of dtomato mice and the mice were sacrificed after injection 3 week (21 days) later. The transduction efficacy test groups (n=3, per group) were control (PBS), AAV2/9Cre alone, AAV2/9Cre/G2 and AAV2/9Cre/G5 in the dTomato heart. The images were analyzed by confocal microscopy (LSM 510) with image J v1.47 (Figure 26 & Figure S2 - S5).

AAV2/9Cre/G2 transduced vessels to a similar extent as AAV2/9Cre/G5 (20.42 ± 7.59 % vs. 19.74 ± 4.69 %), which was higher than AAV2/9Cre only (9.03 ± 4.76 %). The white arrows indicate Cre-positive luminal surface events (= transduced endothelium) of arteries. Furthermore, nano-particle coating enhanced parenchymal transduction. e.g., AAV2/9Cre/G5 achieved 99.86 ± 39.51 A.U. and AAV2/9Cre/G2 86.30 ± 15.69 A.U. compared to the AAV2/9Cre only (39.50 ± 16.00 A.U.) in the dTomato mice mouse hearts.

In summary, nano-particle coating enhances cardiomyocyte transduction in the heart. Moreover, G2 PAMAM coating helps to target inner vessel layers, e.g. endothelium, more efficiently than G5 PAMAM coating of AAV2/9.

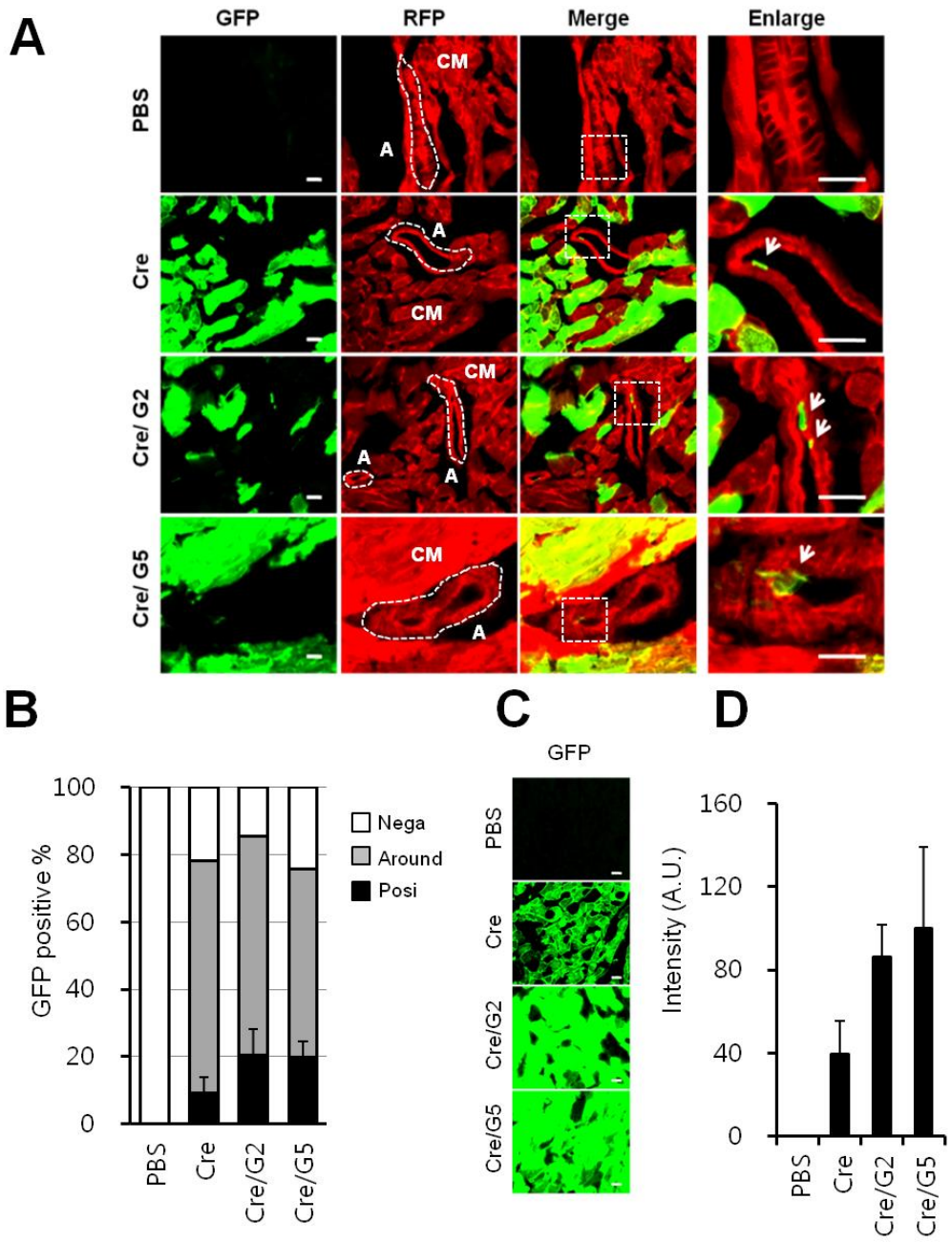

Figure 26 | Transduction efficacy of AAV2/9Cre/G2 or AAV2/9Cre/G5 in dTomato heart. A, Gene delivery efficacy in the arteries. The white arrows were indicated Cre positive expression (green) in endothelium of arteries. GFP; Cre positive expression, RFP; dtomato gene expression, merge; GFP with RFP, enlarge; 3 fold large image of white dashed line square box, A; arteries (white dashed line), CM; cardiomyocyte, Scale Bar; 20 μm. **B**, Demonstration of Cre positive revel (percentage; Cre positive expressed arteries per total arteries), as shown in A. posi (black bars); Cre positive expression in endothelium of arteries, around (gray bars); Cre positive expression of cardiomyocyte in near arteries area, nega (strip bars); Cre negative expression. **C**, Gene delivery efficacy in the cardiomyocyte. GFP; Cre positive expression. Scale Bar; 20 μm. **D**, Intensity (A.U.; arbitrary units) of GFP expression per total RFP area, as shown in **C)**. Values represent the mean ± SD (n=3).

3.13. Specific endothelial transduction of AAV2/9Endo-Cre/G5

AAV2/9Endo-Cre virus particles, as modified to display peptide no.1 (CSLRSPPS) on the surface of AAV2/9 capsid (Varadi K. et al., Gene Therapy 2012 [24]), were coated with 45 μg/mouse of PAMAM dendrimers (G2 or G5). Those were administered into the tail vein of dTomato mice and the mice were sacrificed after injection 3 week (21 days) later. Efficacy of gene delivery was compared between control (PBS), AAV2/9Cre, AAV2/9Endo-Cre, AAV2/9Endo-Cre/G2 and AAV2/9Endo-Cre/G5. As shown, transduction efficiency of endothelium in arteries of Endo-Cre/G5 group (33.73 ± 7.26 %) was higher than in the Endo-Cre/G2 group (9.40 ± 10.23 %), and Endo-Cre alone group (0.0 ± 0.0 %) as well as the Cre group (9.03 ± 4.76). Furthermore, cardiomyocyte transduction efficiency of Endo-Cre groups was reduced (2.87 ± 1.27 A.U.) compared to the Cre group (158.91 ± 18.96 A.U.) when fluorescence intensity was analyzed in the dTomato heart. Additionally, cardiomyocyte transduction efficiencies of Endo-Cre/G2, and Endo-Cre/G5 groups were also reduced (Endo-Cre/G2; 0.37 ± 0.23 A.U., Endo-Cre/G5; 0.32 ± 0.27 A.U.) compared to Endo-Cre group, which, however, was already much lower than the Cre group. As the results show, G5 PAMAM coating improved endothelium transduction to a significant, extent (Figure 27-A). However, Endo groups (Endo alone, Endo-Cre/G2, and Endo-Cre/G5) display reduced cardiomyocyte transduction in heart. It seems that the Endo-peptide coating induces negative selection of the cardiomyocyte compartment, whereas G2 and G5 increase targeting of the endothelium.

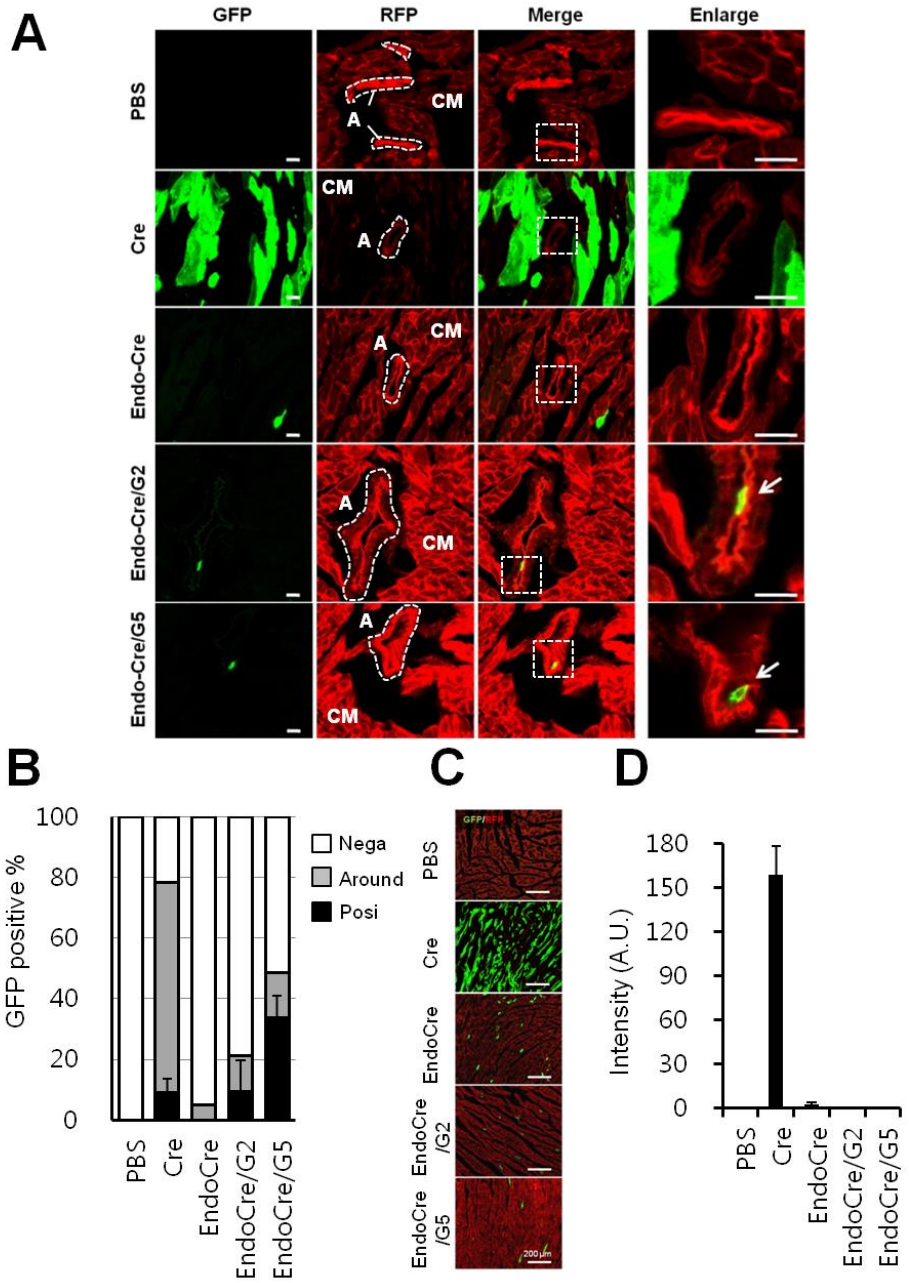

Figure 27 | Transduction efficacy of AAV2/9Endo-Cre /G2 or AAV2/9Endo-Cre /G5 in dTomato heart. A, The white arrows indicate Cre positive expression (green) in endothelium of arteries. GFP; Cre positive expression, RFP; dtomato gene expression, merge; GFP with RFP, enlarge; 3 fold large image of white dashed line square box, A; arteries (white dashed line), CM; cardiomyocyte, scale bar; 20 μm. **B**, Demonstration of Cre positive revel (percentage; Cre positive expressed arteries per total arteries), as shown in A. posi (black bars); Cre positive expression in endothelium of arteries, around (gray bars); Cre positive expression of cardiomyocyte in near arteries area, nega (strip bars); Cre negative expression. **C**, Transduction efficacy in the cardiomyocyte. GFP; Cre positive expression, scale bar; 200 μm. **D**, Intensity (A.U.; arbitrary units) of GFP expression per total RFP area, as shown in **C)**. Values represent the mean ± SD (n=3).

3.14. Endothelial-targeted transduction of AAV2/9Cre/G2P3

AAV2/9Cre virus was modified by linking G2 PAMAM dendrimers with the endothelial-affine peptides P1 and P3 attached to a PEG linker complex (see Methods 2.2.8). Those modified virus particles were administered systemically by tail vein injection of dTomato mice, and the mice were sacrificed 21 days later. In the dTomato mouse heart, transduction efficacy of arteries in the Cre/G2P3 group (43.87 ± 8.70 %) were significantly higher than the Cre/G2P1 group (23.39 ± 5.11 %), the Cre/G2 group (20.42 ± 7.59 %) as well as the Cre alone group (9.03 ± 4.76 %).

Furthermore, transduction efficiency of Cre/G2P1 and Cre/G2P3 groups were higher in the cardiomyocyte compartment Cre/G2P1 (180.00 ± 49.46 A.U.) and Cre/G2P3 (169.64 ± 20.37 A.U.) than in the Cre/G2 group (107.64 ± 38.62 A.U.) in the dTomato mouse hearts (Figure 28).

Moreover, our results show that Cre/G2P3 virus particles transduced endothelium at higher rates than all other transduction groups (43.87 ± 8.70 % of the arteries in the heart). However, it is difficult to derive microcirculatory endothelial transduction efficacies from these morphological studies in mid-size arteries. To independently study general endothelial transduction, we conducted FACS analysis of dTomato mouse hearts digested 3 weeks after transduction and gated for the endothelial marker PECAM-1 (Figure 29). Taken together, combining AAV2/9 with nano-coating (PAMAM G2) and endothelial targeting peptide P3 dramatically increases vessel transduction of murine dTomato hearts. The comparison to P1 (SLRSPPS, cf. Varadi K et al.) indicates a tendency towards a stronger effect of P3, without statistical significance (Figure 27).

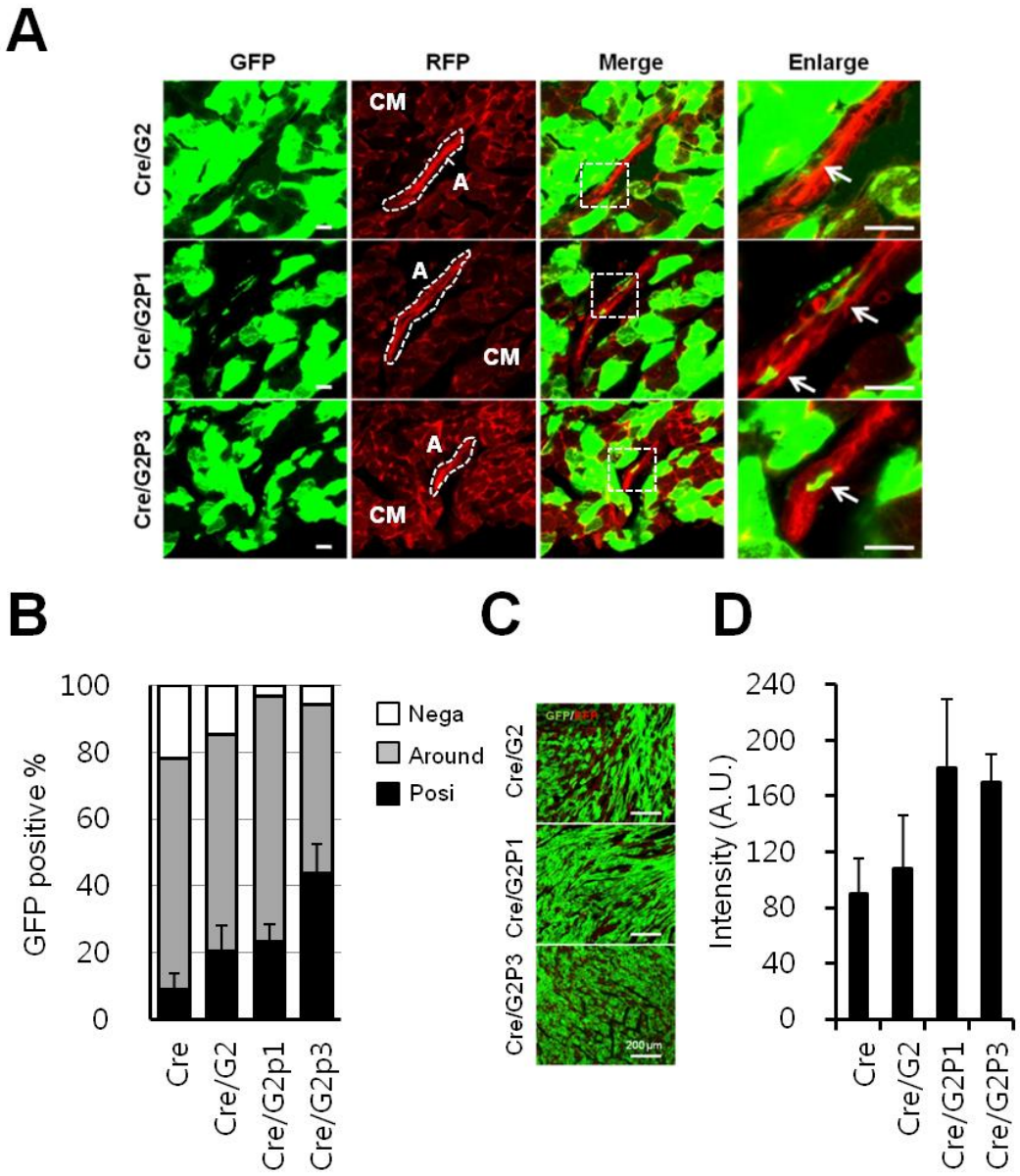

Figure 28 | Transduction efficacy of AAV2/9Cre/G2P1 or AAV2/9Cre/G2P3 in dTomato mice. A, Transduction efficacy in the cardiac artery. The white arrows were indicated Cre positive expression (green) in endothelium of cardiac artery. GFP; Cre positive expression, RFP; dtomato gene expression, merge; GFP with RFP, enlarge; 3 fold large image of white dashed line square box, A; arteries (white dashed line), CM; cardiomyocyte, scale bar; 200 μm. **B**, Demonstration of Cre positive revel (percentage; Cre positive expressed arteries per total arteries), as shown in A. posi (black bars); Cre positive expression in endothelium of arteries, around (gray bars); Cre positive expression of cardiomyocyte in near arteries area, nega (strip bars); Cre negative expression. Values represent the mean ± SD (n=3). **C**, Transduction efficacy in the cardiomyocyte. GFP; Cre positive expression, scale bar; 200 μm. **D**, Intensity (A.U.; arbitrary units) of GFP expression per total RFP area, as shown in **C)**. Values represent the mean ± SD (n=3).

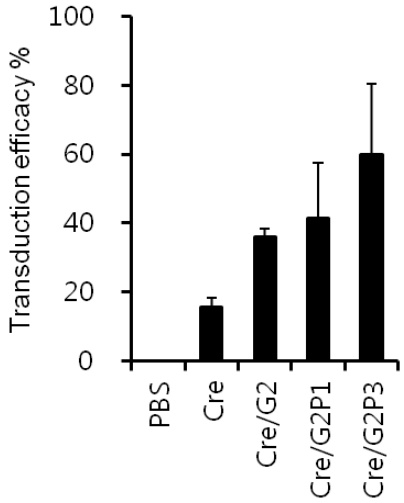

Figure 29 | Whole heart analysis of dTomato mice by FACS. Mouse whole heart dissociated and stained for endothelial cell (PerCP conjugated CD31) after 21 days i.v. injection. Isotype control staining was performed with IgG2a K PerCP. GFP+ cells per total endothelial cells (CD31+), as shown main groups (PBS, Cre, Cre/G2, Cre/G2P1 or Cre/G2P3). Values represent the mean ± SD (n=3).

3.15. Functional evidene for endothelial transduction by AAV2/9-S1FG/G2P3: an in vivo adhesion assay

In order to prove that Cre/C2P3 is capable of endothelial transduction, we selected a transgene which exerts its function only when represented on the luminal surface of the endothelial layer. The fusion protein S1FG is an artificial adhesion molecule based on the SDF-1 (CXCL12) and the mucin backbone taken from fractalkine (CX3CL1). A GPI-anchor was included to link the fusion protein (Figure 30-A) [55]. We compared mice systemically treated with endothelial-targeted Cre/G2P2 with wildtype Cre and saline injection (control). As a read out, non-stimulated adhesion of PMN on the endothelium (cremaster muscle area) was quantified by intravital microscopy 21 days after virus injection. The cremaster venules images were processed by intravital microscopy, a BX 51 WI microscope (Olympus, Munich, Germany) equipped with a charge-coupled device camera (KAPPA CF8 HS) [54], and analyzed by image J v1.47. In this model, the number of adherent neutrophil was more than 5-fold increased in the S1FG/G2P3 group compared with non-coated group S1FG-AAV group and control group, Figure 30-B & C.

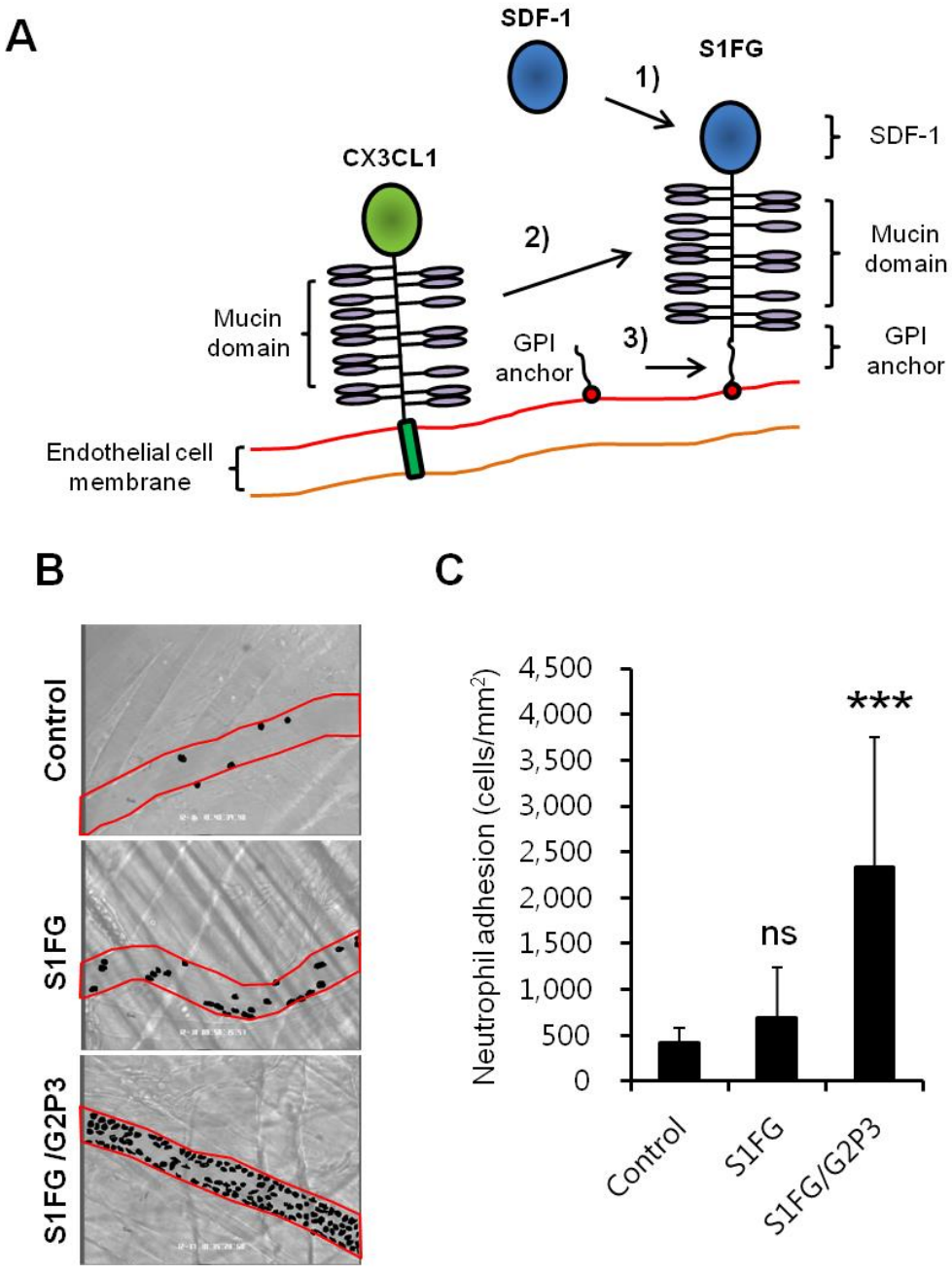

Figure 30 | Functionality of the S1FG fusion protein by intravital microscopy. A, A fusion protein S1FG combined of SDF-1 **1)**, the mucin domain of CX3CL1 **2)**, and the GPI-anchor **3)** [55]. **B**, S1FG enhances adhesion of neutrophil (black dot) in cremaster muscle venules (red box). **C**, Adhesion of neutrophil showed a significant increase with G2P3 coated AAV2/9-S1FG manner. Values represent the mean ± SD (n=4; ns: not significant, ***: P<0.0005, ANOVA t test).

4. DISCUSSION

In the last 15 years, various research groups studied endothelial targeted gene delivery systems by using screening systems. Several approaches engineered AAV2 vectors by expressing phage display peptide libraries on the envelope surface and selecting peptides. Whereas Stuart Nicklin and colleagues focused on human endothelial cells in vitro (Nicklin SA et al., Mol Ther 2001 [49]), Lorraine Work from the same group accomplished improved transduction of lung endothelia in vivo (Work LM et al., Mol Ther 2006 [50]), Yong Hong Chen and coworkers improved brain endothelial transduction and cerebral disease symptoms (cf. Chen YH et al., Nat Med 2009 [47]) and Oliver Müller et al. focused on coronary endothelium (Müller-OJ, Kleinschmidt, Trepel-M et al., Nat Biotech 2003 [51]) by displaying peptides on the surface of the AAV2 envelope. However, direct proof of virus expression on endothelial cells in vivo was not obtained in these earlier studies.

Since AAV serotype 9 was discovered meanwhile, demonstrating efficient transduction of the heart (Zincarelli Carmela et al., Mol Ther 2008 [83]), we focused on this novel envelope, however, leaving the genetic elements of AAV2 in place for biosafety (AAV2 being viewed as not human-pathogenic).

In the current study, we utilized a novel AAV2/9 virus strain to target primary human coronary artery endothelial cells by combining AAV display peptide libraries studies with nanoparticle (PAMAM dendrimer) coating and peptide linkage to the dendrimers for the first time.

4.1. Nanoparticle coating

First, we assessed the role of the chosen biodegradable cationic nanoparticles (polyaminoamide = PAMAM dendrimers), consisting of a diaminobutane as core and branched polyethylenimine of second or fifth generation (termed G2 or G5). We found that coating the AAV2/9 virus capsid with PAMAMs increased transduction of

cardiomyocytic and endothelial cell lines alike in vitro (Fig. 17). This increased transduction efficacy was found for both, the smaller G2 and the larger, wider branched G5 PAMAMs in vitro (Fig.18) and comprised AAV2/6 and AAV2/9 virus pseudostrains. Moreover, cardiomyocyte and endothelial cell transduction was improved in vivo (Fig. 26). Surprisingly, the liver did not display unequivocal results, showing enhanced transduction after G2 than G5 coated AAV2/9 transduction.

Taken together, this observation is in accordance with results from the tumor field, that PAMAM dendrimers facilitate entry into cells which otherwise escape drug therapy, with either antibody or siRNA or pharmacological agents (lit. Wang C et al., Sci Rep 2015 [61]; Ionov M et al., Int J Pharm 2015 [62]; Khatri S et al., J Pharm Bioallied Sci 2014 [63]). However, it should be noted that these biodegradable organic nanoparticles contain biotoxicity, as observed in a topical skin application model recently (Winnicka K et al., Drug Des Devel Ther 2015 [64]) or in vitro cell culture systems (e.g. Movellan J et al., Macromol Biosci 2015 [65]). These observations may explain why a higher rate of dTomato mice was lost during the 21d follow up after transduction when G2 PAMAM nanoparticles were applied (data not shown). However, this study was intended as a proof of principle study, with the concern of biosafety lying still ahead.

4.2. Negative selection by surface-displayed endothelial-targeting peptides

Previously, Varadi K et al. (Varadi K et al., Gene Therapy 2012 [24]) studied peptide modification of the AAV2/9 virus envelope in vitro and reported a ca. 200 times higher transfection efficacy with expression of the SLRSPPS peptide (Ser-Leu-Arg-Ser-Pro-Pro-Ser) than the native envelope in vitro. However, when used in vivo, this virus-peptide combination (termed EndoCre in our study, cooperation OJ. Müller, Heidelberg) did not transduce endothelial cells of the coronary (Fig. 27 & 29) or peripheral microcirculation (Fig. S7) beyond the rate of AAV2/9 wildtype transduction. Thus, a positive selection towards the endothelial cell compartment was not provided by

the SLRSPPS peptide expressed directly on the surface of an AAV2/9 virus envelope. This result confirms the ambiguous results previous attempts to achieve AAV-based microvascular endothelial transduction by direct capsid modification (Nicklin et al., Work et al., Müller et al.) and points to a difference between micro- and macrovessel transduction (e.g. umbilical veins, cf. Varadi K et al., Gene Therapy 2012 [24]) provided by the same vector.

On the other hand, modification of the virus envelope by surface expression of the SLRSPPS peptide (=EndoCre) sufficed to disrupt cardiomyocyte transduction efficacy of the AAV2/9. The cardiomyocyte compartment was shielded from the SLRSPPS-modified envelope of the vector (cf. Fig. 27 C, D), pointing to a negative selection provided by this capsid modification. This finding confirms the fact that envelope structure is decisive for the myotropism of the AAV9 serotype, whose envelope is used in the AAV2/9 pseudotype virus.

4.3. Peptide selection for endothelial targeting

Since other peptides displayed limited efficacy in vivo, we decided to perform our own selection of an endothelial affine peptide. We chose to select for transduction of human endothelial cells (umbilical vein-derived = HUVECs and microvascular = HMECs). An own phage display selection experiment using the M13 CX7C (C; cystein, X; random 7-mer aa) phage display library system (Fig. 19 - 21), followed by 3 rounds of biopanning in an endothelial cell culture (cf. Methods, 2.2.4. panning) yielded 10 peptides. After comparison of both, HUVEC and HMEC transduction as well as homology screening (Fig.21, Table 4), Peptide 3 (CNNSGMRN) was selected. For comparability reasons, we used the SLRSPPS peptide from O. Müller (Heidelberg) as a control peptide.

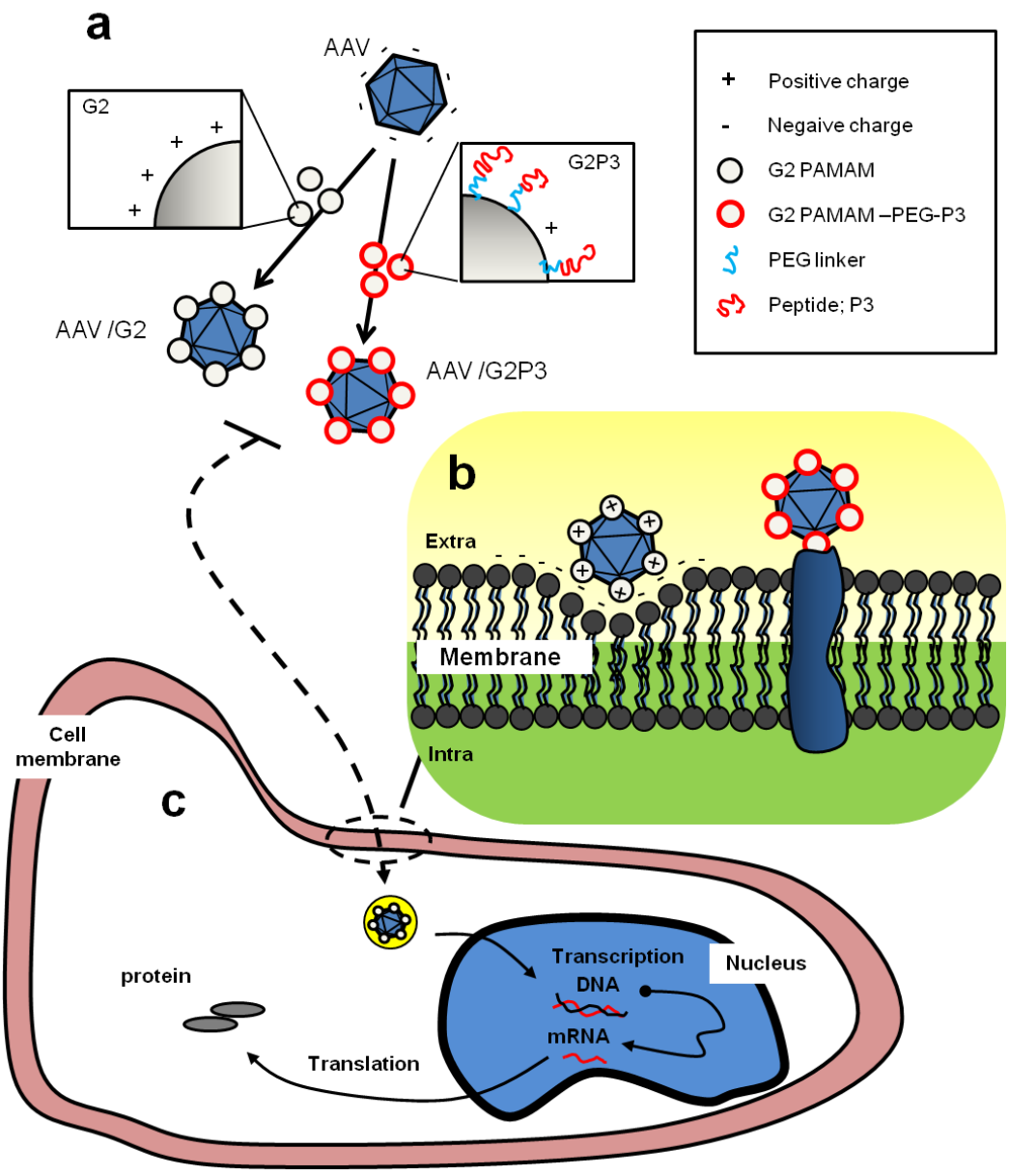

Figure 31 | Schematic representation of cellular uptake by AAV/PAMAM complexes. a, AAV/G2 PAMAM or AAV/surface modified-G2 PAMAM complexes. **b,** Cell membrane targeting by a complexes. **c,** The cellular uptake in endothelial cell [56]. G2: generation 2 PAMAM, G5: generation 5 PAMAM, AAV: adeno associated virus.

4.4. Positive selection by PAMAM-linked endothelial targeting peptides

In a next step, targeting of endothelial cells was successfully performed with achieved with the endothelial cell binding peptide P3 (Asn-Asn-Ser-Gly-Met-Arg-Asn: NNSGMRN), covalently coupled to the G2 PAMAM via a 2 kDa PEG linker (Fig. 31). After combining our own selected P3 with PAMAMs using the PEG-linker, we found for the first time a positive selection effect on endothelial targeting in vivo in coronary microvessels (Fig. 27 & 28). A similar, though slightly less efficient transduction was found, when SLRSPPS (=P1) was linked to PAMAMs, which then were fused to the AAV2/9 envelope.

It is noteworthy that most of the difference obtained between the EndoCre vector (expressing P1 on the surface of the virus envelope) and the AAV/G2P1 vector (displaying P1 on the G2 PAMAM) mainly was the localization of the P1 peptide. Thus, we could demonstrate with the same targeting peptide, that presentation on the tip of a positively charged nanoparticle is superior to the presentation on the virus envelope. Further studies are required to assess whether the positive charge is the main targeting virtue of the nano-particle or whether other (molecular) mechanisms are involved in increasing the transduction efficacy of endothelial cells.

Of note, PAMAM surface modified vectors (Cre/G2P1 and Cre/G2P3) did not lose their ability to efficiently transduce cardiomyocytes. This observation stands in contrast to the weak cardiomyocyte transduction of EndoCre vectors and points to a two step model of virus transduction: whereas the AAV2/9 coat itself suffices for high cardiomyocyte affinity, direct virus coat modification with P1 (=EndoCre) disrupt this behavior (negative selection). However, the repulsion of vectors from cardiomyocytes in itself does not increase endothelial transduction. For this process, positive selection towards endothelial cells is needed, e.g. by a combination of nano-particles with endothelial targeted peptides (e.g. Cre/G2P3 or Cre/G2P1). In future work remodeling

surface of the nano-particles may optimize our approach, such as a half side displayed cationic PAMAM dendron is coupled with another half side displaying the endothelial-targeting peptides (P1 or P3).

4.5. Endothelial targeting: Functional proof of transduction

In previous study, the claim of endothelial transduction was derived from in vitro results and occasional fluorescence microscopy imaging. Rigid ex vivo tracing of transduced endothelial cells as well as functional in vivo bioassays were scarce.

In order to improve accuracy of the claim of endothelial retargeting of an AAV, we developed two test systems: first, a FACS passed assessment of a transduction-dependent recombination event (Cre-based switch from red to green fluorescence) in CD31-positive cells digested from whole hearts of AAV-Cre transduced tomato mice (cf. Fig. 29). In this test system, we confirmed our fluorescence-imaging result in that the combination of G2 PAMAMs and P3 is efficiently transducing coronary microvascular endothelial cells to a higher extent than G2/P1.

Second, we used a novel and unique test system. The basis of this system is an artificial adhesion molecule which – by virtue of its function, recruiting circulating CXCR4 expressing cells, e.g. neutrophils – requires presentation on the luminal surface of an endothelial cell. The artificial adhesion molecule (S1FG) consists of a fusion protein coupling SDF-1/CXCL12 to the mucin backbone domain of fractalkine/CXCL12 and a GPI-membrane anchor. This artificial adhesion molecule has been shown to mediate adhesion of cells expressing CXCR4, the receptor for the SDF-1 ligand (Stachel G et al., Stem cells 2013 [55]). It consists of an SDF-1 chemokine head fused to the mucin domain from fractalkine/CXCL12, which can provide leukocyte recruitment, and a GPI-membrane anchor allowing for firm attachment to the cell membrane, without an intracellular signaling domain (Stachel G et al., Stem cells 2013 [55]).

SDF-1 is well known to mediate neutrophil recruitment via its receptor, CXCR4 (Strydom N et al., Journal of Innate Immunity 2013 [66]; Liehn EA et al., J Am Coll

Cardiol 2011 [67]). We capitalized on the neutrophil-attracting function of this chemokine head by displaying it on an artificial adhesion molecule, which can only exert its purpose when displayed at the luminal site of the endothelium, but not when expressed on the myocytes, as usually accomplished by the unmodified AAV2/9. We followed this process by in vivo microscopy in the cremaster-muscle (cooperation M. Sperandio, WBEx LMU). According to our prediction of a significant increase of endothelial transduction of the AAV2/9-G2P3 compared to the unmodified AAV2/9 pseudotype, neutrophil adhesion to the endothelium of cremaster arterioles was increased by 5.62 fold (Fig. 30). This proof of principle indicates that indeed we were able to display a functionally active adhesion molecule towards the blood flow, and thereby induced firm adhesion of circulating neutrophils. This proof of principle by far exceeds previous experimental approaches, usually histologies of reporter gene expression in anatomical positions suitable with the endothelial lining (White SJ et al., Circ 2004 [48]; Varadi K et al., Gene Ther 2012 [24]). Given notorious difficulties to properly identify endothelial cells without further markers from histological sections, functional testing of unequivocal endothelial properties might be viewed as a more rigid form of proof in this regard.

In summary, we report retargeting of the myotropism of AAV2/9 by displaying endothelial-affine targeting peptides on G2-dendrimers which were fused to the AAV2/9 capsid. G2-P3 fusion to AAV2/9 increased the endothelial transduction rate and provided a 5.6 fold increase of the functionally relevant endothelial expression of S1FG, an artificial adhesion molecule effective only when displayed on the luminal surface of the endothelial lining.

4.6. Endothelial targeting motif of P3 (CNNSGMRN)

Having established a functional role of the newly found peptide CNNSGMRN, we further analyzed the potential molecular mechanism of its endothelial affinity. We found a distinct homology to Stabilin-2.

The Stabilin-2 (as named STAB-2 or endothelial protein) is a high molecular-mass multifunctional transmembrane receptor protein which contains four repeat units (RU), each containing epidermal growth factor (EGF)-like domains (cell/matrix interactions), integrin-binding fasciclin 1(FAS1) domains (protein/protein interactions) and X-link domain (hyaluronic acid binding) in extracellular region. In more detail, four laminin-type EGF-like domains, seven fasciclin-like adhesion domains, three B-(X_7)-B hyaluronan-binding domains, fifteen EGF-like domains, one X-link domain, and one transmembrane region located on the end of C-terminal (cf. Oliver Politz et al., Biochem J 2002 [68]; Kai Schledzewski et al., JCI 2011 [75]). The endothelial targeting peptide P3 (CNNSGMRN) is almost entirely homolog (5 of 6 AA) to the sequence located on the 4^{th} of RU laminin EGF-like domains of mouse Stabilin-2 (GenBank: AAL91684.2), as shown in Fig -32.

Laminin is a major protein of the extracellular membranes that mediate cell adhesion and differentiation. Furthermore, Laminin EGF-like (known as a LE) domains are structural elements of membrane-bound proteins or proteins known to be secreted. They contain repeats of each laminin subunit and the 3D structure of this domain is similar in EGF-like module. The LE domain has been shown to bind with a high affinity to nidogen (a component of the basement membrane).

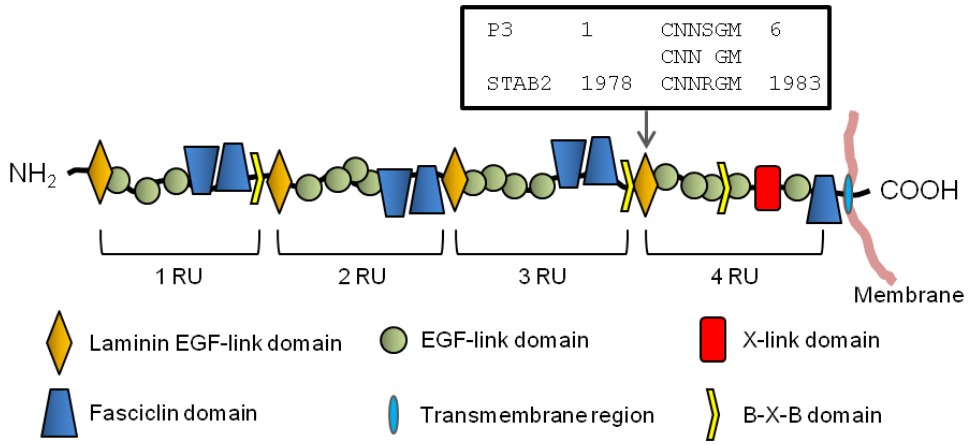

Figure 32 | Domain structure of mStabilin-2. (Modified from Oliver Politz et al., Biochem J 2002 [68]; Seung-Yoon Park et al., Mol Cell Biol 2008 [70]).

The mSTAB-2 is primarily expressed at high level in the sinusoidal endothelial cells of lymph node, liver, spleen, and low level in the heart. Comparison of the full length human protein sequences with mouse STAB-2 gave an identity of 71-79%, as human STAB-2 (cf. Oliver Politz et al., Biochem J 2002 [68]; Kai Schledzewski et al., JCI 2011 [75]). It exerts functions in angiogenesis, receptor scavenging, lymphocyte homing, phagocytosis and cell adhesion (cf. MY Jung et al., Journal of Leukocyte Biology 2007 [69]). The protein interacts with the integrin αMβ2 or αvβ5 which mediate lymphocyte adhesion to the liver sinusoidal endothelium or engulfment of phosphatidylserine (abbreviated Ptd-L-Ser or PS) exposed erythrocytes (cf. Sandra J. Stoll et al., PLOS ONE 2013 [71]; Kim S et al., Mol Cell Biol 2012 [72]; Sung-Jin Lee et al., BLOOD 2011 [74]). It binds to and mediates endocytosis of hyaluronic acid (Megan S. Rost et al., PLOS ONE 2013 [73]; Kai Schledzewski et al., JCI 2011 [75]), and binding to PS receptor enhances the engulfment of apoptotic cells and critical anti-imflammatory fuctions of macrophages (Park SY et al., Mol Cell Biol 2008 [70]; Kim S et al., Mol Cell Biol 2012 [72]). Additionally, it acts as a scavenger receptor for dermatan sulfate (DS), non-glycosaminoglycan (GAG), acetylated low-density lipoprotein (AcLDL), chondroitin sulfate (CS), pro-collagen propeptides and advanced glycation end products

(AGE), and heparin (Hep). The protein was shown to exer several functions in application studies, such as Stabilin-2/HARE mediates systemic clearance of multiple glycosaminoglycans (GAGs) from the vascular and lymphatic circulations. Furthermore, the HA-NPs (HA/nanoparticle complex) study showed the atherosclerotic area via the active targeting procedure. It has been expecting to high potential as the carrier for diagnosis and therapy of atherosclerosis (cf. Lee GY et al., Biomaterials 2015 [76]).

Additionally, the endothelial cell target P3 has homologs located on other proteins, such as neuromedin-B receptor (NMBR), transcription factor AP-2-beta (AP2B), TP53-target gene 5 protein (T53G5), and huntingtin-interacting protein M (HYPM), as shown in Table 5.

Name	Term	5'-	aa sequence	-3'	Length	SP ID
Peptide no.3	P3	1	**CNNSGMRN**	8	8	
Stabilin-2	STAB-2	1978	**CNN**R**GM**..	1983	2559	Q8R4U0
Neuromedin-B receptor	NMBR	71	..**NS**A**MRN**	76	390	O54799
Transcription factor AP-2-beta	AP2B	186	.**NNSGM**..	190	459	Q61313
TP53-target gene 5 protein	T53G5	135	...**SGMRN**	139	290	Q9Y2B4
Huntingtin-interacting protein M	HYPM	74	.**NN**GS**MRN**	80	117	O75409

Table 5 | Other homologous sequence with P3. The under lines are indicate that unmatched aa sequences of endothelial target peptide no.3 compare with other candidate. SP ID; Swiss-Prot ID.

Neuromedin-B receptor (NMBR) is a G protein-linked receptor (GPLR) which endogenous ligand is neuromedin B, such as a subfamily of mammalian bombesin-like peptides (cf. Corjay MH et al., J Biol Chem 1991 [77]; Sainz E et al., J Biol Chem 1998 [82]). The NMBR binds NMB and regulates cell growth, blood pressure, exocrine/endocrine secretions, and glucose level. The receptor has highly affinity with mitogen and growth factor for normal and neoplastic lung.

Transcription factor AP-2 beta (TFAP2B) is an activating enhancer binding protein 2 beta) gene provides instructions for making a protein. A transcription factor is a protein that binds to specific regions of DNA and helps control the activity of particular genes. Transcription factor AP-2β is involved in development in the neural crest. Neural crest

cells migrate to form portions of the nervous system, glands that produce hormones, pigment cells, smooth muscle and other tissues in the heart, and many tissues in the face and skull. Transcription factor AP-2β also appears to play an important role in the development of the limbs. (Feng Zhao et al., Am J Hum Genet 2001 [78]; Shiro Maeda et al., J Hum Genet 2005 [79]).

The p53 regulates growth arrest, tumor suppressor, and apoptosis mediated genes in response to stress signals. It is influencing programmed cell cycle, differentiation, death control mechanisms. TP53-target gene 5 protein (TP53TG5) also known as TP53-inducible gene 5 protein modulates p53 signaling pathways. This protein is highly expressed in brain, small intestine and heart (Isaka S et al., Genes Chromosomes Cancer 2000 [84]).

The hallmark neuropathology of Huntington's disease (HD) is expansion of a polyglutamine segment in huntingtin. Huntingtin interacting protein M, as named HYPM, shown to interact with huntingtin. This protein contains a polyglutamine tract in Huntington's disease. (Peter W. faver et al., Hum Mol Genet 1998 [80]).

It remains to be determined whether P3 exerts its functions due to a Stabilin-2 like function, whereas due to location, time of expression, and type of distribution, other homologies like NMBR, TFAP2ß, TP53TG5 or HYPM appear as less likely candidates for functional homology.

In summary, we report retargeting of the myotropism of AAV2/9 by displaying endothelial-affine targeting peptides on G2 or G5 PAMAM dendrimers which were fused to the AAV2/9 capsid. G2-P3 fusion to AAV2/9 increased the endothelial transduction rate and provided a more than 5-fold increase of the functionally relevant endothelial expression of S1FG, an artificial adhesion molecule effective only when displayed on the luminal surface of the endothelial lining. Thus, in this study we could demonstrate efficient expression of AAV-transduced genes of interest in vitro and in vivo. This finding could be of importance for further use of the AAV vector platform in a variety of experimental models and patient diseases, to provide for example vessel

growth (in ischemia) or vessel degradation (in tumor vessels) as well as vessel regulation (in endothelial dysfunction and vasospasm).

5. SUMMARY

The identification of cell type specific binding ligands and improved transduction efficacy of vector systems (viral or non-viral) are needed for endothelial directed gene therapy. Adeno-associated viral (AAV) vectors are widely used for a long lasting efficacy and low immunogenicity. However, application of this vector in vascular biology is hampered by low transduction rates for vascular and particularly endothelial cells. Here, we attempted to enhance endothelium specificity of AAV based cardiac gene therapy via surface modification of the vector coat. Two principles were combined: first, a 7-mer endothelium targeting peptide, termed P3, was identified in biopanning with a CX7C phage library. Secondly, nanoparticles (generation 2 and 5 PAMAM dendrimers) were coated on the virus envelope surface. Combination of both approaches in an AAV2/9 G2P3 vector enhanced transduction in cardiac and skeletal muscle endothelial cells. Moreover, AAV2/9 G2P3 encoding for an artificial adhesion molecule (S1FG, cf. Stachel et al., Stem cells 2013) was efficient in recruiting circulating leukocytes in a cremaster intra vital microscopy model, whereas an unmodified AAV2/9 encoding for the same transgene did not yield this effect. These results appear as a proof of principle of AAV targeting towards endothelial cells and may have a broad range of applications in biotechnology and nanotechnology.

6. FIGUERS AND TABLES

7. APPENDIX

7.1. Abbreviations

A.U.	astronomical unit
Aa	amino acid
AAV	adeno-associated virus
ACE	angiotensin-converting enzyme
Ad	Adenovirus
APC	antigen presenting cell
ATP	adenosine triphosphate
bEnd.3	mouse brain endothelial cell line
BL	Burkitt's lymphoma
bp	base pair
CAR	coxsackie and adenovirus receptor
cDNA	complementary deoxyribonucleic acid
CO_2	Carbondioxide
DAB	3,3'- Diaminobenzidine
DAPI	4, 6-diamidino-2-phenylindole
DC	dendritic cells
dd	double distilled
DMEM	Dulbecco's Modified Eagle Medium
DMSO	Dimethylsulfoxide
DNA	deoxyribonucleic acid
DTT	Dithiothreitol
E.coli	Escherichia coli
e.g.	lat. Exempli gratia ("for example")
EDTA	ethylenediaminetetraacetic acid

ELISA	enzyme-linked immunosorbent assay
FACS	fluorescence-activated cell sorting
FCS	fetal calf serum
FGFR	fibroblast growth factor receptor
FITC	fluorescein isothiocyanate
g	Gram
g.p.	genomic particles
G2	generation 2 PAMAM dendrimer
G2P1	generation 2 PAMAM -PEG linker -Peptide no.1
G2P3	generation 2 PAMAM -PEG linker -Peptide no.3
G5	generation 5 PAMAM dendrimer
GER	Germany
GFP	green fluorescence protein
Gp	Glycoprotein
h	hour(s)
H&E	hematoxyline and eosin
H_2O	Water
HEK 293	human embryonic kidney cell line
HGFR	hepatocyte growth factor receptor
HL-1	mouse cardiomyocyte cell line
HMECs	human microvascular endothelial cells
HRP	horseradish peroxidase
HSPG	heparan sulphate proteoglycan
i.e.	lat. id est (“that is”)
Ig	Immunoglobulin
IL	Interleukin
IM	infectious mononucleosis
IPTG	isopropyl-1-thio-β-D-galactoside

ITR	inverted terminal repeat
Kb	kilo bases
KCl	potassium chloride
kDa	kilo dalton
l	Liter
LB	Luria Bertani
LCL	lymphoblastoid cell line
LDL(R)	low-density lipoprotein (receptor)
LMP	latent membrane protein
M	Molar
MA	muscular arteries
mg	milligram (1.0E-03 gram)
$MgCl_2$	magnesium chloride
$MgSO_4$	magnesium sulfate
MHC	major histocompatibility complex
min	minute(s)
ml	Milliliter
MLV	murine leukemia virus
mm	Millimeter
mM	Millimolar
mRNA	messenger ribonucleic acid
Na_2HPO_4	disodium hydrogen phosphate
NaCl	sodium chloride
NaH_2PO_4	sodium dihydrogen phosphate
ng	nanogram (1.0E-09 gram)
nm	Nanometer
NPC	nuclear pore complex
nt	Nucleotide

ºC	degree centigrade
OD	optical density
ORF	open reading frame
p.i.	post infection
p.t.	post transduction
PAMAM	poly-amidoamine
PBS	phosphate buffered saline
PCR	polymerase chain reaction
PE	Phycoerythrin
PEG	Polyethylenglycol
PEG linker	NHS -PEG -OPSS linker
PEI	Polyethylenimine
PFA	Paraformaldehyde
Pfu	plaque forming units
pg	pictogram (1.0E-12 gram)
PHA	Phytohemaglutinin
PI	propidium iodide
qPCR	quantitative PCR
rAAV	recombinant adeno-associated viral vector
RNA	ribonucleic acid
rpm	rotations per minute
RT	room temperature
RT-PCR	reverse transcription-polymerase chain reaction
scFv	single-chain fragment of variable region
SDS	sodium dodecyl sulfate
SMA	alpha smooth muscle actin
SOB	super optimal broth
SOT	solid organ transplantation

TAE	Tris acetate EDTA buffer
TBS	Tris buffered saline
TBST	Tris buffered saline tween-20
TE	Tris-EDTA
TEMED	N,N,N,N-tetramethylethlenediamine
TFA	trifluoroacetic acid
TMB	3,3’,5,5’-tetramethylbenzidine
TNF-α	tumor necrosis factor-alpha
TR	terminal repeat
Tris	tris(hydroxymethyl) aminomethane
Tween-20	polyoxyethylene sorbitane monolaurate
U	unit
VCA	viral capsid antigen
Vp	viral particle
VP	viral protein
X-gal	5-Bromo-4-Chloro-3-Indoyl-b-D-galactopyranosid
µg	microgram (1.0E-06 gram)
µl	Microliter
µM	Micromolar

7.2. Supporting informations

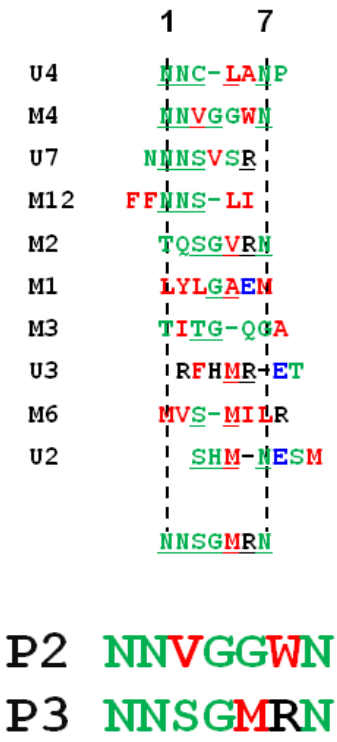

Figure S1 | Alignment analysis of peptide sequences. Alignment analysis program is Clustal W program. **For Fig 21.**

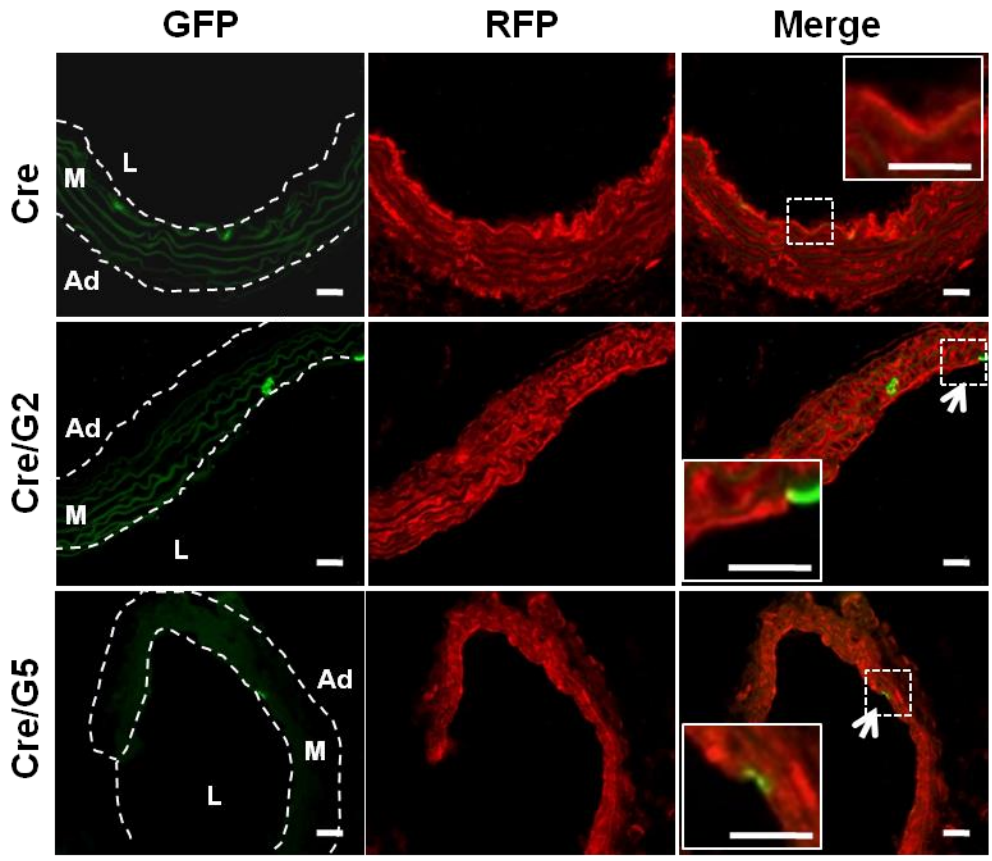

Figure S2 | AAV2/9Cre /G2 or AAV2/9Cre /G5 in elastic artery of dTomato mice. The elastic artery of heart. The white arrows indicate Cre positive expression (green) endothelium in the tunica intima of artery. The white dashed lines are a area of Ad (adventitia of artery), M (media of artery), or L (lumen of artery). Scale Bar; 20 μm. **For Fig 26.**

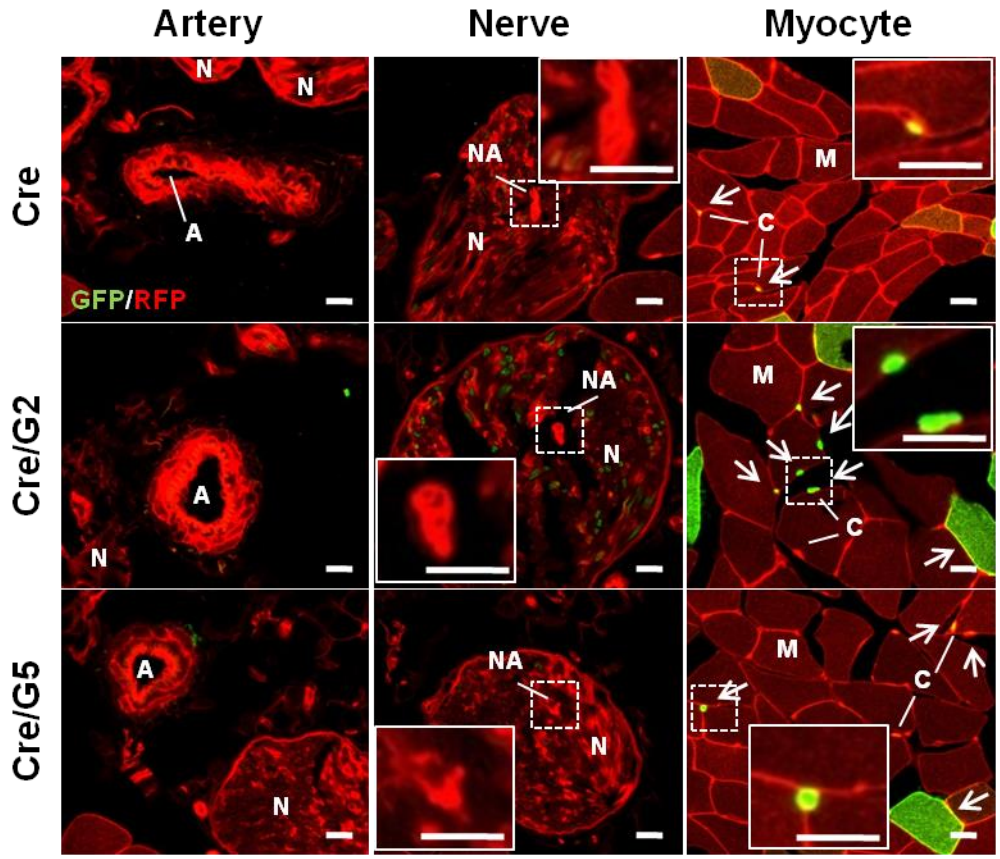

Figure S3 | AAV2/9Cre /G2 or AAV2/9Cre /G5 in hind limb of dTomato mice. The artery (left), nerve (meddle), and myocyte (right) of the hind limb (merge images). The white arrows indicate Cre positive expression (GFP; green) in capillary. A (artery), N (nerve), M (myocyte) or C (capillary). Scale Bar; 20 μm. **For Fig 26.**

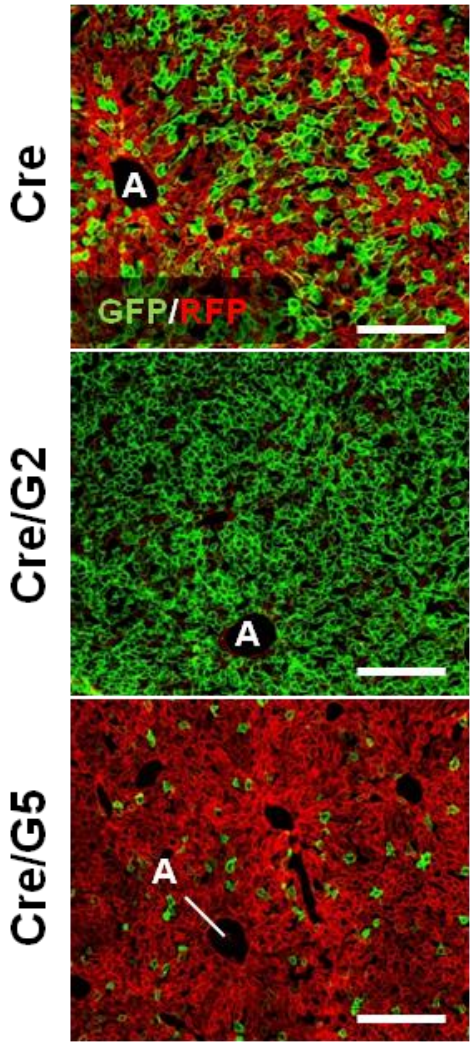

Figure S4 | AAV2/9Cre /G2 or AAV2/9Cre /G5 in liver of dTomato mice. The liver of dTomato mice (merge images). A (artery). Scale Bar; 200 µm. **For Fig 26.**

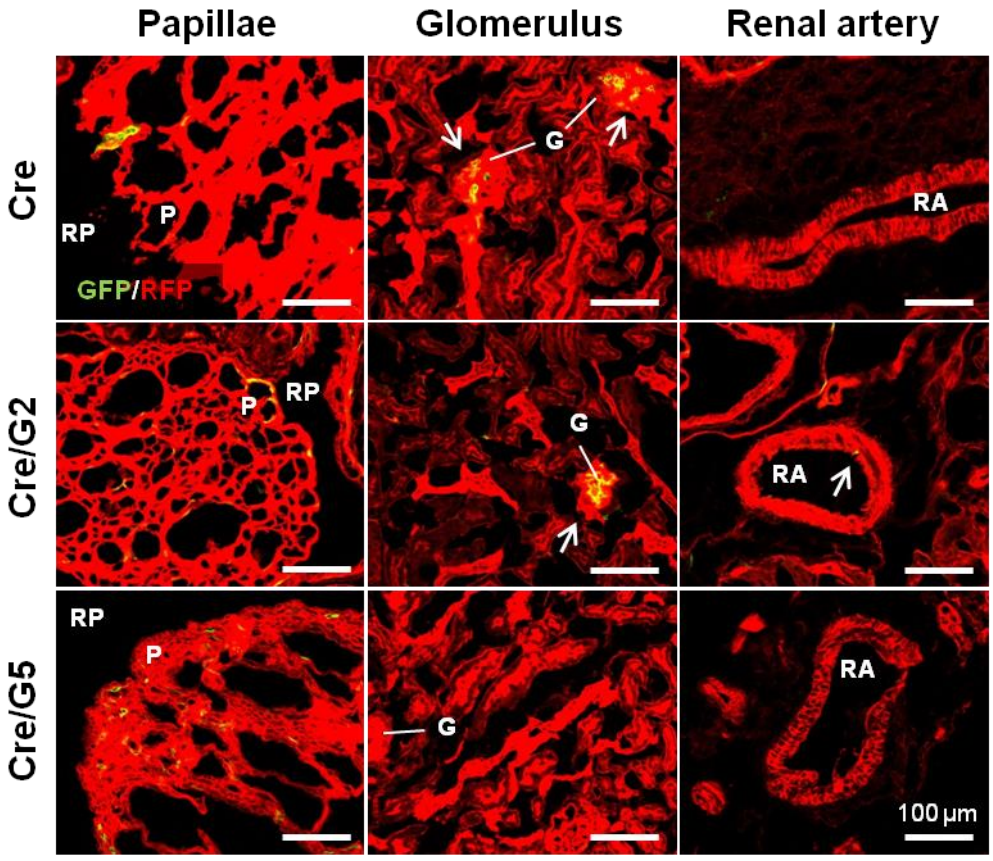

Figure S5 | AAV2/9Cre /G2 or AAV2/9Cre /G5 in kidney of dTomato mice. The papillae (left), glomerulus (meddle), and renal artery (right) of the kidney (merge images). The white arrows indicate Cre positive expression (GFP; green) in glomerulus or renal artery. P (papillae), RP (renal pyramid), G (glomerulus) or RA (renal artery). Scale Bar; 100 μm. **For Fig 26.**

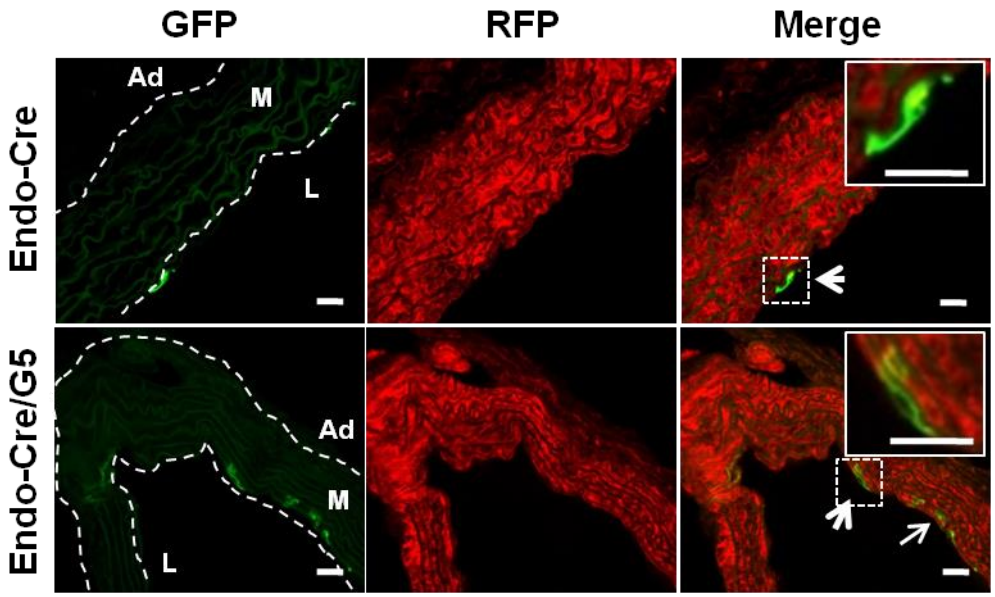

Figure S6 | AAV2/9Endo-Cre /G5 in elastic artery of dTomato mice. The elastic artery of heart. The white arrows indicate Cre positive expression (green) in the tunica intima of artery. The white dashed lines were indicate a area of Ad (adventitia of artery), M (media of artery), or L (lumen of artery). Scale Bar; 20 μm. **For Fig 27.**

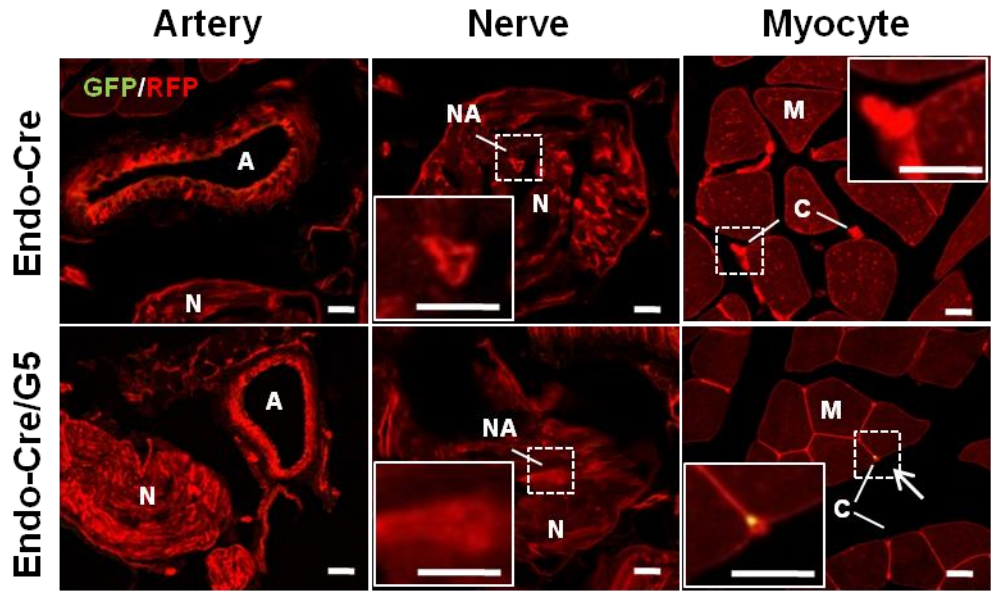

Figure S7 | AAV2/9Endo-Cre /G5 in hind limb of dTomato mice. The artery (left), nerve (meddle), and myocyte (right) of the hind limb. The white arrows were indicated Cre positive expression (GFP; green) in capillary. A (artery), N (nerve), M (myocyte) or C (capillary). Scale Bar; 20 μm. **For Fig 27.**

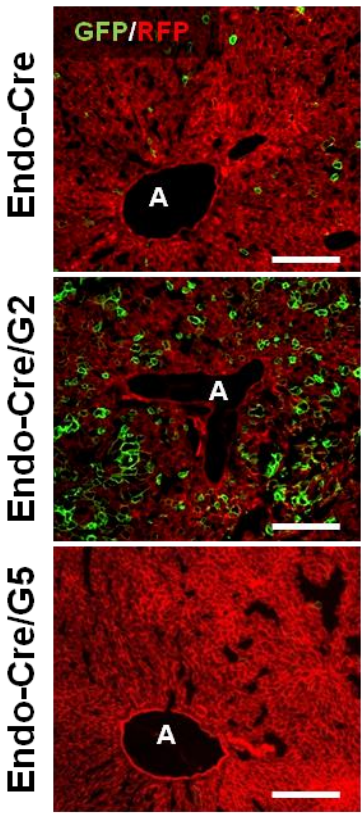

Figure S8 | AAV2/9Endo-Cre /G2 or AAV2/9Endo-Cre /G5 in liver of dTomato mice. The liver of dTomato mice (merge images). A (artery). Scale Bar; 200 μm. **For Fig 27.**

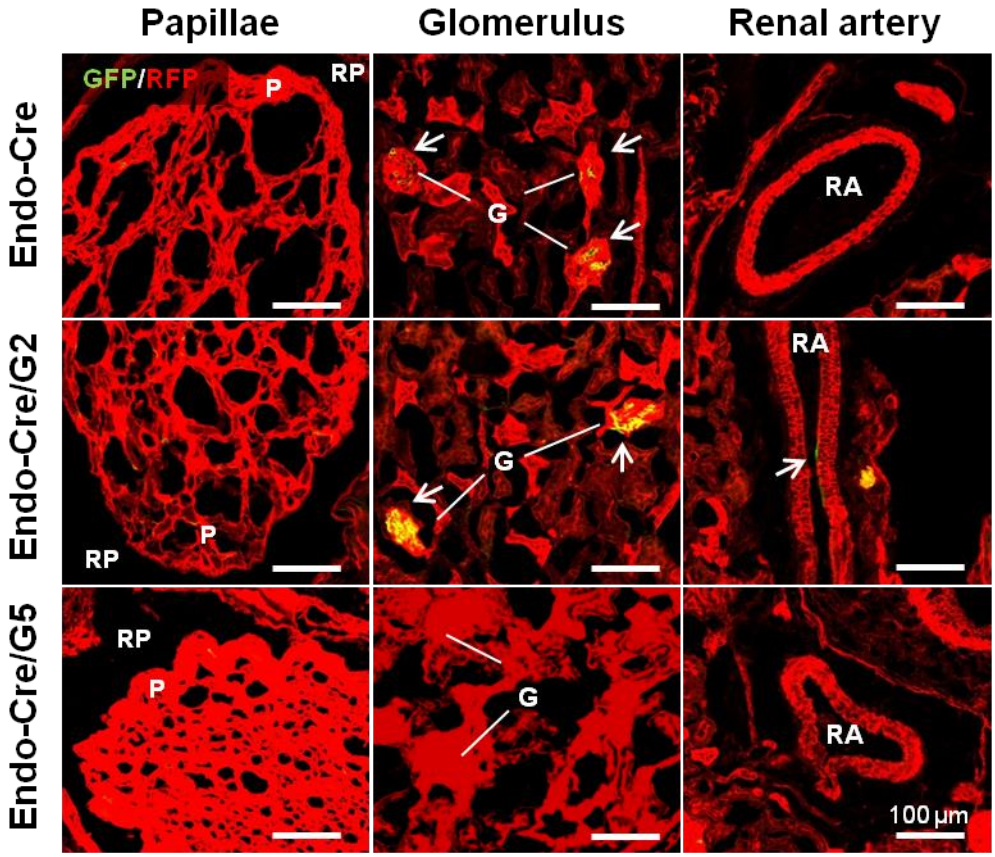

Figure S9 | AAV2/9Endo-Cre /G2 or AAV2/9Endo-Cre /G5 in kidney of dTomato mice. The papillae (left), glomerulus (meddle), and renal artery (right) of the kidney (merge images). The white arrows indicate Cre positive expression (GFP; green) in glomerulus or renal artery. P (papillae), RP (renal pyramid), G (glomerulus) or RA (renal artery). Scale Bar; 100 μm. **For Fig 27.**

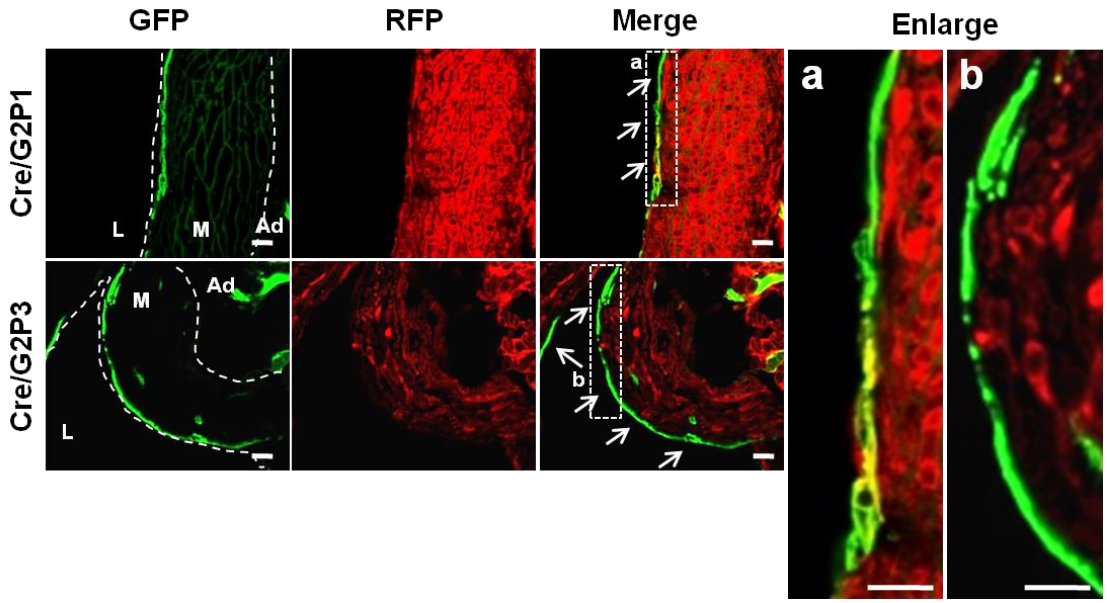

Figure S10 | AAV2/9Cre /G2P1 or AAV2/9Cre /G2P3 in elastic artery of dTomato mice. The elastic artery of heart. The white arrows were indicated Cre positive expression (green) in the tunica intima of aortic artery. The white dashed lines were indicate a area of Ad (adventitia of artery), M (media of artery), or L (lumen of artery). Scale Bar; 20 μm. **For Fig 28.**

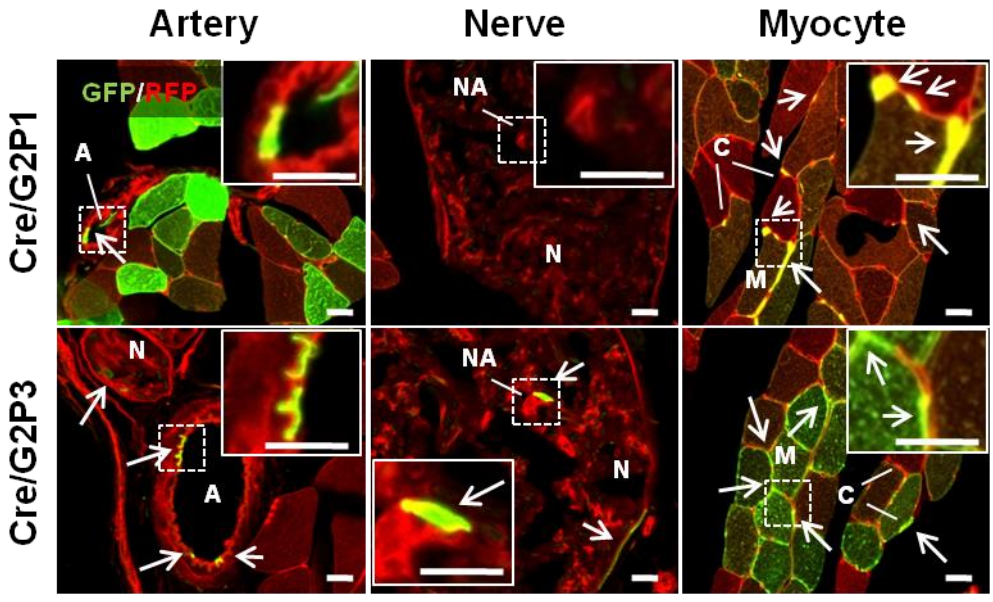

Figure S11 | AAV2/9Cre /G2P1 or AAV2/9Cre /G2P3 in hind limb of dTomato mice. The artery (left), nerve (meddle), and myocyte (right) of the hind limb. The white arrows were indicated Cre positive expression (GFP; green) in capillary. A (artery), N (nerve), M (myocyte) or C (capillary). Scale Bar; 20 μm. **For Fig 28.**

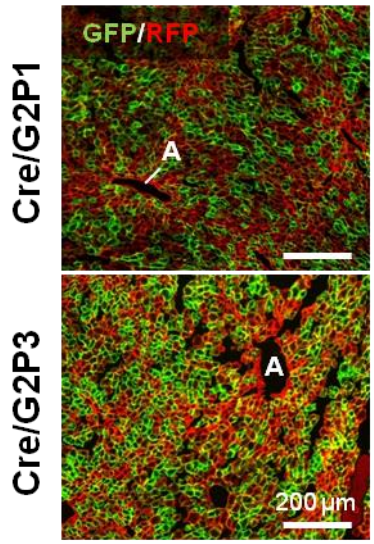

Figure S12 | AAV2/9Cre /G2P1 or AAV2/9Cre /G2P3 in liver of dTomato mice. The liver of dTomato mice (merge images). A (artery). Scale Bar; 200 μm. **For Fig 28.**

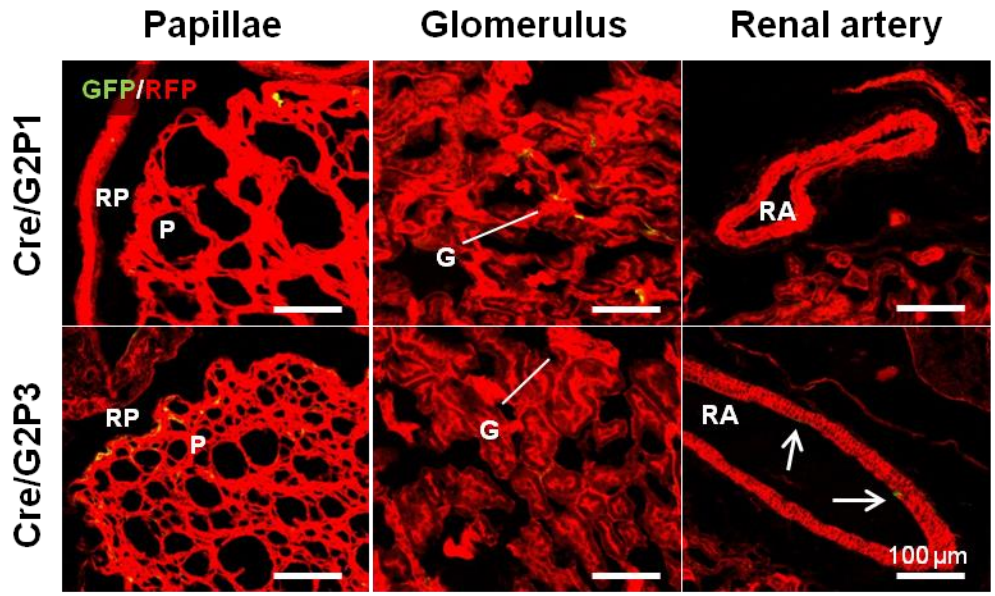

Figure S13 | AAV2/9Cre /G2P1 or AAV2/9Cre /G2P3 in kidney of dTomato mice. The papillae (left), glomerulus (meddle), and renal artery (right) of the kidney (merge images). The white arrows indicate Cre positive expression (GFP; green) in glomerulus or renal artery. P (papillae), RP (renal pyramid), G (glomerulus) or RA (renal artery). Scale Bar; 100 μm. **For Fig 28.**

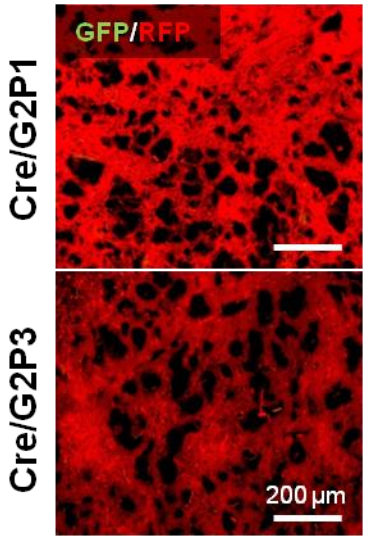

Figure S14 | AAV2/9Cre /G2P1 or AAV2/9Cre /G2P3 in brain of dTomato mice. The brain of dTomato mice (merge images). Scale Bar; 200 μm. **For Fig 28.**

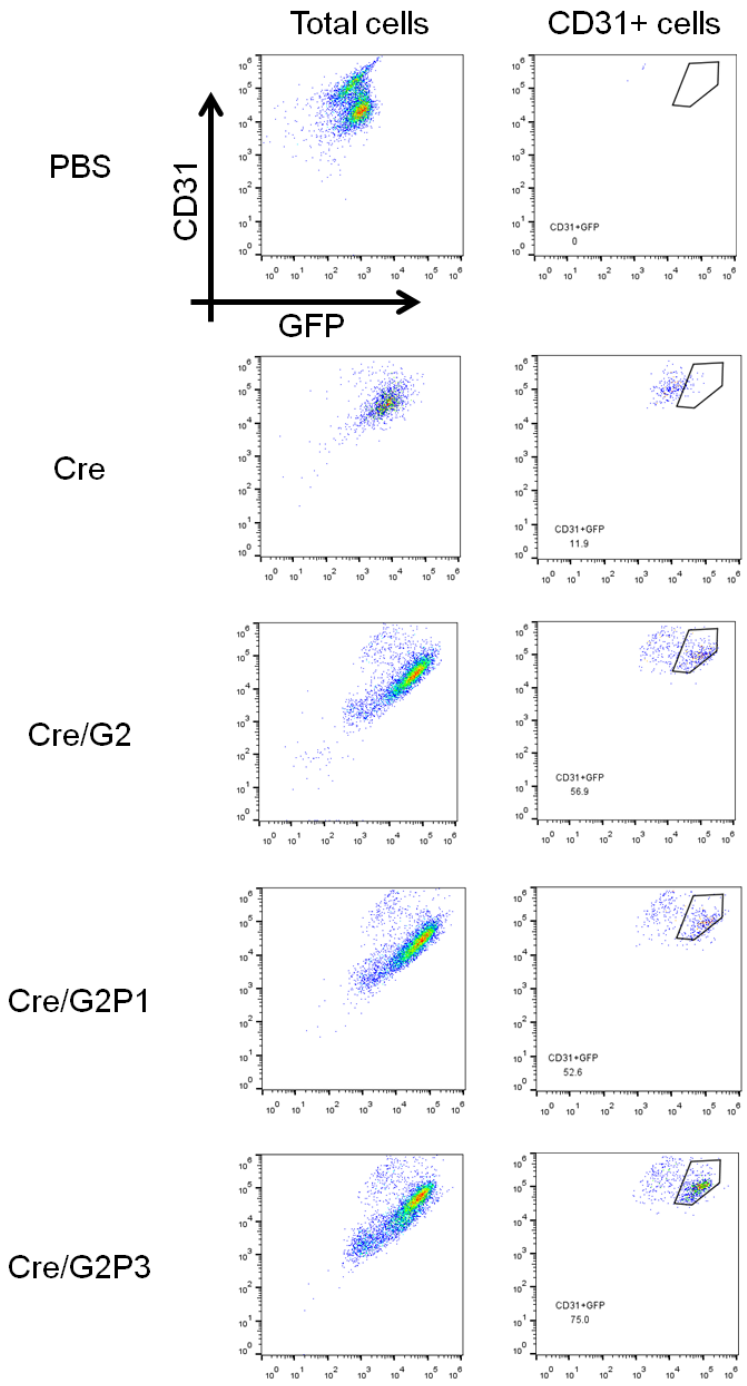

Figure S15 | FACS in whole heart of dTomato mice. For Fig 29.

8. REFERENCES

1. Friedmann T, Roblin R. Gene therapy for human genetic disease? Science 1972; 175(4025): 949-55.
2. Sheridan C. Gene therapy finds its niche. Nat Biotechnol 2011; 29(2): 121-8.
3. Muzumdar MD, Tasic B, Miyamichi K, Li L, Luo L. A global double- fluorescent Cre reporter mouse. Genesis 2007; 45(9): 593-605.
4. Al-Dosari MS, Gao X. Nonviral gene delivery: principle, limitations, and recent progress. AAPS J 2009; 11(4): 671-81.
5. ATCHISON RW, CASTO BC, HAMMON WM. ADENOVIRUS- ASSOCIATED DEFECTIVE VIRUS PARTICLES. Science 1965; 149(3685): 754-6.
6. Gonçalves MA. Adeno-associated virus: from defective virus to effective vector. Virol J 2005; 2(43): 1-17.
7. Tseng YS, Agbandje-McKenna M. Mapping the AAV capsid host antibody response toward the development of second generation gene delivery vectors. Front Immunol 2014; 5(9): 1-11.
8. Dizaj SM, Jafari S, Khosroushahi AY. A sight on the current nanoparticle-based gene delivery vectors. Nanoscale Res Lett 2014; 9(1): 1-9.
9. Xie Q, Bu W, Bhatia S, Hare J, Somasundaram T, Azzi A, Chapman MS. The atomic structure of adeno-associated virus (AAV-2), a vector for human gene therapy. Proc Natl Acad Sci USA 2002; 99(16): 10405-10.
10. Wu Z, Asokan A, Samulski RJ. Adeno-associated virus serotypes: vector toolkit for human gene therapy. Mol Ther 2006; 14(3): 316-27.
11. Russell DW, Kay MA. Adeno-associated virus vectors and hematology. Blood 1999; 94(3): 864-74.
12. Nam HJ, Lane MD, Padron E, Gurda B, McKenna R, Kohlbrenner E, Aslanidi G, Byrne B, Muzyczka N, Zolotukhin S, Agbandje-McKenna M. Structure of adeno-associated virus serotype 8, a gene therapy vector. J Virol 2007; 81(22):

12260-71.

13. Lerch TF, O'Donnell JK, Meyer NL, Xie Q, Taylor KA, Stagg SM, Chapman MS. Structure of AAV-DJ, a retargeted gene therapy vector: cryo-electron microscopy at 4.5 Å resolution. Structure 2012; 20(8): 1310-20.
14. Renata dos Santos Coura and Nance Beyer Nardi. A role for adeno-associated viral vectors in gene therapy. Genetics and Molecular Biology 2008; 31(1): 1-11
15. Ried MU1, Girod A, Leike K, Büning H, Hallek M. Adeno-associated virus capsids displaying immunoglobulin-binding domains permitantibody-mediated vector retargeting to specific cell surface receptors. J Virol 2002; 76(9): 4559-66.
16. Qin D, Trenkwalder T, Lee S, Chillo O, Deindl E, Kupatt C, Hinkel R. Early vessel destabilization mediated by Angiopoietin-2 and subsequent vessel maturation via Angiopoietin-1 induce functional neovasculature after ischemia. PLoS One 2013; 8(4): 1-14 (e61831).
17. Ziegler T, Horstkotte J, Schwab C, Pfetsch V, Weinmann K, Dietzel S, Rohwedder I, Hinkel R, Gross L, Lee S, Hu J, Soehnlein O, Franz WM, Sperandio M, Pohl U, Thomas M, Weber C, Augustin HG, Fässler R, Deutsch U, Kupatt C. Angiopoietin2 mediates microvascular and hemodynamic alterations in sepsis. J Clin Invest 2013; 123(8): 3436–3445.
18. Franz WM, Breves D, Klingel K, Brem G, Hofschneider PH, Kandolf R. Heart-specific targeting of firefly luciferase by the myosin light chain-2 promoter and developmental regulation in transgenic mice. Circ Res 1993; 73: 629–638.
19. Müller OJ, Leuchs B, Pleger ST, Grimm D, Franz WM, Katus HA, Kleinschmidt JA. Improved cardiac gene transfer by transcriptional and transductional targeting of adeno-associated viral vectors. Cardiovasc Res 2006; 70(1): 70-8.
20. Raake PW, Hinkel R, Müller S, Delker S, Kreuzpointner R, Kupatt C, Katus HA, Kleinschmidt JA, Boekstegers P, Müller OJ. Cardio-specific long-term gene expression in a porcine model after selective pressure-regulated retroinfusion of adeno-associated viral (AAV) vectors. Gene Ther 2008; 15: 12–7.

21. Kern A, Schmidt K, Leder C, Muller OJ, Wobus CE, Bettinger K, Von der Lieth CW, King JA, Kleinschmidt JA. Identification of a heparin-binding motif on adenoassociated virus type 2 capsids. J Virol 2003; 77(20): 11072–81.
22. Bish LT, Morine K, Sleeper MM, Sanmiguel J, Wu D, Gao G, Wilson JM, Sweeney HL. AAV9 provides global cardiac gene transfer superior to AAV1, AAV6, AAV7, and AAV8 in the mouse and rat. Hum Gene Ther 2008; 19(12): 1359-68.
23. Sadekar S, Ghandehari H. Transepithelial transport and toxicity of PAMAM dendrimers: implications for oral drug delivery. Adv Drug Deliv Rev 2012; 64(6): 571-88.
24. Varadi K, Michelfelder S, Korff T, Hecker M, Trepel M, Katus HA, Kleinschmidt JA, Müller OJ. Novel random peptide libraries displayed on AAV serotype 9 for selection of endothelial cell-directed gene transfer vectors. Gene Ther 2012; 19(8): 800-9.
25. Mueller J, Gaertner FC, Blechert B, Janssen KP, Essler M. Targeting of tumor blood vessels: a phage-displayed tumor-homing peptide specifically binds to matrix metalloproteinase-2-processed collagen IV and blocks angiogenesis in vivo. Mol Cancer Res 2009; 7(7): 1078-85.
26. Lee SM, Lee EJ, Hong HY, Kwon MK, Kwon TH, Choi JY, Park RW, Kwon TG, Yoo ES, Yoon GS, Kim IS, Ruoslahti E, Lee BH. Targeting bladder tumor cells in vivo and in the urine with a peptide identified by phage display. Mol Cancer Res 2007; 5(1): 11-9.
27. Scott JK1, Smith GP. Searching for peptide ligands with an epitope library. Science 1990; 249(4967): 386-90.
28. Devlin JJ, Panganiban LC, Devlin PE. Random peptide libraries: a source of specific protein binding molecules. Science 1990; 249(4967): 404-6.
29. Vetter A, Virdi KS, Espenlaub S, Rödl W, Wagner E, Holm PS, Scheu C, Kreppel F, Spitzweg C, Ogris M. Adenoviral vectors coated with PAMAM dendrimer

conjugates allow CAR independent virus uptake and targeting to the EGF receptor. Mol Pharm 2013; 10(2): 606-18.

30. Thurn KT, Brown E, Wu A, Vogt S, Lai B, Maser J, Paunesku T, Woloschak GE. Nanoparticles for applications in cellular imaging. Nanoscale Res Lett 2007; 2(9): 430-41.
31. DONALD A. TOMALIA, JEAN M. J. FRE´CHET. Discovery of Dendrimers and Dendritic Polymers: A Brief Historical Perspective. Journal of Polymer Science: Part A: Polymer Chemistry 2002; 40: 2719–2728.
32. D. A. Tomalia, H. Baker, J. Dewald, M. Hall, G. Kallos, S. Martin, J. Roeck, J. Ryder, and P. Smith. A new class of polymers: Starburst-Dendritic Macromolecules. Polymer J 1985; 17(1): 117-132.
33. Magdalena Labieniec, Cezary Watala. PAMAM dendrimers- diverse biomedical applications. Facts and unresolved questions. Cent Eur J Biol 2009; 4(4): 434–451.
34. Donald A. Tomalia. The dendritic state. Materialstoday 2005; 34-46.
35. Abbott NJ1, Rönnbäck L, Hansson E. Astrocyte-endothelial interactions at the blood-brain barrier. Nat Rev Neurosci 2006; 7(1): 41-53.
36. Adamson RH, Clough G. Plasma proteins modify the endothelial cell glycocalyx of frog mesenteric microvessels. J Physiol 1992; 445: 473-86.
37. Kitchens KM, El-Sayed ME, Ghandehari H. Transepithelial and endothelial transport of poly (amidoamine) dendrimers. Adv Drug Deliv Rev 2005; 57(15): 2163-76.
38. Voigt J, Christensen J, Shastri VP. Differential uptake of nanoparticles by endothelial cells through polyelectrolytes withaffinity for caveolae. Proc Natl Acad Sci USA 2014; 111(8): 2942-7.
39. Scott RA, Panitch A. Glycosaminoglycans in biomedicine. Wiley Interdiscip Rev Nanomed Nanobiotechnol 2013; 5(4): 388-98.
40. Adage T, Piccinini AM, Falsone A, Trinker M, Robinson J, Gesslbauer B, Kungl

AJ. Structure-based design of decoy chemokines as a way to explore the pharmacological potential of glycosaminoglycans. Br J Pharmacol 2012; 167(6): 1195-205.

41. Smith GP. Filamentous fusion phage: novel expression vectors that display cloned antigens on the virion surface. Science 1985; 228(4705): 1315-7.
42. Barbas CF 3rd, Kang AS, Lerner RA, Benkovic SJ. Assembly of combinatorial antibody libraries on phage surfaces: the gene III site. Proc Natl Acad Sci USA 1991; 88(18): 7978-82.
43. Huang JX, Bishop-Hurley SL, Cooper MA. Development of anti-infectives using phage display: biological agents against bacteria, viruses, and parasites. Antimicrob Agents Chemother 2012; 56(9): 4569-82.
44. Smith J, Kontermann RE, Embleton J, Kumar S. Antibody phage display technologies with special reference to angiogenesis. FASEB J 2005; 19(3): 331-41.
45. Fukunaga K, Taki M. Practical tips for construction of custom Peptide libraries and affinity selection by using commercially available phage display cloning systems. J Nucleic Acids 2012; 295719: 1-9.
46. Sauer B, Henderson N. Site-specific DNA recombination in mammalian cells by the Cre recombinase of bacteriophage P1. Proc Natl Acad Sci USA 1988; 85(14): 5166-70.
47. Chen YH, Chang M, Davidson BL. Molecular signatures of disease brain endothelia provide new sites for CNS-directed enzyme therapy. Nat Med 2009; 15: 1215–1218.
48. White SJ, Nicklin SA, Büning H, Brosnan MJ, Leike K, Papadakis ED et al. Targeted gene delivery to vascular tissue in vivo by tropism-modified adeno-associated virus vectors. Circulation 2004; 109: 513–519.
49. Nicklin SA, Buening H, Dishart KL, de Alwis M, Girod A, Hacker U et al. Efficient and selective AAV2-mediated gene transfer directed to human vascular

endothelial cells. Mol Ther 2001; 4: 174–181.

50. Work LM, Büning H, Hunt E, Nicklin SA, Denby L, Britton N et al. Vascular bed-targeted in vivo gene delivery using tropism-modified adeno-associated viruses. Mol Ther 2006; 13: 683–693.
51. Müller OJ, Kaul F, Weitzman MD, Pasqualini R, Arap W, Kleinschmidt JA et al. Random peptide libraries displayed on adeno-associated virus to select for targeted gene therapy vectors. Nat Biotechnol 2003; 21: 1040–1046.
52. Grimm D, Lee JS, Wang L, Desai T, Akache B, Storm TA et al. In vitro and in vivo gene therapy vector evolution via multispecies interbreeding and retargeting of adenoassociated viruses. J Virol 2008; 82: 5887–5911.
53. Pacak CA, Mah CS, Thattaliyath BD, Conlon TJ, Lewis MA, Cloutier DE et al. Recombinant adeno-associated virus serotype 9 leads to preferential cardiac transduction in vivo. Circ Res 2006; 99: e3–e9.
54. Markus Sperandio, Aravinda Thatte, Dan Foy, Lesley G. Ellies, Jamey D. Marth, and Klaus Ley, Severe impairment of leukocyte rolling in venules of core 2 glucosaminyltransferase–deficient mice. Blood 2001; 97: 3812-19.
55. Stachel G, Trenkwalder T, Götz F, El Aouni C, Muenchmeier N, Pfosser A, Nussbaum C, Sperandio M, Hatzopoulos AK, Hinkel R, Nelson PJ, Kupatt C. SDF-1 Fused to a Fractalkine Stalk and a Gpi Anchor Enables Functional Neovascularization. Stem cells 2013; 31(9): 1795-805
56. Kelly CV, Liroff MG, Triplett LD, Leroueil PR, Mullen DG, Wallace JM, Meshinchi S, Baker JR, Orr BG, Banaszak Holl MM. Stoichiometry and Structure of Poly(amidoamine) Dendrimer-Lipid Complexes. ACS Nano 2009; 3(7): 1886-96.
57. Jolanta F. Kukowska-Latallo, Kimberly A. Candido, Zhengyi Cao, Shraddha S. Nigavekar, Istvan J. Majoros, Thommey P. Thomas, Lajos P. Balogh, Mohamed K. Khan, and James R. Baker Jr. Nanoparticle targeting of anticancer drug improves therapeutic response in animal model of human epithelial cancer. Cancer Res

2005; 65(12): 5317-24.

58. Jiezhong Chen, Renfu Shao, Xu Dong Zhang, and Chen Chen. Applications of nanotechnology for melanoma treatment, diagnosis, and theranostics. Int J Nanomedicine 2013; 8: 2677–2688.
59. Lekli I, Mukherjee S, Ray D, Gurusamy N, Kim YH, Tosaki A, Engelman RM, Ho YS, Das DK. Functional recovery of diabetic mouse hearts by glutaredoxin-1 gene therapy: role of Akt-FoxO-signaling network. Gene Ther 2010; 17(4): 478-85
60. van Til NP, Stok M, Aerts Kaya FS, de Waard MC, Farahbakhshian E, Visser TP, Kroos MA, Jacobs EH, Willart MA, van der Wegen P, Scholte BJ, Lambrecht BN, Duncker DJ, van der Ploeg AT, Reuser AJ, Verstegen MM, Wagemaker G. Lentiviral gene therapy of murine hematopoietic stem cells ameliorates the Pompe disease phenotype. Blood 2010; 115(26): 5329-37
61. Wang C, Hu J, Lu M, Gu H, Zhou X, Chen X, Zen K, Zhang CY, Zhang T, Ge J, Wang J, Zhang C. A panel of five serum miRNAs as a potential diagnostic tool for early-stage renal cell carcinoma. Sci Rep 2015; 5(5): 7610
62. Ionov M, Lazniewska J, Dzmitruk V, Halets I, Loznikova S, Novopashina D, Apartsin E, Krasheninina O, Venyaminova A, Milowska K, Nowacka O, Gomez-Ramirez R, de la Mata FJ, Majoral JP, Shcharbin D, Bryszewska M. Anticancer siRNA cocktails as a novel tool to treat cancer cells. Part (A). Mechanisms of interaction. Int J Pharm 2015; 485(1-2): 261-9
63. Khatri S, Das NG, Das SK. Effect of methotrexate conjugated PAMAM dendrimers on the viability of MES-SA uterine cancer cells. J Pharm Bioallied Sci 2014; 6(4): 297-302
64. Winnicka K, Wroblewska M, Sosnowska K, Car H, Kasacka I. Evaluation of cationic polyamidoamine dendrimers' dermal toxicity in the rat skin model. Drug Des Devel Ther 2015; 5(9): 1367-77
65. Movellan J, González-Pastor R, Martín-Duque P, Sierra T, de la Fuente JM,

Serrano JL. New Ionic bis-MPA and PAMAM Dendrimers: A Study of Their Biocompatibility and DNA-Complexation. Macromol Biosci 2015;.

66. Strydom N, Rankin SM. Regulation of Circulating Neutrophil Numbers under Homeostasis and in Disease. Journal of Innate Immunity 2013; 5:304-14.
67. Liehn EA, Tuchscheerer N, Kanzler I, et al. Double-Edged Role of the CXCL12/CXCR4 Axis in Experimental Myocardial Infarction. J Am Coll Cardiol 2011; 58:2415-23.
68. Politz O, Gratchev A, McCourt PA, Schledzewski K, Guillot P, Johansson S, Svineng G, Franke P, Kannicht C, Kzhyshkowska J, Longati P, Velten FW, Johansson S, Goerdt S. Stabilin-1 and -2 constitute a novel family of fasciclin-like hyaluronan receptor homologues. Biochem J 2002; 15(362): 155-64.
69. Jung MY, Park SY, Kim IS. Stabilin-2 is involved in lymphocyte adhesion to the hepatic sinusoidal endothelium via the interaction with alphaM beta2 integrin. J Leukoc Biol 2007; 82(5): 1156-65.
70. Park SY, Kim SY, Jung MY, Bae DJ, Kim IS. Epidermal Growth Factor-Like Domain Repeat of Stabilin-2 Recognizes Phosphatidylserine during Cell Corpse Clearance. Mol Cell Biol 2008; 28(17): 5288-98.
71. Stoll SJ, Bartsch S, Kroll J. HOXC9 Regulates Formation of Parachordal Lymphangioplasts and the Thoracic Duct in Zebrafish via Stabilin 2. PLoS One 2013; 8(3): e58311.
72. Kim S, Park SY, Kim SY, Bae DJ, Pyo JH, Hong M, Kim IS. Cross Talk between Engulfment Receptors Stabilin-2 and Integrin alphav beta5 Orchestrates Engulfment of Phosphatidylserine-Exposed Erythrocytes. Mol Cell Biol 2012; 32(14): 2698-708.
73. Rost MS, Sumanas S. Hyaluronic Acid Receptor Stabilin-2 Regulates Erk Phosphorylation and Arterial - Venous Differentiation in Zebrafish. PLoS One 2014; 9(2): e88614.
74. Lee SJ, Park SY, Jung MY, Bae SM, Kim IS. Mechanism for

phosphatidylserine-dependent erythrophagocytosis in mouse liver. Blood 2011; 117(19): 5215-23.

75. Schledzewski K, Géraud C, Arnold B, Wang S, Gröne HJ, Kempf T, Wollert KC, Straub BK, Schirmacher P, Demory A, Schönhaber H, Gratchev A, Dietz L, Thierse HJ, Kzhyshkowska J, Goerdt S. Deficiency of liver sinusoidal scavenger receptors stabilin-1 and -2 in mice causes glomerulofibrotic nephropathy via impaired hepatic clearance of noxious blood factors. J Clin Invest 2011; 121(2): 703-14.
76. Lee GY, Kim JH, Choi KY, Yoon HY, Kim K, Kwon IC, Choi K, Lee BH, Park JH, Kim IS. Hyaluronic acid nanoparticles for active targeting atherosclerosis. Biomaterials 2015; (53): 341-8.
77. Corjay MH, Dobrzanski DJ, Way JM, Viallet J, Shapira H, Worland P, Sausville EA, Battey JF. Two Distinct Bombesin Receptor Subtypes Are Expressed and Functional in Human Lung Carcinoma Cells. J Biol Chem 1991; 266(28): 18771-9.
78. Zhao F, Weismann CG, Satoda M, Pierpont ME, Sweeney E, Thompson EM, Gelb BD. Novel TFAP2B mutations that cause Char syndrome provide a genotype-phenotype correlation. Am J Hum Genet 2001; 69(4): 695-703.
79. Maeda S, Tsukada S, Kanazawa A, Sekine A, Tsunoda T, Koya D, Maegawa H, Kashiwagi A, Babazono T, Matsuda M, Tanaka Y, Fujioka T, Hirose H, Eguchi T, Ohno Y, Groves CJ, Hattersley AT, Hitman GA, Walker M, Kaku K, Iwamoto Y, Kawamori R, Kikkawa R, Kamatani N, McCarthy MI, Nakamura Y. Genetic variations in the gene encoding TFAP2B are associated with type 2 diabetes mellitus. J Hum Genet 2005; 50(6): 283-92.
80. Faber PW, Barnes GT, Srinidhi J, Chen J, Gusella JF, MacDonald ME. Huntingtin interacts with a family of WW domain proteins. Hum Mol Genet 1998; 7(9): 1463-74.
81. Mayer U, Pöschl E, Gerecke DR, Wagman DW, Burgeson RE, Timpl R. Low

nidogen affinity of laminin-5 can be attributed to two serine residues in EGF-like motif gamma 2III4. FEBS Letters 1995; 365(2-3): 129-132.

82. Sainz E, Akeson M, Mantey SA, Jensen RT, Battey JF. Four amino acid residues are critical for high affinity binding of neuromedin B to the neuromedin B receptor. J Biol Chem 1998; 273(26): 15927-32.
83. Zincarelli C, Soltys S, Rengo G, Rabinowitz JE. Analysis of AAV serotypes 1-9 mediated gene expression and tropism in mice after systemic injection. Mol Ther 2008;16(6): 1073-80.
84. Isaka S, Takei Y, Tokino T, Koyama K, Miyoshi Y, Suzuki M, Takahashi E, Azuma C, Murata Y, Nakamura Y. Isolation and characterization of a novel TP53-inducible gene, TP53TG5, which suppresses growth and shows cell cycle-dependent transition of expression. Genes Chromosomes Cancer 2000; 27(4): 345-52.
85. Yang L, Xiao X. Creation of a cardiotropic adeno-associated virus: the story of viral directed evolution. Virol J 2013; 11;10:50
86. Drew PJ, Shih AY, Kleinfeld D. Fluctuating and sensory-induced vasodynamics in rodent cortex extend arteriole capacity. Proc Natl Acad Sci U S A 2011; 108(20): 8473-8.

9. PUBLICATIONS

1. **Seungmin Lee**, Judy Ng, Rabea Hinkel, Oliver Müller, Peter Nelson, Markus Sperandio, Manfred Ogris, Christian Kupatt. Nanoparticles optimize peptide-guided AAV-retargeting towards microvascular endothelium. (Manuscript prep.)
2. **Seungmin Lee**. Identification of a H3N2 Hong-Kong influenza virus binding receptors by homolog mining a single immune scFv M13 phage library. (Manuscript prep.)
3. Rabea Hinkel, Philipp Lange, Björn Petersen, Elena Gottlieb, Judy Ng, Stefanie Finger, Jan Horstkotte, **Seungmin Lee**, Michael Thormann, Maike Knorr, Chiraz El-Aouni, Peter Boekstegers, Bruno Reichart, Philip Wenzel, Heiner Niemann, Christian Kupatt. Heme oxygenase 1 gene therapy provides cardioprotection via control of postischemic inflammation in a preclinical pig model. **JACC 2015;** 66(2): p.154-165.
4. Trenkwalder T, Deindl E, Bongiovanni D, **Lee S,** Schunkert H, Kupatt C, Hinkel R. Thymosin-β4-mediated therapeutic neovascularization: role of the PI3K/AKT pathway. **Expert Opin Biol Ther 2015;** 4: p. 1-11.
5. Rabea Hinkel, Teresa Trenkwalder, Bjoern petersen, Wira Husada, Florian Gesenhues, **Seungmin Lee**, Ewald Hannappel, Ildiko Bock-Marquette, Daniel Theisen, Laura Leitner, Peter Boekstegers, Czeslaw Cierniewski, Oliver J. Mueller, Ferdinand le Noble, Ralf H.Adams, Christine Weinl, Alfred Nordheim, Bruno Reichart, Christian Weber, Eric Olson, Guido Posern, Elisabeth Deindl, Heiner Niemann & Christian Kupatt. MRTF-A controls vessel growth and maturation by increasing the expression of CCN1 and CCN2. **Nature comm 2014;** 5: p. 3970.
6. Qin Di, Trenkwalder T, **Lee S**, Chillo O, Deindl E, Kupatt C, Hinkel R. Early vessel destabilization mediated by Angiopoietin-2 and subsequent vessel

maturation via Angiopoietin-1 induce functional neovasculature after ischemia. **PLoS One 2013;** 8(4): p. e61831.

7. Ziegler T, Horstkotte J, Schwab C, Pfetsch V, Weinmann K, Dietzel S, Rohwedder I, Hinkel R, Gross L, **Lee S**, Hu J, Soehnlein O, Franz WM, Sperandio M, Pohl U, Thomas M, Weber C, Augustin HG, Fässler R, Deutsch U, Kupatt C. Angiopoietin 2 mediates microvascular and hemodynamic alterations in sepsis. **J Clin Invest 2013;** 123(8): p. 3436–3445.
8. Yeong Su Ha, Hwa Young Lee, Gwang Il An, Jonghee Kim, Wonjung Kwak, Eun-Ju Lee, **Seung-Min Lee**, Byung-Heon Lee, In-San Kim, Takele Belay, Woonghee Lee, Byeong-Cheol Ahn, Jaetae Lee, Jeongsoo Yoo. Synthesis and evaluation of a radioiodinated bladder cancer specific peptide. **Bioorg Med Chem 2012;** 20(14): p. 4330-5.
9. **Seung-Min L**, Gil-Suk Y, Eun-Sang Y, Tae-Gyun K, In-San K, Byung-Heon L. Application of phage display to discovery of tumor-specific homing peptides: developing strategies for therapy and molecular imaging of cancer. **Methods Mol Biol 2009;** 512: p. 355-63.
10. **Lee SM**, Lee EJ, Hong HY, Kwon MK, Kwon TH, Choi JY, Park RW, Kwon TG, Yoo ES, Yoon GS, Kim IS, Ruoslahti E, Lee BH. Targeting bladder tumor cells in vivo and in the urine with a peptide identified by phage display. **Mol Cancer Res 2007;** 5(1): p. 11-9.

10. ACKNOWLEGEMENTS

First of all, I would like to thank to my supervisor Prof. Dr. med. Christian Kupatt for his scientific support and guidance. I appreciate, given to me the freedom works in my PhD thesis. He was always accommodative to the suggestions, which stimulated the independent thinking. It is not only a great honor but also a valuable enrichment for my future career and life.

Special thanks to my second supervisor Dr. dvm. Rabea Hinkel for her helpful advice, support and encouragement. I am very grateful to Mr. Kieu Cuong (Med I, LMU München, Germany), and Frau, Elisabeth Ratt (Med I, LMU München, Germany) for excellent technical support about production of AAV. Without their help this thesis would not have been as successful. A big thanks to Prof. Dr. med. Oliver J. Müller (Med III, Heidelberg, Germany) for support about AAV vectors. Special thanks to Prof. Dr. Manfred Ogris (Clinical Pharmacy and Diagnostics, Vienna, Austria) for his suggestion and support about purification of nanoparticles. Thanks a lot to Prof. Dr. med. Markus Sperandio (Walter-Brendel-Center, LMU München, Germany) for scientific support, as the whole mount images of the cremaster muscle. Thanks Dr. Judy Ng for help about FACS analysis of whole mice heart.

Furthermore, I would like to express deep thanks to members of Klinikum Grosshadern LMU München. Who is Dr. med. Guo Yang, Dr. med. Di Qin, and Dr. med. Teresa T. Thanks to Dr. Alexandra Kerstin Maria Vetter, and Dr. Christian N.

Finally, I want to express thanks to my family, my father, mother, and sisters. They care me so much and always give me a good motivation. Without them, I would not be myself as I am these days.